Flow instabilities of PP filled with crosslinked EPDM rubber: using rheology to understand and control its occurrence

by

Nikoo Ghahramani

B.Sc., Amirkabir University of Technology, Tehran, Iran, 2014
M.Sc., Amirkabir University of Technology, Tehran, Iran, 2017

A THESIS SUBMITTED IN PARTIAL FULFILLMENT OF
THE REQUIREMENTS FOR THE DEGREE OF

DOCTOR OF PHILOSOPHY

in

THE FACULTY OF GRADUATE AND POSTDOCTORAL STUDIES
(Chemical and Biological Engineering)

THE UNIVERSITY OF BRITISH COLUMBIA

(Vancouver)

September 2021

The following individuals certify that they have read, and recommend to the Faculty of Graduate and Postdoctoral Studies for acceptance, the dissertation entitled:

Flow instabilities of PP filled with crosslinked EPDM rubber: using rheology to understand and control its occurrence

submitted by Nikoo Ghahramani in partial fulfillment of the requirements for

the degree of Doctor of Philosophy

in Chemical and Biological Engineering

Examining Committee:

Savvas G. Hatzikiriakos, Chemical and Biological Engineering, UBC
Supervisor

Mark Martinez, Chemical and Biological Engineering, UBC
Supervisory Committee Member

Jeffrey Giacomin, Chemical Engineering, Queen's University
External Examiner

Simcha Srebnik, Chemical and Biological Engineering, UBC
University Examiner

Reza Vaziri, Civil Engineering, UBC
University Examiner

Additional Supervisory Committee Members:

Sheldon Green, Mechanical Engineering, UBC
Supervisory Committee Member

Antonios Doufas, ExxonMobil Chemical Company
Supervisory Committee Member

Krishnan Iyer, ExxonMobil Chemical Company
Supervisory Committee Member

Abstract

Thermoplastic vulcanizates (TPVs) are polymer blends that have good processability like their thermoplastic phase and good elasticity like their elastomeric phase. They consist of a high amount of dynamically cured rubber particles which make flow instability such as melt fracture intense and complicated. In this study a comprehensive rheological analysis is performed to gain a deep understanding of TPVs' flow instabilities and identify the key parameters that control them.

First, a thorough linear viscoelastic analysis is performed using several groups of TPVs which are systematically different in curing level, types of polymer components, and cured rubber content. All the TPVs show a non-terminal behavior reaching to an equilibrium modulus at low frequencies/high relaxation times. The equilibrium modulus, G_y, is an indication of the existence of yield stress and the linear modulus, $G(t)$ can be modeled by a simple power-law model in the form of $(G(t) - G_y) \propto t^{-p}$, where t is the time. A yield stress is also observed in the extensional tests and the relationship between extensional and shear yield stress is investigated.

Due to the presence of oil and high amount of rubber particles, TPVs show wall slip. The multimode integral Kaye-Bernstein-Kearsley-Zapas (KBKZ) constitutive model considering wall slip is applied to study and model the TPVs' non-linear behavior. To incorporate slip into the model, a new way is used by applying a fraction of imposed nominal strain to match the experimental data. Moreover, it is assumed that the material does not slip in the linear unyielding region i.e., for shear stresses less than the yield stress. Applying these assumptions, the KBKZ captures the experimental data well.

Finally, to study processing parameters that affect the melt fracture phenomenon, capillary experiments are performed. It is observed that TPVs slip massively in capillary flow. Surface fracture of the TPVs gets better with shear rate indicating that the origin of melt fracture is different with that of TPV's pure component. Yield stress controls flow instability of the TPVs and to overcome and/or mitigate melt fracture, high shear rates are needed to cause flow and eliminate unyielded regions in the complex geometries used in real processing.

Lay Summary

Thermoplastic vulcanizates are polymer blends which contain a high amount of rubber particles that are dispersed in a thermoplastic matrix. Due to the presence of a high amount of rubber, they exhibit yield stress i.e. the applied forces should be higher than a certain value to cause flow. TPVs also slip massively and exhibit surface distortions (melt fracture) when they flow out of dies in processing. In this thesis, the rheological properties of (TPVs) are studied in detail and used to understand the origin of flow instability such as melt fracture.

Preface

This thesis entitled “Flow Instabilities of PP Filled with Crosslinked EPDM Rubber: Using Rheology to Understand and Control its Occurrence” presents the research the author performed during her PhD study under the supervision of Professor Savvas G. Hatzikiriakos. Rheology and flow behavior of different groups of TPVs have been extensively studied to fully understand their flow instabilities.

The following journal papers have been published or submitted for publication from the research work presented in this dissertation:

Chapter 5 has been prepared based on a published manuscript.
Ghahramani, N., Iyer, K., Doufas, A., Hatzikiriakos, S.G., (2020). Rheology of thermoplastic vulcanizates (TPVs). Journal of Rheology, 64(6), pp.1325-1341.

The materials covered in chapter 6 is based on a published manuscript.
Ghahramani, N., Iyer, K., Doufas, A., Hatzikiriakos, S.G., (2021). Rheological modelling of Thermoplastic Vulcanizates (TPVs) using the Kaye–Bernstein, Kearsley, Zapas (K–BKZ) constitutive law. *Physics of Fluids*, 33(8), p.083107.

Chapter 7 has been prepared based on a published manuscript.
Ghahramani, N., Zhang, S., A Iyer, K., Doufas, A.K. and Hatzikiriakos, S.G., 2021. Melt fracture and wall slip of thermoplastic vulcanizates. *Polymer Engineering & Science*, *61*(4), pp.942-958. Capillary experiments were done by Shiling Zhang.

All manuscripts were written by the author of this thesis and revised by the supervisor (Prof. S.G. Hatzikiriakos) and the other co-authors.

Table of Contents

List of Tables

List of Figures

List of Symbols

C_t	Cauchy-Green tensor
C_t^{-1}	Finger tensor
^oC	The degree Celsius (centigrade)
D	Die diameter (m)
E_a	Energy of activation (J/mol)
f	Fraction
G	Relaxation modulus (Pa)
G^*	Complex modulus (Pa)
G'	Storage modulus (Pa)
G"	Loss modulus (Pa)
$G_c^{"}$	Loss modulus coefficient (constant) (Pa)
G_c	Relaxation modulus constant (proportionality constant)
G_y	Equilibrium relaxation modulus (Pa)
G_y'	Equilibrium storage modulus (Pa)
G_c'	Storage modulus coefficient (constant) (Pa)
$h(\gamma)$	Damping function
I_{C_t}	First invariant of the Cauchy-Green tensor
L	Die length (m)
m (t-t')	Memory function
M_w	Weight average molecular weight (g/mol)
n	Material constant used in the damping function
N_1	First normal stress difference (Pa)
N_2	Second normal stress difference (Pa)
p	Power-law exponent
ΔP	Pressure drop (Pa)

ΔP_{end}	Ends pressure (Pa)
Q	Volumetric flow rate (m^3/s)
R	Die radius (m)
T	Temperature (K)
t	Time (s)
V_s	Slip velocity (m/s)

Greek symbols

β	Material constant used in the damping function
γ	Strain
$\dot{\gamma}$	Shear rate (s^{-1})
$\dot{\gamma}_A$	Apparent shear rate (s^{-1})
$\dot{\gamma}_{A,S}$	Apparent shear rate corrected for the effect of slip (s^{-1})
γ_y	Yield strain
γ_n	Nominal strain
$\dot{\gamma}_{nR}$	Nominal shear rate (s^{-1})
$\dot{\gamma}_R$	True shear rate (s^{-1})
δ	Damping factor
$\dot{\varepsilon}$	Hencky strain rate
η	Viscosity (Pa.s)
η^*	Complex viscosity (Pa.s)
η_E^+	Uniaxial tensile stress growth coefficient (Pa.s)
η^+	Shear stress growth coefficient (Pa.s)
θ	Material constant defining the ratio of the normal stress differences
λ	Relaxation time (s)
σ	Stress (Pa)
σ_A	Apparent shear stress (Pa)

σ_y	Shear yield stress (Pa)
σ_W	Wall shear stress (Pa)
$\sigma_{y,C}$	Crossover yield stress (Pa)
τ_R	Characteristic time (s)
ω	Frequency (s^{-1})

List of Abbreviations

CD	Crosslinked density
ENR	Epoxidized natural rubber
EPDM	Ethylene propylene diene monomer
EOC	Ethylene-octene copolymer
EVM	Ethylene-vinyl acetate rubber
GMF	Gross melt fracture
HDPE	High-density poly(ethylene)
K-BKZ	Kaye-Bernstein-Kearsley-Zapas
LCB	Long chain branching
LVE	Linear viscoelasticity
NBR	Nitrile butadiene rubber
NR	Natural rubber
PDI	Polydispersity index
PLA	Poly(lactic acid)
PP	Poly (propylene)
PVDF	Poly (vinylidene fluoride)
SiR	Silicon rubber
TPE	Thermoplastic elastomer
TPV	Thermoplastic vulcanizate
tTS	Time-temperature superposition

Acknowledgements

First and foremost, I would like to thank my supervisor Prof. Savvas G. Hatzikiriakos for his sincere support, advice and encouragement throughout my PhD research. Without his guidance, this work would never have been done. I would also like to acknowledge my supervisory committee members Professor Mark Martinez, Dr. Sheldon Green, Dr. Antonios Doufas and Dr. Krishnan Iyer for their time and helpful comments.

Sincere gratitude to my wonderful colleagues and friends Shohre, Shiling, Tanja, Benjamin, Marziyeh, Tina, Ziyue, Marina, Muaad, Zhe, Shahryar, Yu, Zahra, and Ali for their heartwarming friendships and for their great support along my journey over the past three years.

I would also like to thank my roommate Parya for all her support, encouragement, and effort to create a peaceful environment to live.

My acknowledgement also goes to ExxonMobil Chemical Co. for their research grant that provided the necessary financial support and the materials for this research.

The most profound and loving thanks go to my family; my wonderful sisters and brothers, Soybeh, Pourya, Sandia, and Arya for their endless love, encouragement and caring, and my cousin Pardis who was always there through my ups and downs. My deepest gratitude goes to my parents, Hedayat and Najimeh whom supported me and loved me each and every day.

Dedication

To my lovely parents

تقدیم به پدر و مادر عزیزم

1 Introduction

Generally, polymer blends can be categorized into two broad classes: miscible and immiscible. In the first category polymers exist in a homogeneous, single phase state with properties typically different from their primary components. In the second category, the blend forms two distinct phases. There is a third category of polymers blends which is technologically compatible blends or alloys. These blends exist in two or more phases in micro-scale but show macroscopic properties similar to a single phase material [1].

Thermoplastic elastomers (TPEs) are immiscible polymer blends that contain a thermoplastic and a rubbery phase (category 2). Therefore, while they show high elastic properties similar to traditional vulcanized rubbers, they have a good processability analogous to thermoplastics [2]. TPEs are widely used in footwear, wire insulation, medical devices and sporting goods and adhesives [3,4]. TPEs can be classified into two following categories. The first category is thermoplastic block copolymers and the second thermoplastic blends including thermoplastic-rubber blends undergoing a dynamic vulcanization process. These blends are referred to as thermoplastic vulcanizates (TPVs). In TPVs, a high content of rubber ($> 50\, wt.\%$) is simultaneously crosslinked and dispersed in a thermoplastic matrix [2].

Different TPV blends such as ethylene propylene diene monomer (EPDM)/polypropylene (PP) [2,5–11], ethylene-octene copolymer/polypropylene (PP) [12], epoxidized natural rubber/PP [13], natural rubber /PP [14], Natural rubber/high density polyethylene (HDPE) [15], nitrile butadiene rubber/PP TPVs [16], oil resistant ethylene-vinyl acetate rubber /poly(vinylidene fluoride) (PVDF) TPVs [17], high temperature resistant silicon rubber /PVDF TPVs [18], bio-based TPVs, such as poly (lactic acid) /Natural Rubber TPVs [19] have been studied in the literature. The subject of the present thesis is rheology and processing of TPVs.

Most of TPV properties such as mechanical, electrical, and rheological properties are highly influenced by their microstructure [10,20,21]. In order to reach the matrix disperse morphology at the end, a co-continuous morphology is required at the beginning of the melt mixing process [1] and the inversion from a co-continuous phase to a matrix disperse phase is the key factor in the

fabrication of TPVs [2]. It should be mentioned that a fine dispersion of rubber particles is required to obtain good mechanical properties [2].

Due to TPVs' complex microstructure, a substantial knowledge of the parameters affecting their processability is required. Rheological properties determine the processing behavior of TPVs. Therefore, understanding thoroughly their rheological behavior can be extremely useful to optimize the processability of TPVs and reduce major processing problems i.e., flow instability (slip and melt fracture). Although the rheological properties of TPVs have been investigated to some extent, there is no systematic and comprehensive study on rheological properties of TPVs in terms of their structure and composition and their correlation with the processability. Thus, this thesis aims to perform a thorough experimental study on the structural and rheological properties of TPVs attempting to obtain a better understanding of their flow behavior and their relation with processability, essentially targeting at improving their processing.

1.1 Production of TPVs

TPVs are usually produced by melt blending. They can be produced by either a continuous process using compounders (mixing extruders) or co-rotating twin screw extruders or batch process by internal mixers [1]. There are three main feeding procedure for producing TPVs, illustrated in **Figure 1-1**. In methods 1 and 2 rubber and plastic are mixed together at high temperature, and high shear rates. On the other hand, in method 3 rubber and crosslinking agent undergo a cold mixing to form a pre-mix. Afterwards, this premix is blended with the plastic and vulcanized simultaneously. The difference between method 1 and 2 is that in method 1, the rubber-plastic pre-mix goes through a cold mixing with the crosslinking agent., Then the dynamic vulcanization is applied to the mixture under high temperature and high shear rate. However, in method 2, the rubber-plastic pre-mix is mixed to crosslinking agent and vulcanized at the same time [2].

1.2 Formation Mechanism

Two factors are of high importance during the preparation of TPVs, namely the phase inversion and the fine dispersion of the rubber phase into the plastic matrix. Three different mechanisms have been proposed for phase inversion. Machado et al. [22] proposed a mechanism for the phase inversion in the manufacturing of PP/EPDM TPVs depicted in **Figure 1-2**. They hypothesized that before vulcanization of the rubber phase, the plastic droplets are dispersed in the rubber matrix

due to the high phase ratio of the rubber to the plastic phase (**Figure 1-2-a**). Then at the early stage of the dynamic vulcanization, the viscosity of the rubber phase increases which results in a co-continuous structure (**Figure 1-2-b**). Subsequently, the rubber phase forms an unstable fibrillar structure (**Figure 1-2-c**). Finally, with more increment in the crosslinking density, the viscosity of the rubber phase increases dramatically which results into an increase of the stress on the rubber phase and as a result the rubber phase breaks up into particles (**Figure 1-2-d**).

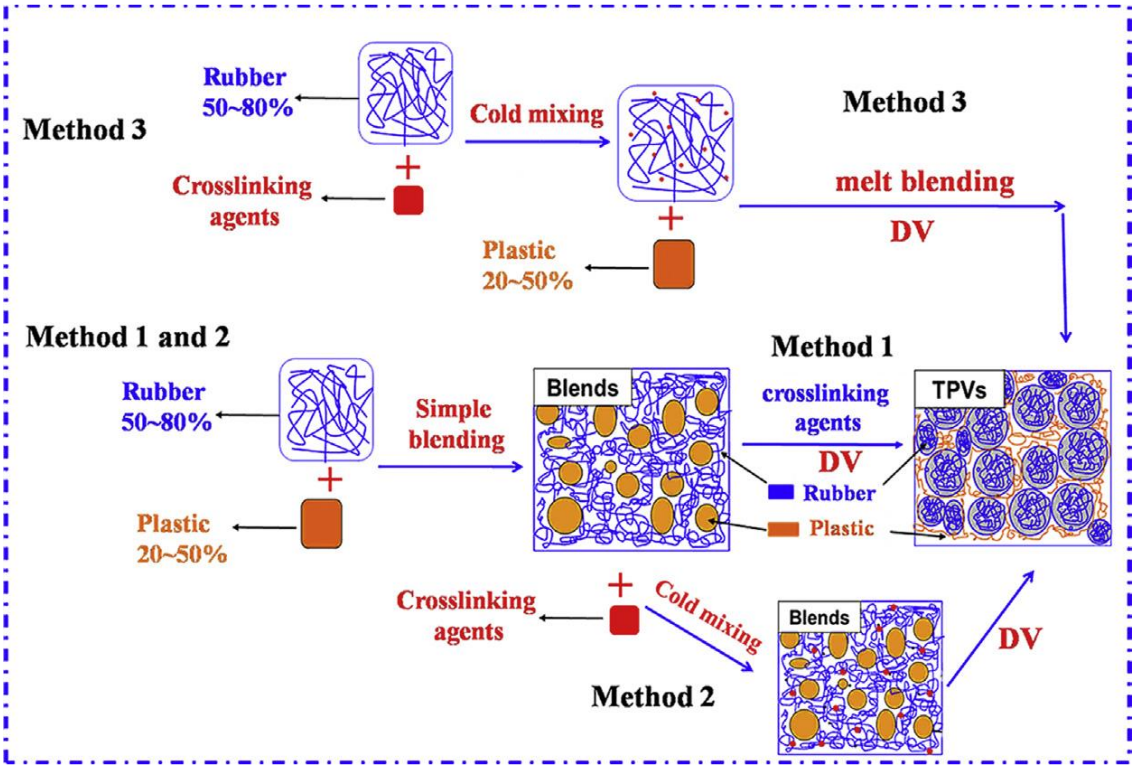

Figure 1-1. Schematic figure of preparation methods of TPVs adopted from [2]

Goharpey et al. [23] proposed another mechanism, depicted in **Figure 1-3**. The proposed model consists of four stages. First, the melt-melt dispersion before the onset of curing where the rubber droplet breakup and coalescence occur simultaneously. In the second stage, the rubber micro-droplets formed by the breakup of the rubber phase, cannot coalescence, instead, they can be transformed into micro-particles forming agglomerations. As the vulcanization proceeds, the interfacial adhesion between the two phases increases. In the last stage, due to the shrinkage of the

rubber particle (lower the surface energy), the rubber agglomerations break down to rubber micro-particles which results into a fine dispersion and thus phase inversion.

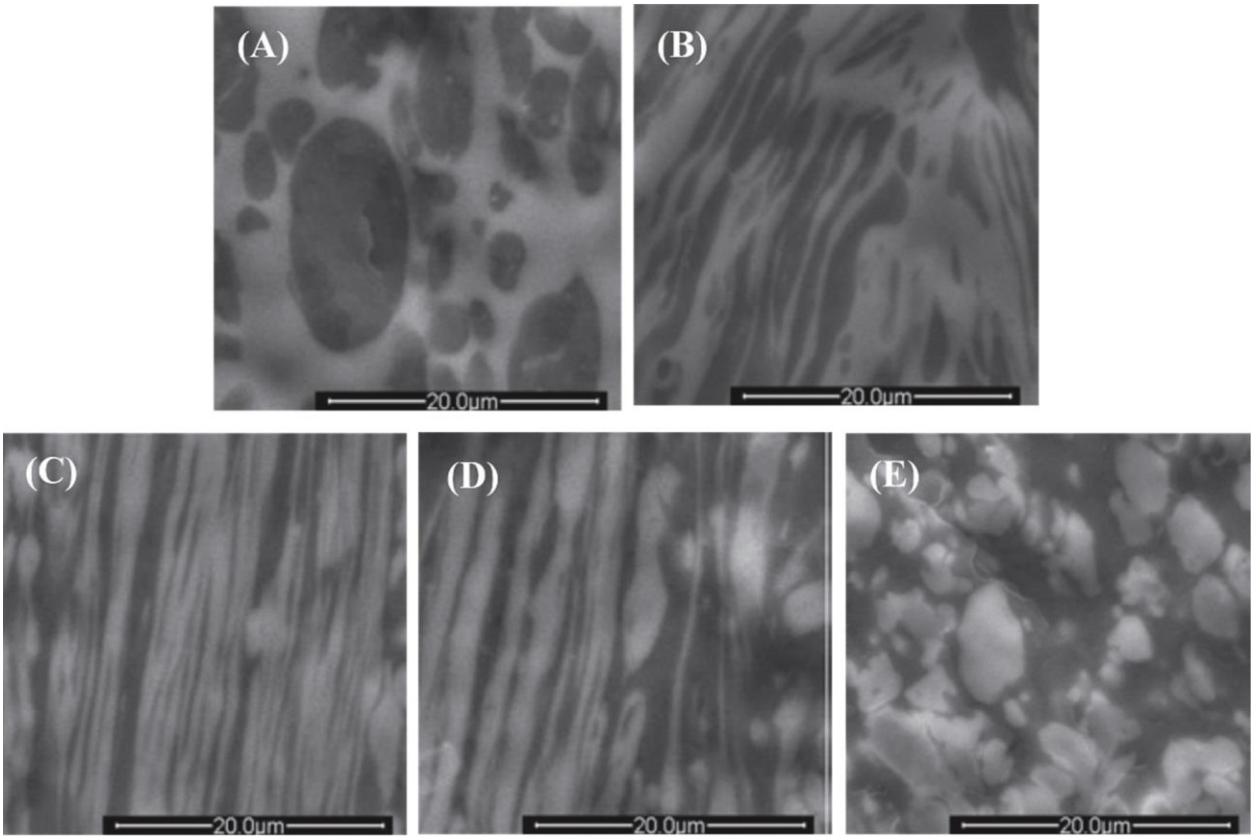

Figure 1-2. Morphological development mechanism proposed for the phase inversion of EPDM/PP blends during dynamic vulcanization adopted from [2,22].

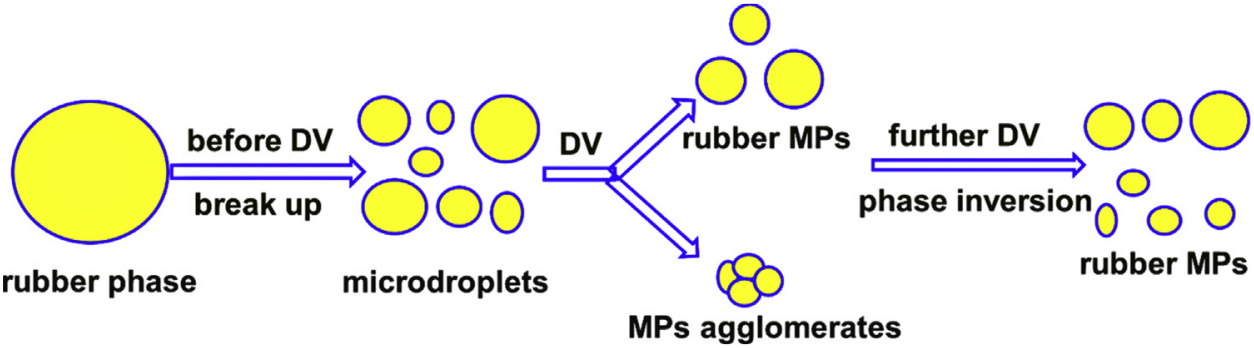

Figure 1-3. Schematic diagram of the proposed mechanism for the development of PP/EPDM blends during dynamic vulcanization adopted from [2,23].

2 Literature Review

One of the main advantages of TPVs over traditional cured rubbers is their processability, which is determined by their rheological behavior. Therefore, rheological studies of TPVs have received significant attention in the literature. The rheological properties can be studied by using parallel-plate modular compact rheometers as well as capillary rheometers. It should be noted that since TPVs contain a high amount of cured rubber particles, their rheological properties are significantly different than uncured blends due to the formation of a strong cured rubber network [2].

In order to do rheometry with modular compact rheometers, polymeric samples are placed between two circular plates (parallel-plate geometry). The upper plate is gradually lowered to touch the sample and compresses it until building up a high normal force. Due to buildup of the high normal force, the gap cannot be controlled at an exact specified value, and as such cone-and-plate geometry is not a good choice for TPVs. Instead, the parallel-plate geometry having a normal force controlled moving profile is a better choice. It should also be noted that during sample preparation for the rheometry, if the measuring plate approaches the sample at high velocity, a high normal force builds up abruptly which cannot be subsequently relaxed. Therefore, a low velocity moving profile near the sample surface coupled with stopping controlled by normal force is suggested as a good moving profile before starting the rheological measurements. Another important point is that to reduce slip, the TPV samples should be placed in the convectional oven at the desired temperature for around 30 minutes before starting the measurement.

Due to the existence of the strong rubber network, TPVs are expected to show yield stress [24] as well they are expected to slip violating the no-slip boundary condition of fluid mechanics [25,26]. Thus, in addition to structural parameters such as rubber/thermoplastic ratio, pure polymers' structure, and curing content, two major phenomena that dictate the rheological behavior of TPVs are yield stress and wall slip. Therefore, in this thesis, emphasis is placed on the study and explanation of these two phenomena. Finally, the melt fracture of the TPVs as a criterion for their processability has been emphasized in this thesis as well. Melt fracture is manifested as surface distortion on the surface of polymers when the flow exits a die and typically occurs if the flow rate exceeds a critical value.

2.1 Structural Parameters Affecting Rheology of TPVs

TPVs microstructure highly influences their properties such as mechanical and rheological [10,20,21]. As it was mentioned above, TPVs' rheological properties are of high importance because they affect their processability and can be used to understand and optimize it [27,28]. Since there is a strong rubber network in TPVs due to the presence of the cured rubber particles, their complex viscosity at low shear rates are much higher than that of the thermoplastic matrix [29–31]. There are other significant parameters such as the ratio of rubber phase to plastic phase, the size of the rubber domains, the curing level of the rubber phase, and the addition of plasticizers and fillers which determine their rheological properties [13,27–29,32–36]. It has been widely reported that by increasing the crosslinking agent concentration, the crosslinking density increases and consequently the complex viscosity is enhanced accordingly [1,18,23]. Generally, while a small amount of filler has only a minor effect, a large amount increases the viscosity of TPVs, [1]. It has also been reported that incorporating filler disrupts the rubber network and decreases the complex modulus, G^*, of TPVs [37].

2.1.1 Effect of polymer type

Goharpey et. al. [23] studied several sets of PP/EPDM blends with different PP viscosity. They reported that by increasing the PP melt viscosity, the EPDM/PP viscosity ratio decreases, which results in a better dispersion of rubber aggregates and consequently more stabilized morphology and better mechanical properties of the TPE samples. Prut et. al. [38] also compared PP/oil-free EPDM TPVs to PP/Oil-extended EPDM ones and reported that the processability of oil-extended TPVs are significantly better than the oil free ones.

2.1.2 Effect of the composition ratio (R/P)

With increasing the rubber concentration in TPVs, the number and density of the rubber particles increase and form a strong rubber network. In addition, the rubber phase has much higher shear viscosity than that of the thermoplastic phase. Therefore, the viscosity increases with the concentration of rubber particles. Meanwhile, because the thickness of the plastic ligaments decreases with increasing the rubber content, it also causes an increase in the viscosity of TPVs and deterioration of processability [2].

2.1.3 Effect of the content of crosslinking agent

It has also been widely reported in various TPVs systems that with increase of the crosslinking agent both the crosslinked density (CD) and the viscosity of TPVs increase, which can have a negative impact on their processability [2,17,27]. Although the rigidity of the rubber particles increases with CD, it decreases the deformability of the system, resulting in strengthening of the rubber network in TPVs [29,39]. Moreover, an increase in the curing agent concentration could result in the formation of smaller rubber particles in TPVs, and consequently an increase in viscosity of TPVs [34]. Unbound/uncontrolled increase of viscosity typically have negative effects on the processability.

2.2 Yield Stress

TPVs contain a high amount of rubber particles dispersed in a polypropylene matrix. As such they are expected to possess a yield stress. At large deformations and shear rates, the continuous rubbery network will eventually yield and flow and possibly destruction and reformation of the network will be occurring [18,27]. Determining the yield stress is of high importance in studying the flow behavior of these materials as it can be correlated with the curing degree, percentage of curing agent and level of particle dispersion (quality control). Li et al. [24] reported that the higher rubber content results in higher modulus, viscosity and yield stress in PP/EPDM TPVs.

2.2.1 Ways of obtaining yield stress

There are different ways of measuring and calculating yield stress such as fitting models to their flow curve (shear stress versus shear rate), creep test experiments, oscillatory amplitude sweep, as well as strain recovery experiments [40]. Among them, fitting of the flow curve and oscillatory amplitude sweep are the most common. Examples on yield determination are given below.

To determine the yield stress using flow curve, the experimental data are fitted by an equation and yield stress would be the extrapolation of shear stress at diminishingly values of the shear rate (**Figure 2-1**). On the other hand, calculating yield stress based on oscillatory amplitude sweep can be done via two methods. First, the stress that the material starts deviating from linear viscoelastic behavior that represents the point where initial plastic deformations are forming. Second, stress related to the crossover of storage and loss moduli can also be used particularly when the loss

modulus exhibits a maximum which indicated the occurrence of flow. The crossover could be related to yield stress since it points out to a strain above which loss modulus gets a higher value than storage modulus; therefore, dissipation or fluid like behavior surpasses solid like behavior. It is noted that this point should be considered as yield stress with caution because the definition of G' and G'' is only valid in linear viscoelastic region. However the crossover is definitely in the non-linear region [40]. Both methods are presented in **Figure 2-2**. One way to define the onset of non-linearity initiation is to find a point where the storage modulus drops to 90% of its limiting (plateau) value [41]. Using the strain related to this point and stress-strain curve, the yield stress can be calculated.

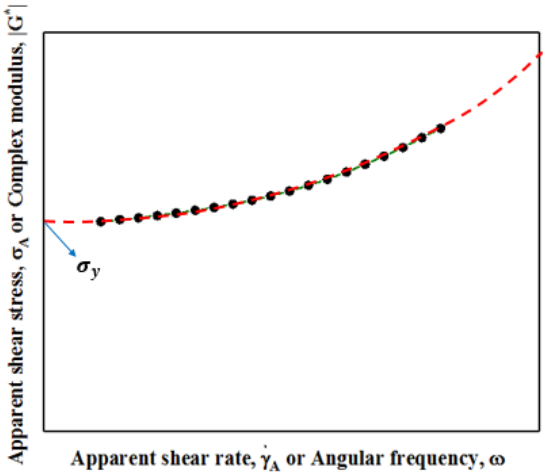

Figure 2-1. Typical flow curve of a yield stress fluid showing the extrapolation to shear rate equal to zero.

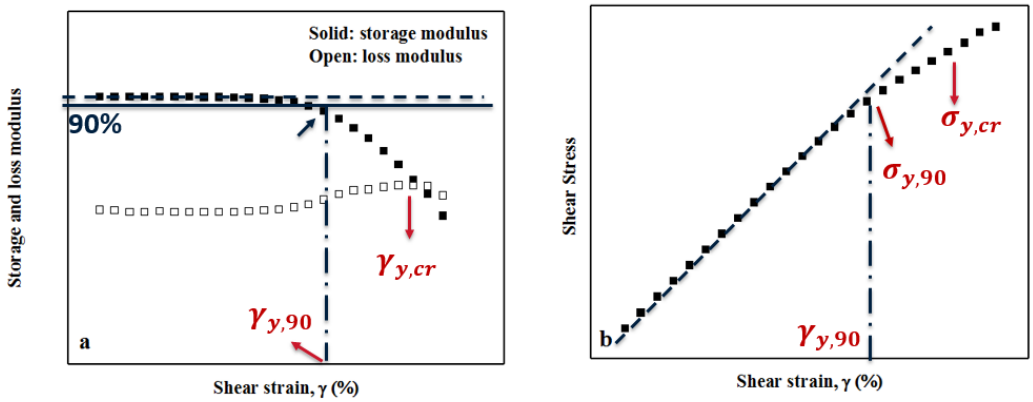

Figure 2-2. Using 90% and crossover methods to find yield stress in strain amplitude sweep test a) viscoelastic moduli vs. shear strain amplitude, and b) Stress vs. shear strain amplitude obtained from the same test. (Typically, these curves are plotted in a log-log scale)

The flow curves can be obtained using both capillary and modular compact rheometers. However, since TPVs show wall slip due to the presence of strong rubber network, determining the yield stress from flow curves from capillary rheometry might not be of high accuracy.

Yield stress in simple shear flow field has been well characterized [40,42,43]. However, polymeric materials experience complex flow fields including elongational components in many real processes such as extrusion, squeezing, blade coating, etc. where the material undergoes a shrinkage in one direction while being extended in the perpendicular direction [44]. Therefore, studying the extensional yield stress would be extremely helpful to understand the behavior of yield stress fluids in these flow fields.

2.3 Slip Velocity

Due to the presence of oil and rubbery phase these systems are expected to exhibit wall slip phenomena. It has been reported that molten linear polymers such as polyethylene, and elastomers slip no matter how small the applied shear stresses are. In addition slip velocity increases with increase of temperature, decrease of molecular weight and polydispersity [45,46].

A review of wall slip phenomena in polymers can be found in [45]. Ebrahimi [47] has explained different methods for analyzing experimental data to determine the wall slip of polymers in detail. A common method to determine slip velocity is based on the gap dependence measurements of flow curves in simple geometries (parallel plate and capillary), known as Mooney method [48]. In this method, the flow curves at different gaps are determined experimentally and if there is a gap dependence **Figure 2-3-a**, the experimental data from simple shear flow can be analyzed based on Equation 2-1, which can be easily derived by using the velocity profiles under slip and no-slip depicted in **Figure 2-4**.

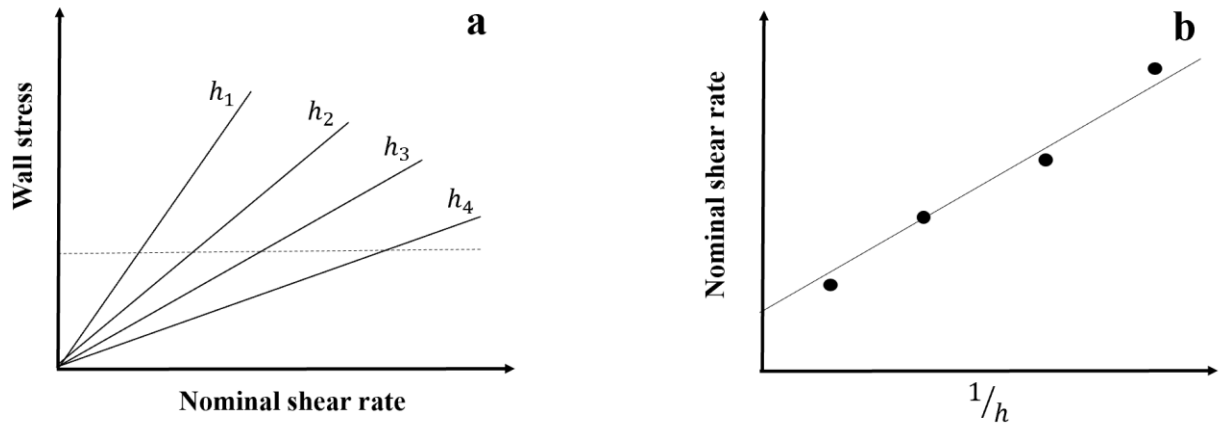

Figure 2-3. Depiction of Mooney method a) flow curve at different gaps, and b) nominal shear rate vs. $\frac{1}{h}$ at a specific wall stress.

$$\dot{\gamma}_{nR} = \dot{\gamma}_R + \frac{2V_s}{h} \qquad 2\text{-}1)$$

where $\dot{\gamma}_{nR}$ and $\dot{\gamma}_R$ are nominal and true shear rates at the edge of the disk, respectively, V_s is slip velocity and h is the gap between the plates. At a fixed shear stress value, the $\dot{\gamma}_{nR}$ is plotted versus 1/h, with the slope of the line to be equal to 2Vs (**Figure 2-3-b**). The procedure is repeated for several wall shear stress values to result the functional dependence of slip velocity on wall shear stress.

Figure 2-4. Velocity profiles in simple shear flow under no-slip and slip boundary conditions.

The slip velocity in pressure driven capillary flows (**Figure 2-5**) can be calculated from Eq. 2-2

$$\dot{\gamma}_A = \dot{\gamma}_{A,S} + \frac{4V_s}{R} = \dot{\gamma}_{A,S} + \frac{8V_s}{D} \qquad 2\text{-}2)$$

where $\dot{\gamma}_A$, and $\dot{\gamma}_{A,S}$ are the apparent shear rate and apparent shear rate corrected for the effect of slip, respectively, R is the radius and D is the diameter of the capillary die [47]. Similar to simple shear, at a fixed shear stress value the apparent shear rate $\dot{\gamma}_A$ is plotted versus 1/D, with the slope of the line to be equal to 8Vs. The procedure is repeated for several wall shear stress values to result the functional dependence of slip velocity on wall shear stress.

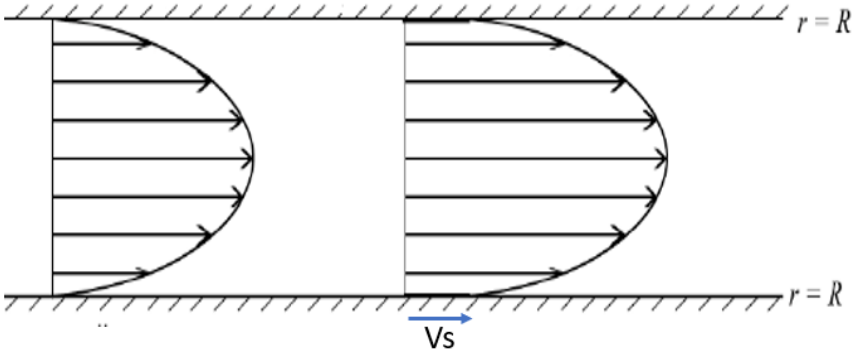

Figure 2-5. Velocity profiles in capillary flow under no-slip and slip boundary conditions.

Another method to determine slip velocity is based on the deviation of flow curve from LVE [45]. A similar approach to the gap dependency is used here, as well (**Figure 2-6**), which means that at a specific shear stress, the slip velocity is obtained from Eq. 2-3

$$8V_s = (\dot{\gamma}_A - \dot{\gamma}_{A,S}).D \qquad 2\text{-}3)$$

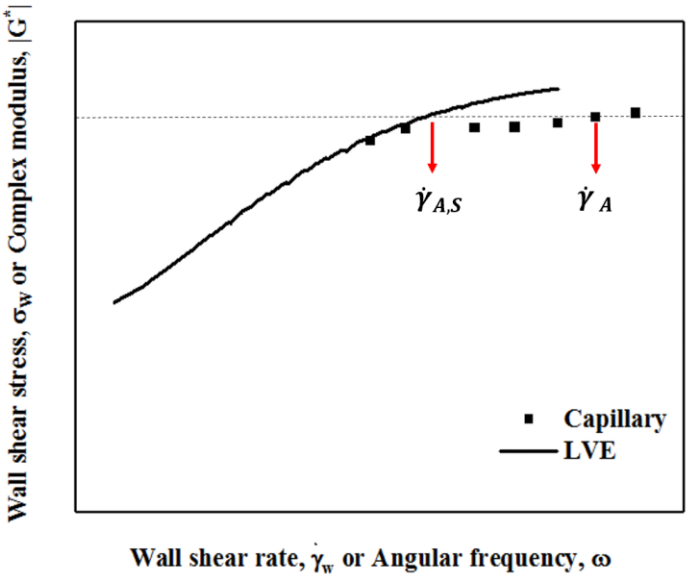

Figure 2-6. Flow curve deviation from LVE which can be used to calculate slip velocity.

2.4 Melt Fracture

During the extrusion of most polymers when the wall shear stress exceeds a critical value, melt fracture phenomena, such as sharkskin (small amplitude periodic distortions occurring on the surface of the melt), stick-slip or oscillating melt fracture and gross melt fracture (GMF) (large amplitude/ chaotic distortions affecting the whole volume of the melt), have been known to occur [49,50]. **Figure 2-7** shows images for the various types of melt fracture. Typically, by increasing shear rate, extrudate shows smooth surface, sharkskin, stick-slip, and gross melt fracture respectively (**Figure 2-7**).

Sharkskin is of great importance as it is the first instability that occurs and thus the first problem to be addressed. This periodic distortion that is only limited to the surface of the extrudate, is a function of die geometry, temperature, and molecular structure [49]. Stick-slip instability is characterized by oscillation in the pressure or shear rate in controlled throughput capillary extrusion. It can also be observed on the extrudate surface as alternating rough and smooth regions resulting from the transition from weak to strong slip condition. It can be also distinguished from a plateau or discontinuity (a transition zone) in the flow curve (**Figure 2-8**). Typically, stick-slip instability occurs at shear rates above sharkskin and below gross melt fracture. However, there are cases in which gross melt fracture happens at shear rates below stick-slip melt fracture. Stick-slip is dependent on capillary length, capillary length-to-diameter ratio, die temperature, molecular weight, and molecular weight distribution.

GMF is a profound chaotic distortion that involves the whole cross section of the extrudate. Therefore, it is frequently referred to as “volume melt fracture” as opposed to sharkskin which is a “surface melt fracture”. GMF is a result of severe instability of the melt at the entrance of a converging die while sharkskin forms at the die exit. Although helical melt fracture is a type of GMF, sharkskin can also cause a helical distortion that is limited to the surface. Since sharkskin occurs at shear rates lower that GMF, it is an important issue as it restricts the production rate and needs to be first addressed [49].

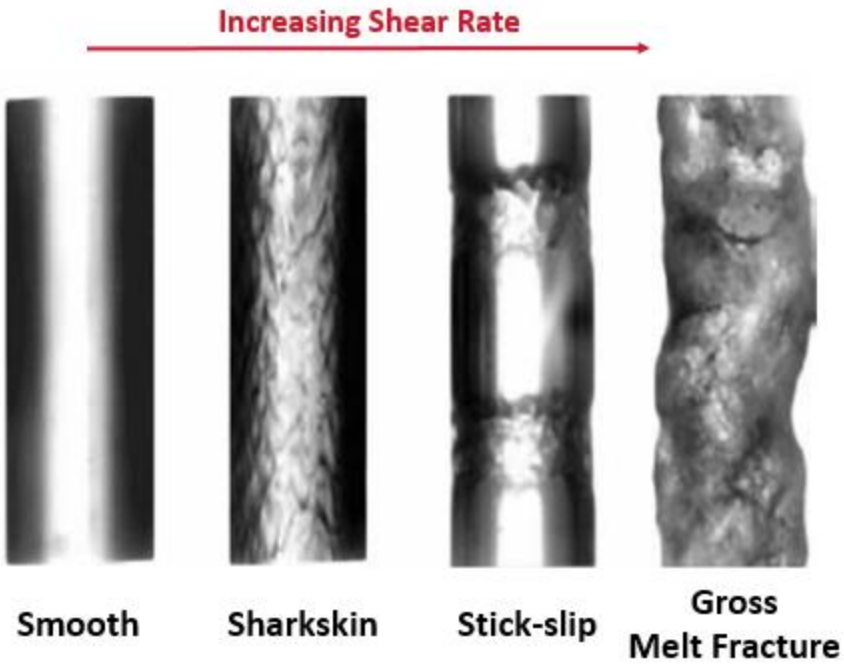

Figure 2-7. Various types of melt fracture. Adopted from [49].

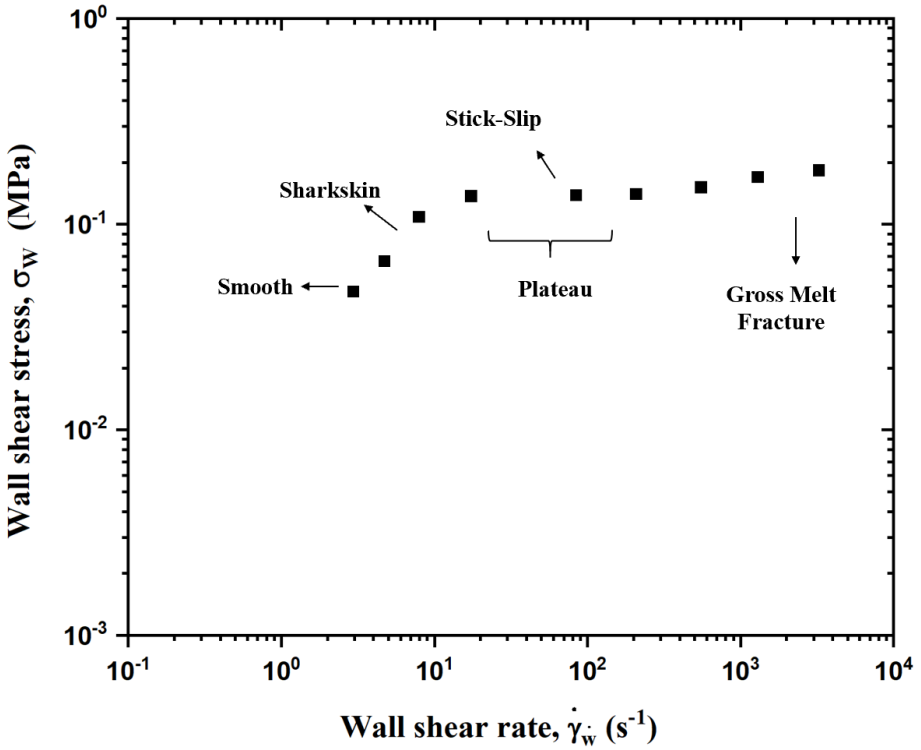

Figure 2-8. Typical extrudate instability occurrence on a flow curve

These phenomena can be problematic in the processing of polymers by setting an upper limit to the throughput applied during extrusion. PPs and EPDMs (basic constituents of TPVs) exhibit these phenomena. Many reports exist in the literature for PPs [35,36] and EPDMs [51,52]. However, very few studies exist on the TPV melt fracture in the literature. Most of these studies are not systematic as they do not address explicitly the role of the molecular characteristics of constituent polymers of TPVs, their relative composition, curing degree and temperature. The single study by Wu et.al. [53] on TPV melt fracture reported that by increasing the time of TPV extrusion via performing the extrusion twice, also with increasing the extrusion temperature and time, smoother extrudate surfaces are achieved.

2.5 Knowledge Gap

PP/EPDM TPVs have been investigated in both industry and academia to a certain extend. There are several studies specifically on linear [5,6,11,23,54] and nonlinear [9,55] rheological properties, studying mainly the effects of various parameters such as the amount of processing oil, curing level and composition, and molecular architecture of constituent polymers on TPVs' microstructure and properties. To the best of my knowledge, there is no study on the influence of microstructure and molecular architecture on both linear and non-linear rheological properties of TPVs in both shear and extension. For instance, how yield stress values determined in shear manifest themselves in extension.

While the rheology of TPVs in drag shear flow has been studied to a certain extent, their flow behavior in pressure driven flows needs further attention [24,56]. The presence of oil and rubbery phase causes TPV systems to exhibit wall slip phenomena [45,46]. Such studies on the wall slip phenomena of TPVs during their flow in contact with solid walls do not exist. It is extremely useful to derive slip velocity relationships for these systems in modeling TPV extrusion for process optimization.

Moreover, these highly elastic systems exhibit melt fracture phenomena that manifest themselves as distortions on the surface of extruded TPV samples [53]. While several melt fracture studies exist for polymer melts such as polyethylenes [57–59], polypropylenes [60,61], polystyrenes [62], polydimethylosiloxanes [63], polylactides and polycaprolactones [64–66], fluoropolymers [67],

polybutylenes [68], ionomers [69] as well as polymer blends and composites [70–73], specific studies focused on TPVs are rare.

To wrap it up, as rheological properties of TPVs determine their processability, there is an evident need to have a deep understanding of rheological behavior of TPVs to reduce their significant processing flaw in the industry which is melt fracture. Therefore, the three main elements of the present thesis, is (i) a systematic rheological study of a series of TPVs having different compositions including determination of yield stress (ii) study of the slip behavior of TPVs in simple shear and pressure driven drag flows (iii) a comprehensive study of the instabilities of TPVs in capillary flow. The objectives of this PhD thesis are discussed in detail in the next chapter.

3 Objectives and Thesis Organization

3.1 Research Objectives

This work is essentially aiming to use rheology as a powerful tool to completely understand the flow behavior of TPVs and subsequently reduce or eliminate TPVs' processing troubles originated from flow instabilities. The main objective of this work is to perform a thorough systematic study on the linear and non-linear rheological behavior of TPVs, determine the main parameters affecting their flow instabilities and correlate rheological parameters to their processability as this can be reflected from the occurrence of flow instabilities such as melt fracture. The main question to answer is how to optimize the formulation of TPVs to avoid and/or postpone flow instabilities such as melt fracture (distortions on the surface of final products) to higher rates of production.

In more detail, the following objectives of this PhD study are:

1 To perform a thorough rheological characterization of several TPVs and the critical parameters that affect both their linear and nonlinear (shear and extensional) rheology. The rheology of TPVs will be compared with that of their constituent components, namely the uncured EPDM and PP.

2 To determine and draw relationships between the yield stress values in shear and extension and see how the yield stress values determined in shear (easily observed) manifest themselves in extension (never studied and observed before).

3 To study the effect of the degree of curing and plastic/rubber (P/R) ratio on the rheological properties of TPVs in relation to the rheology of their main constituents, PP and EPDM

4 To study the wall slip of TPVs in simple shear and capillary flow relative to the slip behavior of their constituent individual components (PP and EPDM).

5 To model the rheological behavior of PPs, EPDMs, and TPVs using the integral constitutive relationship of K-BKZ

6 To study the melt fracture behavior of several TPVs as a function of shear rate, temperature, molecular characteristics of constituent polymers, degree of curing, and concentration of

filler will be studied relative to the melt fracture of their individual components (PP and EPDM).

7 To develop interrelationships between the rheological properties (yield stress) and processability.

3.2 Thesis Organization

The organization of this dissertation is as follows. A brief introduction of thermoplastic vulcanizates (TPVs), their properties and fabrication mechanism is presented in Chapter 1. In Chapter 2 a literature review on the structural and processing parameters affecting TPVs' rheological and processing properties is discussed. The research objectives and thesis organization are presented in Chapter 3. In Chapter 4, the materials used in this study are presented, their composition and their method of fabrication. Details of the apparatuses used in this study, including a rotational rheometer (AntonPaar MCR 502 or AntonPaar MCR 702 equipped with cone-and-plate or parallel-plate geometry and partitioned plate fixture), a capillary rheometer (Instron), an Olympus MIC-D digital microscope (to take images of the polymer samples extruded) are also presented in Chapter 4. The experimental methodology associated with these experimental techniques is also described.

Chapter 5 is focused on the linear rheological properties of TPVs and their constituent polymers used in their fabrication. Use of the K-BKZ model to model the rheological properties is also presented. The yield stresses of these materials were determined in both shear and extensional flows (objectives 1, 2, and 3). This chapter is based on a published paper (N. Ghahramani, K. Iyer, A.K. Doufas and S.G. Hatzikiriakos, "Rheology of Thermoplastic Vulcanizates (TPVs)," J. Rheology, **64,** 1325-1341 (2020)

Chapter 6 presents the non-linear rheological behavior of TPVs behavior in shear and extensional flow fields. The K-BKZ constitute model is considered to model their rheological behavior including the inclusion of yield stress and wall slip (objectives 4, 5). This chapter is based on a paper recently submitted to Physics of Fluids.

Finally, in Chapter 7 the wall slip and melt fracture of TPVs are investigated in order to gain a better understanding of TPVs' processing. Relationships between yield stress and extensional

rheological properties with the processability of these polymers are also presented and discussed. The flow instabilities (melt fracture) are also studied in capillary extrusion and detailed images are presented to identify and illustrate these instabilities. (Objectives 6 and 7). This thesis is concluded in Chapter 8 where recommendations for future work are also presented.

4 Materials and Experimental Methods

4.1 Materials

Two different polypropylenes (PPs, one linear labelled as L-PP and one branched labelled as B-PP) and two ethylene propylene diene monomer rubbers (EPDMs, one linear labelled as L-EPDM and one branched labelled as B-EPDM) were obtained from ExxonMobil Chem., Co. (Baytown, TX, USA) listed in **Table 4-1**, which are the main constituents of the fabricated TPVs listed in **Table 4-2**. **Table 4-1** lists the molecular characteristics of the basic constituent resins, including the weight molecular weight M_w, Polydispersity Index (PDI), and the degree of long chain branching (LCB-g'). Both EPDMs contain oil (L-EPDM: 42.9 wt. %, B-EPDM: 50 wt.%).

Table 4-1. Polymers that are the main constituents of the TPVs studied in the present work and their molecular characteristics.

Sample*	M_w (kg/mol)	PDI	LCB-g'	Activation energy, E_a (kJ/mol)	Vertical shift factor (b_T)
L-PP (linear)	562	7.5	1.00	18.5	1.00 to 1.08
B-PP (branched)	540	19	0.86	26.5	1.00 to 1.25
L-EPDM (linear)	610	2.5	1.00	13.9	1.00 to 1.05
B-EPDM (branched)	509	4	0.87	15.5	0.97 to 1.00

Table 4-2 list the various TPVs and their compositions examined in this work. These materials were also obtained from ExxonMobil for this study. **Table 4-2** specifies two groups of TPVs. The main difference is that TPVs in Group A (PP: 27.5 wt. %, EPDM: 72.5 wt. %) contain a higher % wt. of crosslinked rubber and higher % wt. of PP compared to those of Group B (PP: 35 wt. %, EPDM : 65 wt. %). As such, TPVs of Group B have higher hardness (70-75 Shore A) relative to the TPVs of Group A (60-65 Shore A). As also seen the level of curing or curing degree varies as an important factor to be studied in the present work. The amount of EPDM used in all TPVs was

more than 50wt% in PP/EPDM blends, which will be evident from the linear viscoelastic properties of these polymers [1,27]. This set of TPVs are mostly commercial.

A new series of TPVs has been prepared by ExxonMobil where the composition has been varied in a more systematic way (**Table 4-3**). The rheological study of these series can shed light into the relative effects of various parameters related to their composition.

Table 4-2. Characteristics of TPVs used in this study (commercial polymers).

Sample		PP-Type	EPDM-Type	Cure level
(Group A)	TPV1	B-PP	L-EPDM	High
	TPV2	L-PP	L-EPDM	High
	TPV3	L-PP	L-EPDM	Normal
	TPV4	L-PP	B-EPDM	Normal
(Group B)	TPV5	B-PP	L-EPDM	High
	TPV6	L-PP	L-EPDM	High
	TPV7	L-PP	L-EPDM	Normal
	TPV8	L-PP	B-EPDM	Normal

Table 4-3. Characteristics of TPVs whose composition is varied systematically.

Formulation (phr)	B-EPDM	L-EPDM	L-PP	B-PP	filler	oil	curative	accelerative	total
S1	175.00	-	45.30	-	44.00	66.75	5.00	1.11	337.16
S2	175.00	-	45.00	-	44.00	65.00	7.50	1.67	338.17
S3	175.00	-	44.54	-	44.00	62.38	11.25	2.51	339.68
S4	175.00	-	-	45.30	44.00	66.75	5.00	1.11	337.16
S5	175.00	-	-	45.00	44.00	65.00	7.50	1.67	338.17
S6	175.00	-	-	44.54	44.00	62.38	11.25	2.51	339.68
S7	-	200.00	45.30	-	44.00	41.75	5.00	1.11	337.16
S8	-	200.00	45.00	-	44.00	40.00	7.50	1.67	338.17
S9	-	200.00	44.54	-	44.00	37.38	11.25	2.51	339.68
S10	-	200.00	-	45.30	44.00	41.75	5.00	1.11	337.16
S11	-	200.00	-	45.00	44.00	40.00	7.50	1.67	338.17
S12	-	200.00	-	44.54	44.00	37.38	11.25	2.51	339.68

*All samples are cured using a phenolic resin with the amounts listed in the table

**Acid chloride salts are used as accelerator

4.2 TPVs Sample Preparation

ExxonMobil Co. prepared all TPV samples used in this work. The procedure of sample preparation is as follows:

EPDM was fed into the feed throat of an extruder. The thermoplastic resin (polypropylene) was also fed into the feed throat along with other reaction rate control agents such as zinc oxide and stannous chloride. Fillers, such as clay and carbon black, were also added into the extruder feed throat. Process oil was injected into the extruder at two different locations along the extruder. The curative was injected into the extruder after the rubber, thermoplastics and fillers commenced blending. The second process oil (post-cure oil) was injected into the extruder after the curative injection. Rubber crosslinking reactions were initiated and controlled by balancing a combination of viscous heat generation due to application of shear, barrel temperature set point, use of catalysts, and residence time. The extrusion mixing was carried out at 325 revolutions per minute (RPM). A barrel metal temperature profile in °C, ranging from barrel section near feed throat down towards the die was maintained at 160 to180 °C (wherein the last value is for the die) was used.

The TPV samples were cut to fit into an atomic force microscope (AFM) sample holder (Leica) and then cryo-microtomed in the desired plane at -120 °C using a Leica Ultramicrotome. All samples were dried in a desiccator before AFM imaging. The AFM images were collected using a Bruker Dimension Icon AFM. The scans were acquired with a cantilever of spring constant of 42 N/m, and resonance frequency of ~320 kHz. The data channels monitored were height and phase. **Figure 4-1** below presents typical TPV morphologies of two of the TPVs examined in this work indicating bi-continuous morphology with typical domain sizes of the order $\sim 1\mu m$.

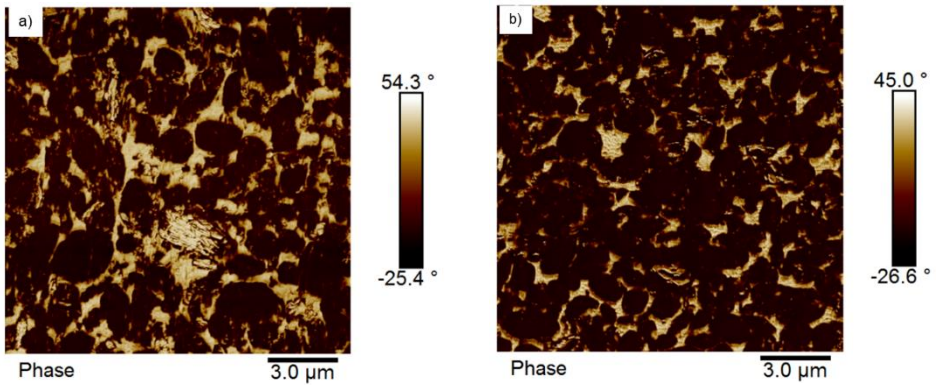

Figure 4-1. Representative AFM micrographs showing the morphology in two TPV samples: a) TPV1 and b) TPV4

4.3 Rheological Measurements

4.3.1 Rotational rheometer

A rotational rheometer (Anton Paar, MCR-501) with parallel-plate geometry is used to study the linear viscoelastic (LVE) properties of the polymers listed in **Table 4-1** to **4-3**. The following tests are performed to study their rheological response. First frequency sweep tests are carried out at different temperature ranges depending on the polymer (190-220^{o}C for PP, 130-210^{o}C for EPDMs, 190-220^{o}C for TPVs). Maximum temperature for EPDMs is slightly lower to avoid ant degradation or crosslinking at high temperatures. Then master curves of the linear viscoelastic moduli are constructed using the time-Temperature Superposition (tTS) principle and the results are presented at the reference temperature of T_{ref}=190^{o}C.

The Anton Paar MCR 702 rheometer equipped with a cone partitioned-plate geometry (**Figure 4-2-a**) is used for experiments in the nonlinear viscoelastic region, such as stress relaxation and start-up of steady shear of pure componentsand TPVs. Using the partitioned plate geometry, significantly reduces the edge fracture which occurs during non-linear measurements using regular geometries [74].

Uniaxial extensional experiments are conducted at various temperatures same with those used in shear) using the second generation Sentmanat Extensional Rheometer (SER2) fixture, **Figure 4-2-b**. Specimen of these polymers are prepared as films with a thickness of about 0.6 mm (PPs and EPDMs) and 0.3 mm (TPVs), respectively. Various Hencky strain rates are used in the range of 0.1 to 5 s^{-1} for pure components and 0.001-0.5 s^{-1} for TPVs.

4.3.2 Capillary rheometer

An Instron pressure driven constant-speed capillary rheometer, **Figure 4-3**, is used to study the effect the wall slip of TPVs in capillary flow and compare it with that obtained from rotational rheometry (Anton Paar MCR-702). This comparison will address the consistence of slip measurements. Two capillary dies of different diameter, D (0.43 mm and 0.89mm) and fixed length-to-diameter ratio, L/D=33 to keep the pressure approximately constant at a given shear stress value, are used to study the slip behavior of basic constituent polymers and TPVs. Capillary dies of fixed diameter (D = 0.89 mm) and various L/D (4, 14 and 33) are used to identify and apply

the end pressure correction to the experimental data in order to determine the true flow curves of PPs, EPDMs and TPVs. An Olympus MIC-D digital microscope is used for taking various images of the collected extrudate samples.

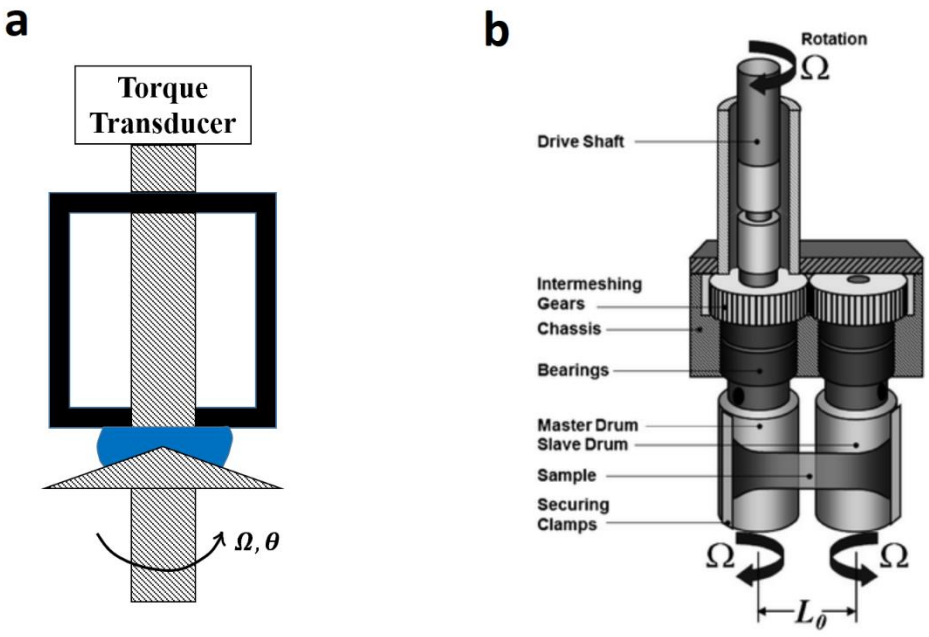

Figure 4-2. Schematics of the a) rotational rheometer equipped with the cone partitioned-plate and b) uniaxial extensional fixture that is used in conjunction with a rotational rheometer.

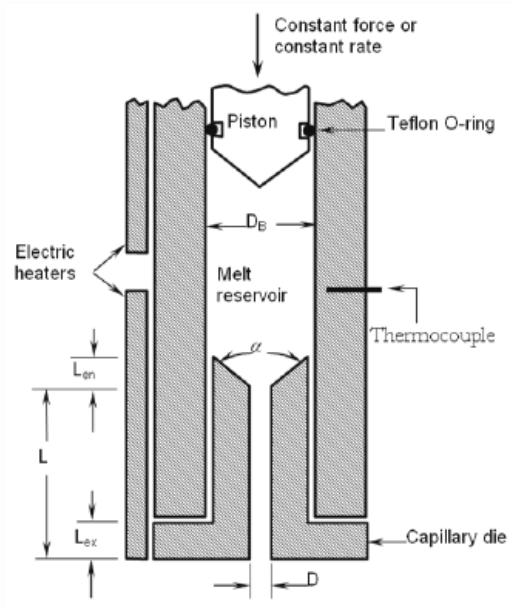

Figure 4-3. Schematic representation of the capillary rheometer.

5 Rheology of Thermoplastic Vulcanizates (TPVs)

In this chapter, the rheology of several TPVs is studied with focus on their linear viscoelasticity. The rheological behavior of their base components, namely, PP and EPDM is also performed in detail. The effects of long chain branching of the primary constituents (prior to crosslinking), the level of curing, and the amount of crosslinked rubber on their rheology are studied in detail and found to affect the rheology to various degrees. The rheology of TPVs in relation to their base polymers is also discussed in detail. The rheological data are modeled by using an integral constitutive equation, known as the K-BKZ model which is presented next.

5.1 Theoretical Background

The K-BKZ constitutive model proposed by Wagner [75] and modified by Luo and Tanner [76] was used to model the rheology of individual TPV constituents (PP and EPDM):

$$\bar{\bar{\tau}} = \frac{1}{1-\theta}\int_{-\infty}^{t}\sum_{k=1}^{N}\frac{G_k}{\lambda_k}exp\left(-\frac{t-t'}{\lambda_k}\right)exp\left[-n\left(\beta I_{C_t^{-1}} + (1-\beta)I_{C_t} - 3\right)^{\frac{1}{2}}\right][C_t^{-1}(t') + \theta C_t(t')]dt' \qquad 5\text{-}1)$$

where λ_k and G_k are the relaxation times and relaxation modulus coefficients, N is the number of relaxation modes, n and β are material constants, and I_{C_t}, $I_{C_t^{-1}}$, are the first invariants of the Cauchy-Green tensor C_t and its inverse C_t^{-1}, the Finger strain tensor. The parameter n can be determined from step-strain experiments in simple shear by the determination of the single exponential Wagner damping function, $h(\gamma) = exp(-n\gamma)$, and the parameter β can be calculated from fitting uniaxial extension experiments. The material constant θ is given by

$$\frac{N_2}{N_1} = \frac{\theta}{1-\theta} \qquad 5\text{-}2)$$

where N_1 and N_2 are the first and second normal stress differences, respectively. It is noted that θ is not zero for polymer melts, which possess a non-zero second normal stress difference [38]. Its usual range is between -0.1 and -0.2 in accordance with experimental findings and numerical simulations [38,39]. Its effect on the predictions are minor [77,78].

The relaxation modulus (Maxwell model) $G(t) = G_k\, exp(-(t-t')/\lambda_k)$ is suitable for the modeling of the individual constituent polymers (PPs and EPDMs) as presented and discussed

below. However, a much simple power–law form is suitable for the relaxation modulus of TPVs, nearly universal for all TPVs (discussed below in detail and used for modelling the TPV rheological behavior in Chapter 6).

5.2 Results and Discussion

5.2.1 Rheology of pure polymeric constituents of TPVs

As explained above various rheological tests were performed to determine the parameters of the K-BKZ model for each polymer listed in **Table 4-1**. **Figure 5-1**- **Figure 5-4** present the rheological results for all polymers in the same order as listed in **Table 4-1**. The linear viscoelastic moduli (G' and G'') have been used to determine the relaxation moduli and relaxation times $\{G_k, \lambda_k\}$ of each polymer, the stress relaxation after the imposition of sudden strain data to determine the parameter *n* (in the damping function of Equation 5-1) and the uniaxial extensional data to determine the parameter (in the damping function of Equation 5-1). The normal stress ratio has been assumed constant and equal to -0.15 for all polymers in the absence of experimental data, although typical data for polymers melts report values between -0.2 and -0.1 [79]. As shown by Tomkovic et al. [80] the results are nearly insensitive to the value of $-N_2/N_1$ when this ratio is kept within the range of {0.1, 0.2}. The continuous lines in **Figure 5-1** - **Figure 5-4** represent the fits of the K-BKZ model. The fitted parameters in the K-BKZ model for all polymers simulated are listed in **Table 5-1**.

The main conclusions drawn from **Figure 5-1**- **Figure 5-4** are as follows: First, the linear viscoelasticity (LVE) of EPDMs are more complex compared to that of their PP counterparts as more Maxwell relaxation times are needed (typically 6 relaxation modes for PPs versus 10 relaxation modes for EPDMs). Due to their elastomeric nature, no terminal relaxation has been reached for both EPDMs; in fact, a tendency for a plateau in G' at low frequencies is observed, which is typical for elastomers. The viscosity material functions and viscoelastic moduli of EPDMs are nearly one order of magnitude higher compared to those of PPs (**Figure 5-5**). Although B-PP is branched, its complex viscosity is lower than that of L-PP throughout the angular frequency range, which is due to its lower molecular weight. The slightly higher complex viscosity of B-EPDM compared to that of L-EPDM is also due to the branched structure of B-EPDM.

However, from the practical point of view both EPDMs have similar linear viscoelastic moduli (**Figure 5-5**).

No strain hardening is observed for L-PP and L-EPDM (**Figure 5-1-d** and **Figure 5-3-d**) due to their linear molecular architecture. Unlike L-PP and L-EPDM, B-PP and B-EPDM exhibit strong strain hardening as can be observed from **Figure 5-2-d** and **Figure 5-4-d**, which is a sign of the presence of long chain branching in their structure. A stronger strain hardening is shown by B-PP compared to that of B-EPDM due to its higher degree of strain hardening (LCB-g′ values listed in **Table 4-1**). Similar conclusions can be drawn by inspecting the values of the energy of activation, E_a, listed in **Table 4-1**. First the E_a for both PPs are lower than the reported values in the literature 27-40 kJ/mol [81–83]. This might be attributed to the use of Nitrogen that avoided degradation. The activation energy, E_a, of B-PP is clearly higher than the one for L-PP due to its branched microstructure [59,84] . The E_a for L-EPDM (linear) is as low as E_a=13.9 kJ/mol. The EPDM has unsaturated covalent bonds that can react at temperatures above 145^{o}C, and therefore the activation energy is low. Typical reported values for the E_a for EPDMs vary significantly $E_a = 10 - 50$ kJ/mol [54,85,86] depending on the molecular architecture. For example, the E_a value for B-EPDM (branched) E_a=15.5 kJ/mol is higher compared to that of L-EPDM (linear) E_a=13.9 kJ/mol indicative of its long chain branching structure.

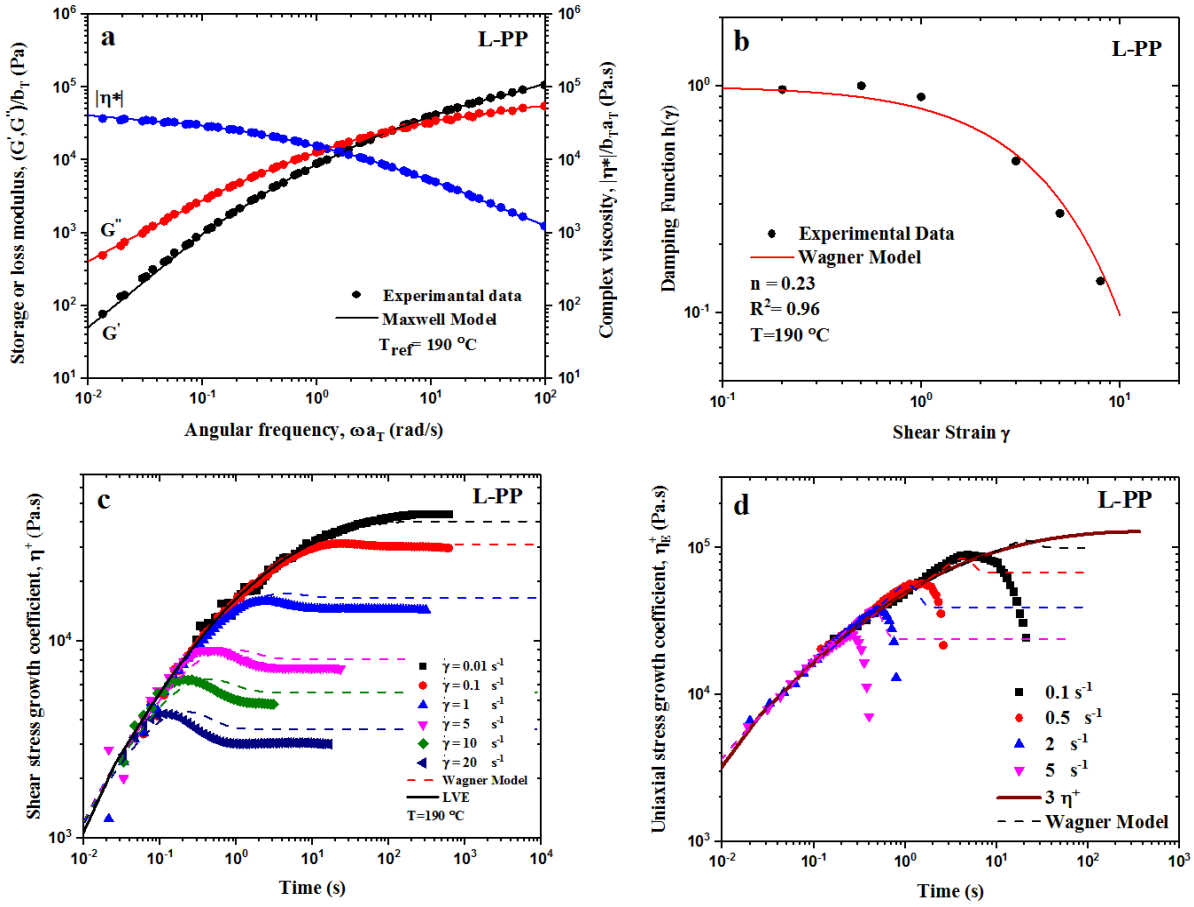

Figure 5-1. (a) The linear viscoelastic moduli G′, G″ and complex viscosity $|\eta *|$, (b) the damping function $h(\gamma)$ in shear, (c) the shear stress growth coefficient in start-up of steady shear, $\eta^+$and (d) the uniaxial tensile stress growth coefficient in start-up of uniaxial extension, η_E^+ for L-PP (**Table 4-1**) at 190°C. Continuous lines are fits of the K-BKZ/Wagner model to the experimental data with the values of the parameters listed in **Table 5-1**.

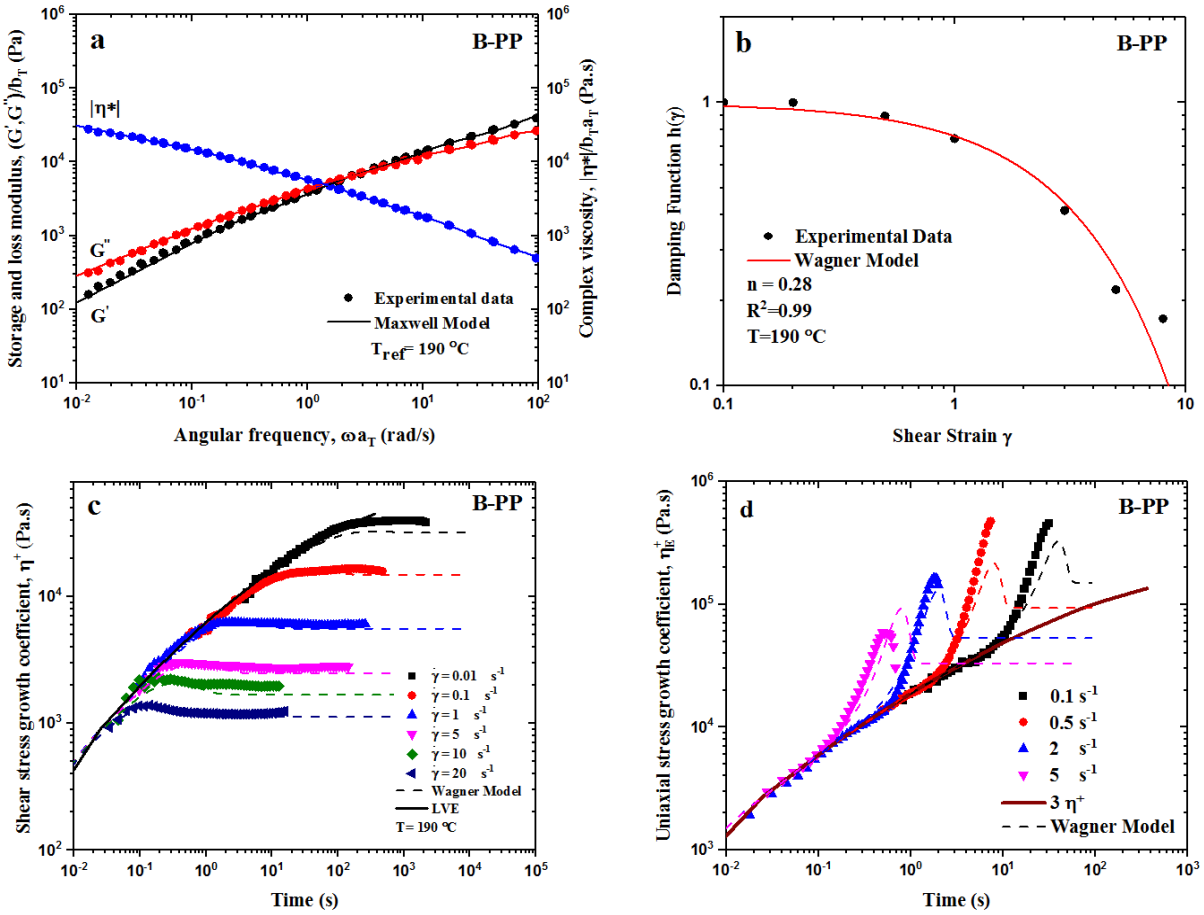

Figure 5-2. (a) The linear viscoelastic moduli G′, G″ and complex viscosity $|\eta *|$, (b) the damping function $h(\gamma)$ in shear, (c) the shear stress growth coefficient in start-up of steady shear, $\eta^{+}$and (d) the uniaxial tensile stress growth coefficient in start-up of uniaxial extension, η_E^{+} for B-PP (**Table 4-1**) at 190°C. Continuous lines are fits of the K-BKZ/Wagner model to the experimental data with the values of the parameters listed in **Table 5-1**.

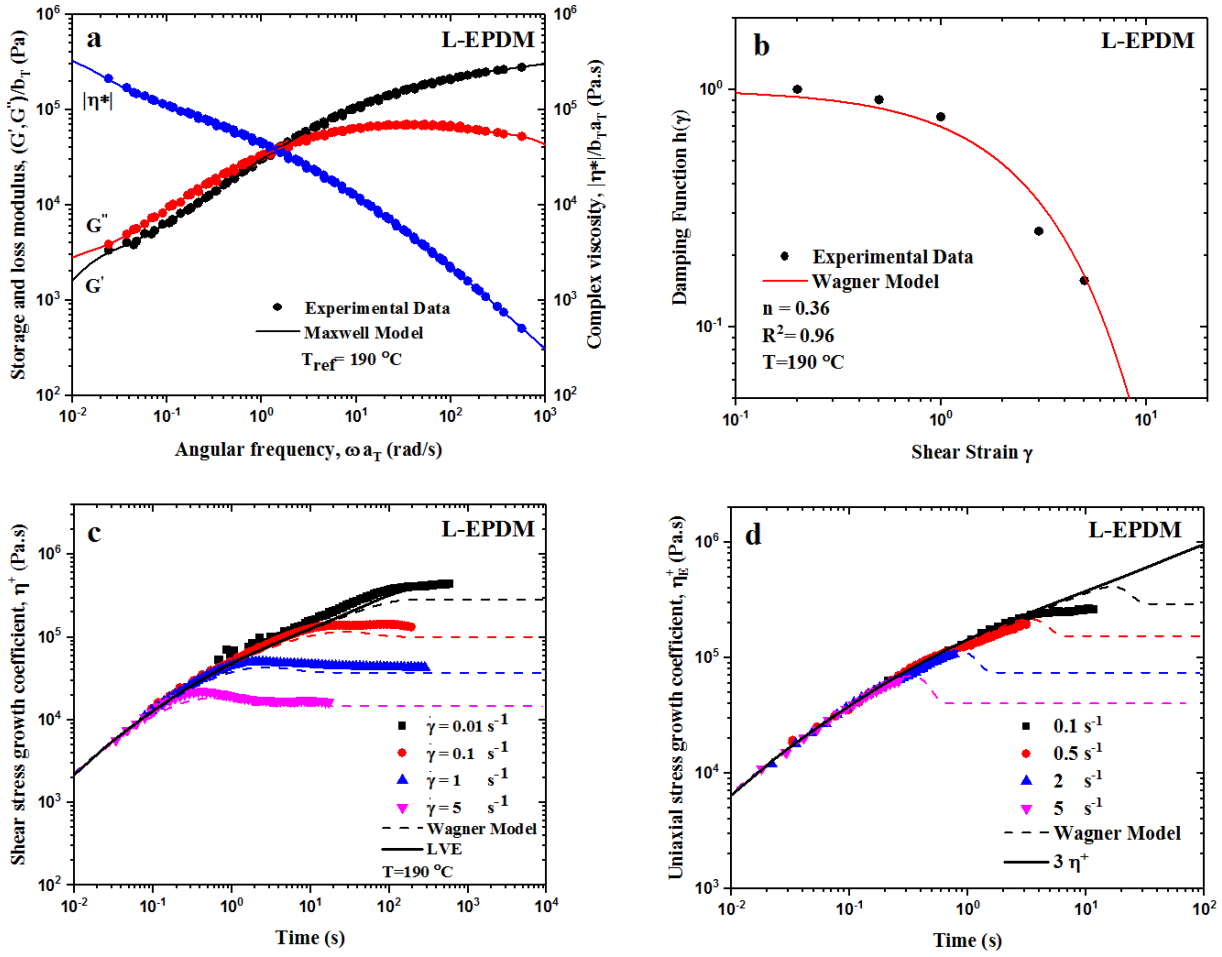

Figure 5-3. (a) The linear viscoelastic moduli G′, G′′ and complex viscosity $|\eta *|$, (b) the damping function $h(\gamma)$ in shear, (c) the shear stress growth coefficient in start-up of steady shear, $\eta^{+}$and (d) the uniaxial tensile stress growth coefficient in start-up of uniaxial extension, η_E^{+} for L-EPDM (**Table 4-1**) at 190°C. Continuous lines are fits of the K-BKZ/Wagner model to the experimental data with the values of the parameters listed in **Table 5-1**.

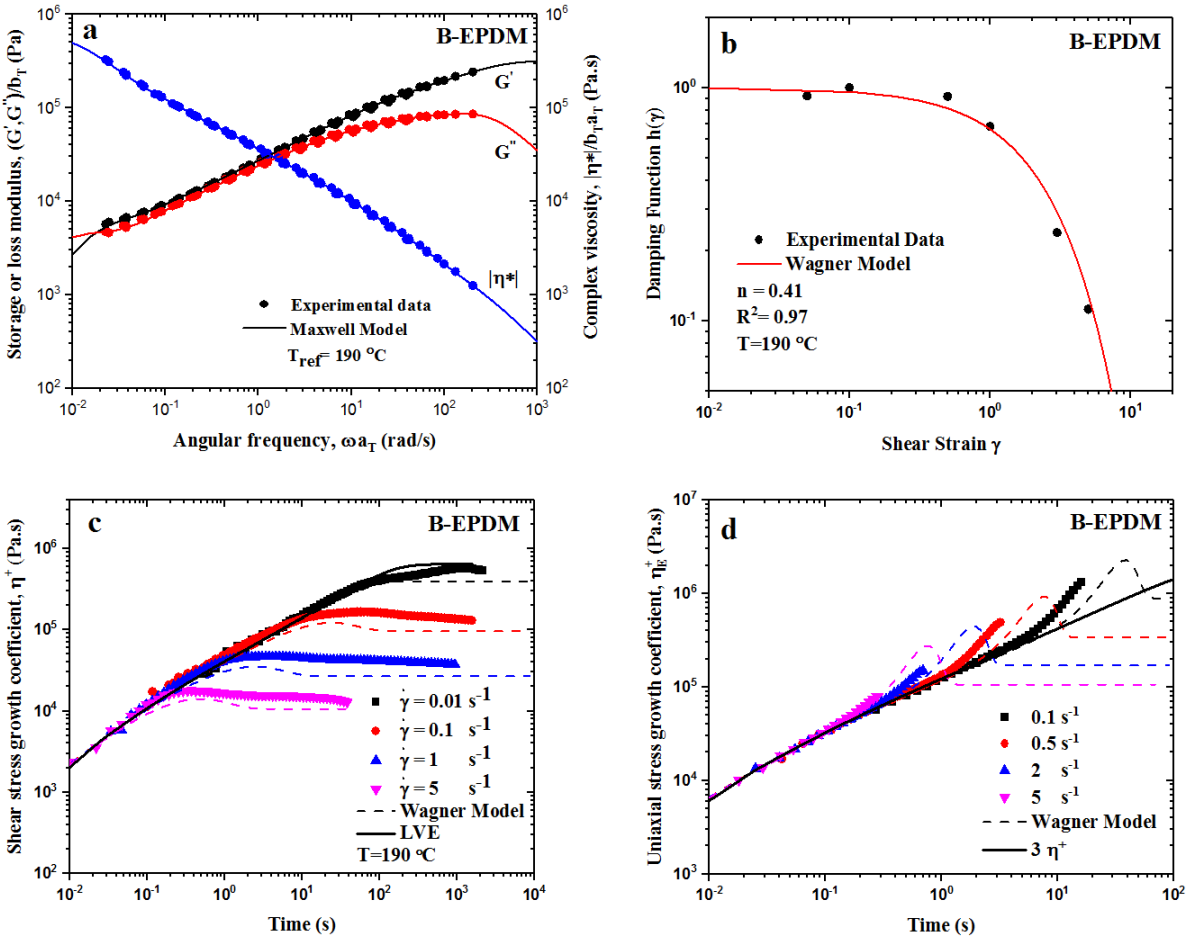

Figure 5-4. (a) The linear viscoelastic moduli G′, G″ and complex viscosity $|\eta *|$, (b) the damping function $h(\gamma)$ in shear, (c) the shear stress growth coefficient in start-up of steady shear, $\eta^{+}$and (d) the uniaxial tensile stress growth coefficient in start-up of uniaxial extension, η_E^{+} for B-EPDM (**Table 4-1**) at 190°C. Continuous lines are fits of the K-BKZ/Wagner model to the experimental data with the values of the parameters listed in **Table 5-1**.

Table 5-1. The Maxwell relaxation spectrum and nonlinear rheological parameters for the K-BKZ/Wagner model (Eq.4) of all polymers listed in **Table 4-1** at T_{ref} = 190°C.

Relaxation time λ_k(s)	**Relaxation modulus G_k (Pa)**	**Relaxation time λ_k(s)**	**Relaxation modulus G_k (Pa)**
Sample L-PP		**Sample B-PP**	
0.009	95201	0.009	49263
0.070	40786	0.087	14008
0.373	19552	0.656	5294
1.971	5990	5.058	1565
10.370	1144	39.18	402
58.840	139	350.3	71
n=0.23, β =1, θ = -0.15		n=0.28, β =0.02, θ = -0.15	
Sample L-EPDM		**Sample B-EPDM**	
0.177	34512	0.818	5196
0.008	60070	0.016	70989
0.820	18848	85.13	6422
9.007	4986	8.536	5863
2.357	11990	0.327	17403
0.379	22222	2.281	8772
0.025	53037	0.056	50479
0.0705	48082	0.818	8117
0.001	69134	0.004	123397
91.240	3486	0.157	26516
n=0.36, β =1, θ =-0.15		n=0.41, β =0, θ =-0.15	

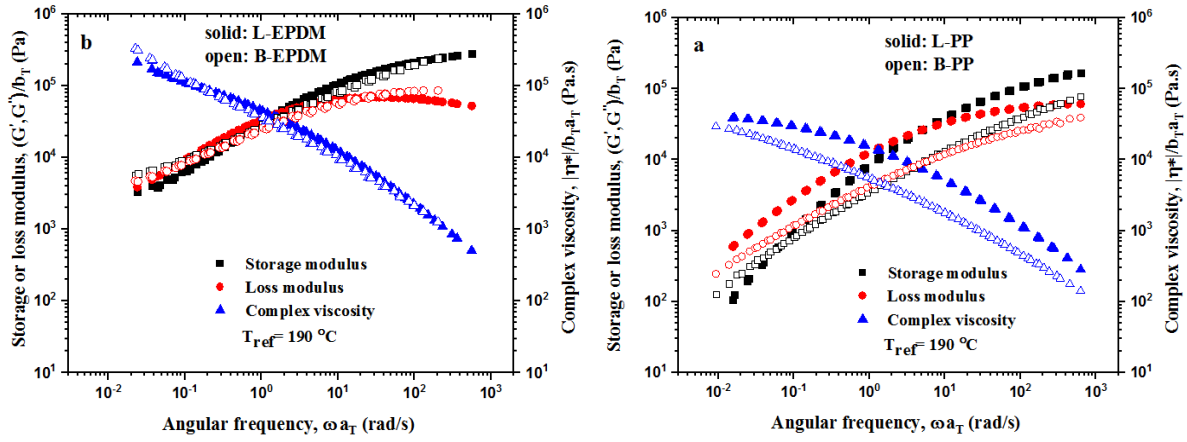

Figure 5-5. Comparison of the viscoelastic moduli of the two PPs and the two EPDMs listed in **Table 4-1** at T_{ref}=190°C. Note the much higher material functions of L-PP(linear) compared to B-PP (branched) and the similar material functions of the two EPDMs. It is also noted that EPDMs have in general material functions about 1 order of magnitude greater than those of PPs.

5.2.2 Linear viscoelasticity of TPVs

As discussed above the linear viscoelastic behavior of all TPVs listed in **Table 4-2** was studied in detail and compared to that of their basic constituents. The results are presented in this section.

Strain sweep: Figure 5-6 presents strain sweep results for TPV8 at three different temperatures using a frequency of 0.1 Hz. As seen, the temperature does not have a significant effect on the elastic response, G′ (same observation for all TPVs examined). While G′′ decreases with increase of temperature as expected, a small increase of G′ has been observed with increase of temperature (counterintuitive observation). The elastic modulus G′ of TPV is possibly dominated by the presence of rubber (entropic effect) giving rise to this small increase which has been universally observed for all TPVs. The effect of temperature is more significant on the viscous response of the material, G′′. In fact, the G′′ exhibits a maximum, which is related to the onset of flow/shear melting (increase of viscous response), although flow should have been initiated at the point where G′′ starts increasing [87]. The existence of this maximum is an indication of the existence of yield stress. In fact a sequence of processes start at the point where G′′ starts increasing (increase of dissipation implying flow initiation) that is also the point where the stress ($|G*|$)-strain γ relationship deviates from linearity [43,87,88]. This is where destruction (yielding) of the rubber network starts and reconstruction due to the movement of matrix (PP) and thus the maximum in G′′ appears [43,87–89]. Two methods to estimate the yield stress were used. The first one is the transition from linear to non-linear regime [42]. To consistently determine the limiting value of strain for linear viscoelastic response and the stress for shear yielding, σ_y, we consider the strain at which G′ drops to 90% of its linear viscoelastic value at which the strain value is defined as $\gamma_y$which we refer to as the yield strain [41] [39]. **Table 5-2** lists the yield strain,γ_y, and the related yield stress, σ_y, of different TPVs at 190°C. Typical values of $\sigma_y$are in the range from 3.6 to 7.8 kPa. TPVs 1-4 (Group A) overall possess higher yield stresses due to the relatively higher amounts of crosslinked rubber particles. In addition, the effect of curing degree renders the materials stiffer and thus they fail at a smaller stress and strain. For example, compare TPV2 with TPV3 and TPV6 with TPV7 which only differ in the level of curing. TPV3 and TPV7 fail at a higher strain and shear stress. The more crosslinked system is more likely to form stronger rubber network (more discussion below) and hence yields at a lower strain. On the other hand, the less crosslinked rubber

might form smaller domains and can result in a weaker network that is more amenable to larger strains.

Another method to determine the yield stress is using the crossover of G′ and G′′, labelled as $\sigma_{y,C}$ with values listed in **Table 5-2** (3-4 times higher). It should be mentioned that although this point is traditionally associated with yield, it must be made with caution as the definition of G′ and G" are only valid in the linear regime and the crossover point is certainly in the non-linear flow regime [40]. However, although yield stress is defined as a single point, it should be realized that the process of yield occurs over a wide range of shear stress values (distribution of values rather than a single point), where parts of the fluid yield locally at different values particularly for inhomogeneous fluids. Therefore, the two yield stress values listed in **Table 5-2** provide the range over which the yield process is initiated and completed (transition from solid-like to fluid-like behavior).

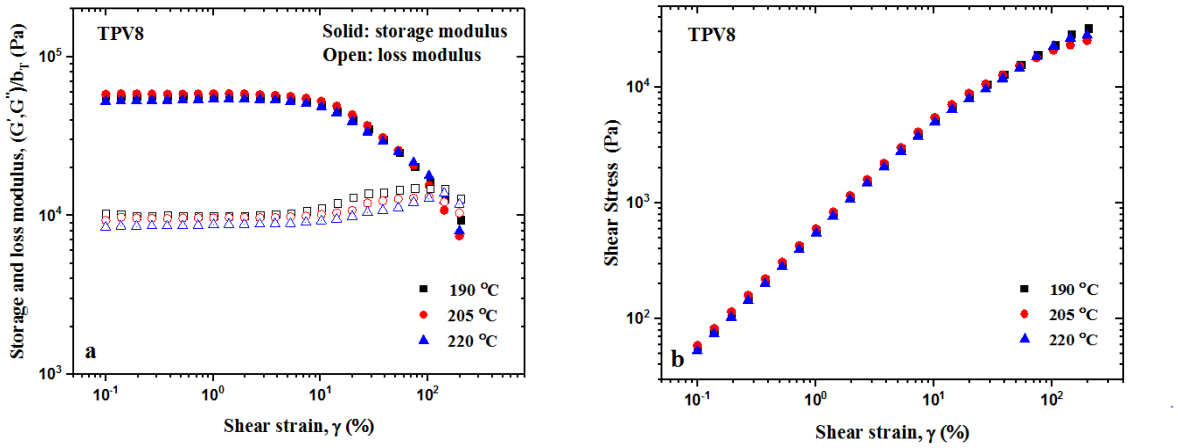

Figure 5-6. Strain sweep experiments for TPV8 at various temperatures (190-220°C) to determine the limiting values of strain for linear viscoelastic response and the stress and strain for shear yielding (flow).

Table 5-2. Yield strains and related critical yield stresses of TPVs listed in **Table 4-2** at *T*=190 ℃.

Sample	Yield strain, γ_y (%)	Yield stress, σ_y (kPa)	Yield stress at crossover, $\sigma_{y,C}$ (kPa)
TPV 1	5.3	4.6	18.5
TPV 2	7.6	6.4	15.4
TPV 3	11.3	7.8	22.5
TPV 4	8.4	4.8	18.9
TPV 5	6.0	3.6	12.3
TPV 6	7.0	5.1	22.7
TPV 7	10.4	6.0	22.7
TPV 8	8.8	4.6	25.7

5.2.3 Viscoelastic spectrum of TPVs

Several factors that influence the LVE of TPVs is examined in this section. **Figure 5-7** depicts the viscoelastic moduli of TPV2 (left) and TPV3 (right) compared with those of their constituent polymers at T_{ref}=190°C to see how the LVE response of the individual constituents of TPVs affects their LVE behavior. At higher frequencies, the TPV response is controlled by the segmental dynamics of its constituent polymers (Rouse time response) and as such the LVE moduli of TPVs are between those of their constituent polymers (closer to the response of the matrix which is the PP). However, at lower frequencies the effect of the cured EPDM interface with the matrix (PP) plays a significant role as there is no sign of terminal relaxation or tendency for relaxation. Both G′ and G″ show solid-like behavior with a small dependence on frequency (G′ much higher than G″). This is typically observed for all TPVs independent of the type of constituent polymeric components, curing degree (high or normal), and level of crosslinked rubber concentration (high in Group A or low in Group B). Considering the particle network existence in TPVs, which results in a non-terminal behavior in storage modulus (storage modulus does not take value zero when frequency is going to zero), the "simple" mode of relaxation known as power-law relaxation typically observed in the response of foods such as dough and yogurt [58-59] can be applied:

$$G' = G'_c(\omega\tau_R)^p + G'_y \ and \ G'' = G''_c(\omega\tau_R)^p \qquad 5\text{-}3)$$

Where G'_c and G''_c are the storage and loss moduli coefficients (constants), τ_R is a characteristic time in the transition zone from unyielding to yielding zone and p is the power-law coefficient indicating the dependence of $G' \ and \ G''$on frequency, ω. This characteristic time τ_R can be

calculated as the inverse frequency at which the power-law expression $G' = G'_{c,i}\omega^p = G'_y$ holds ($G'_{c,i} = G'_c\omega^p$). Based on this definition of τ_R, $G'_c = G'_y$, and Eq. 5-3 is reduced to:

$$G'/G'_y = 1 + (\omega\tau_R)^p \ and \ \ G''/G'_y = (G''_c/G'_y)(\omega\tau_R)^p \qquad 5\text{-}4)$$

The term G'_y (equilibrium modulus) indicates the existence of yield stress and it is related to the rubber network strength. It also correlates with both the yield stress, and yield strain (see discussion below).

Based on Equations 5-3, the following model can be written, which provides a direct link between the microstructure of the material and its linear rheological properties with a minimum number of parameters (mainly the exponent *p*, the constants G'_c and G'_y) within the context of linear viscoelasticity [41,90,91].

$$\tau = \int_{-\infty}^{t} G(t-t')\dot{\gamma}(t')dt' \qquad 5\text{-}5)$$

Where *G*(t) is the relaxation modulus and $\dot{\gamma}$ is the shear rate. The form of the relaxation modulus function can be written in view of Eq 5-3, as:

$$G(t) = G_c t^{-p} + G_y \qquad 5\text{-}6)$$

Obviously, $G_y = G'_y$ in view of Eq. 5-3 ($G''(0) = 0$).

Since the damping factor, $tan\delta(\omega)$=$G^{"}(\omega)/G'(\omega)$ is small in case of the TPVs, Eq. 5-7 can be used to calculate the relaxation modulus [92].

$$G(t) \cong \ G'(\omega) - 0.560G^{"}(\omega/2) + 0.200G^{"}(\omega) \qquad 5\text{-}7)$$

Stress relaxation test was also performed to compare the accuracy of Eq. 5-7 with the experimental data. **Figure 5-8** depicts fits of typical experimental data by means of the proposed relaxation model (Eqs 5-3 and 5-6). **Table 5-3** summarizes the parameters of the storage modulus of all TPVs studied in the present work at 190°C. The equilibrium modulus, G'_y and G'_c for the samples with higher rubber amount (TPV1-4 of Group A) and higher curing degrees (TPV2 vs TPV3 and TPV6 vs TPV7 see **Table 4-2** for details) are higher, indicating that the level of curing and amount of crosslinked rubber form stronger networks. Thus, the G'_y value can be used as a measure of the network strength. However, a stronger network (stiffer material) may fail and yield at smaller shear

stress values and smaller yield strains. This can be seen from **Figure 5-9**, where the yield stressσ_y, and yield strain, γ_y, are plotted as functions of the equilibrium modulus G_y' (note the relationship between these quantities, $\sigma_y = G_y'\gamma_y$). The trends are similar in both groups of TPVs (A and B) for both the yield stresses and strains indicating consistency of the results. A maximum appears in both yield strain and yield stress at an optimum network strength (G_y'). This (strongest network) is formed by combining the two linear polymers (PP and EPDM) in the network at a medium curing level. A high curing degree increases the network strength (high G_y'), and as stiffer fails at lower yield strains, thus resulting smaller yield stress values. In addition, it appears that the use of the B-EPDM weakens the network and results in the smallest yield stress values in both Groups of TPVs (TPV4 and TPV8). These parameters (σ_y, G_y', γ_y) are expected to have a significant impact on the processing of these materials.

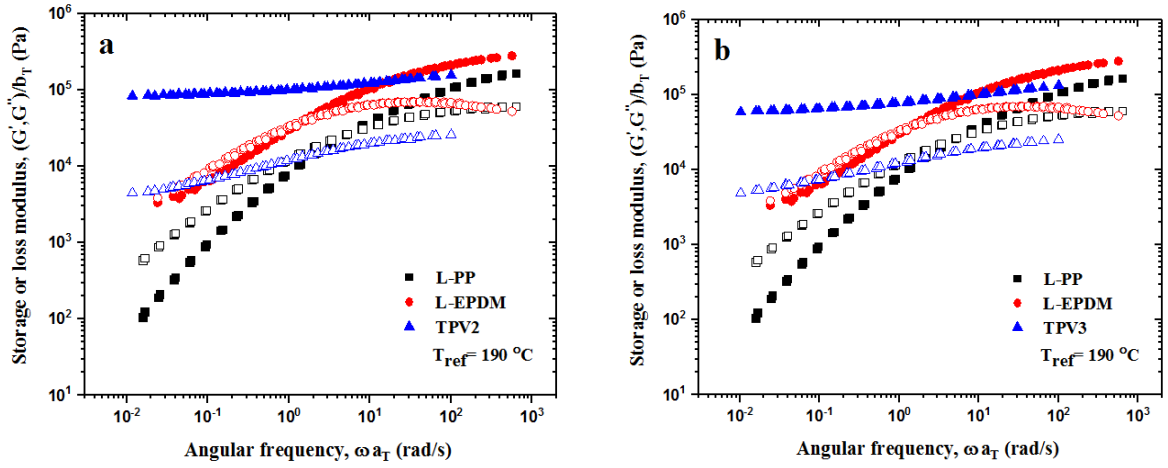

Figure 5-7. The linear viscoelastic moduli of a) TPV2 and b) TPV3 compared with the corresponding moduli of their constituents at T_{ref}=190°C. Solid symbols represent storage modulus and open symbols represent loss modulus.

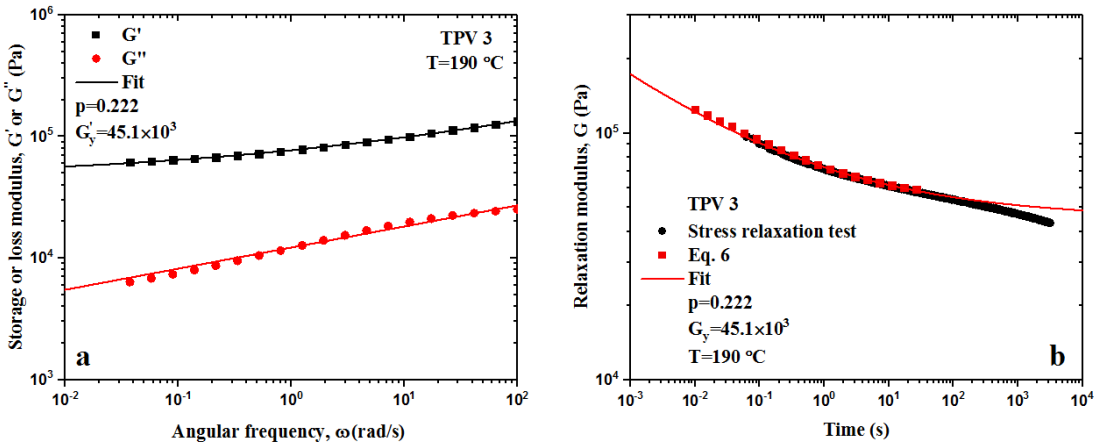

Figure 5-8. Fitting the experimental data with the model of Eqs 5-3 and 5-6 to determine the parameters listed in **Table 5-3** a) storage and loss moduli, and b) shear stress and relaxation modulus.

Table 5-3. Parameters of the storage modulus function (Eq 5-3) of all TPVs at T=190 ℃.

Sample	G_y' (kPa)	τ_R (s)	p
(Group A)			
TPV1	78.3	0.003	0.258
TPV2	69.7	0.027	0.231
TPV3	45.1	0.213	0.222
TPV4	33.3	2.864	0.200
(Group B)			
TPV5	61.8	0.009	0.274
TPV6	55.6	0.049	0.270
TPV7	39.8	0.191	0.257
TPV8	28.7	0.928	0.234
Universal constants of Eq 5-3 for all TPVs, p = 0.215 and $G_c''/G_y' = 0.34$			

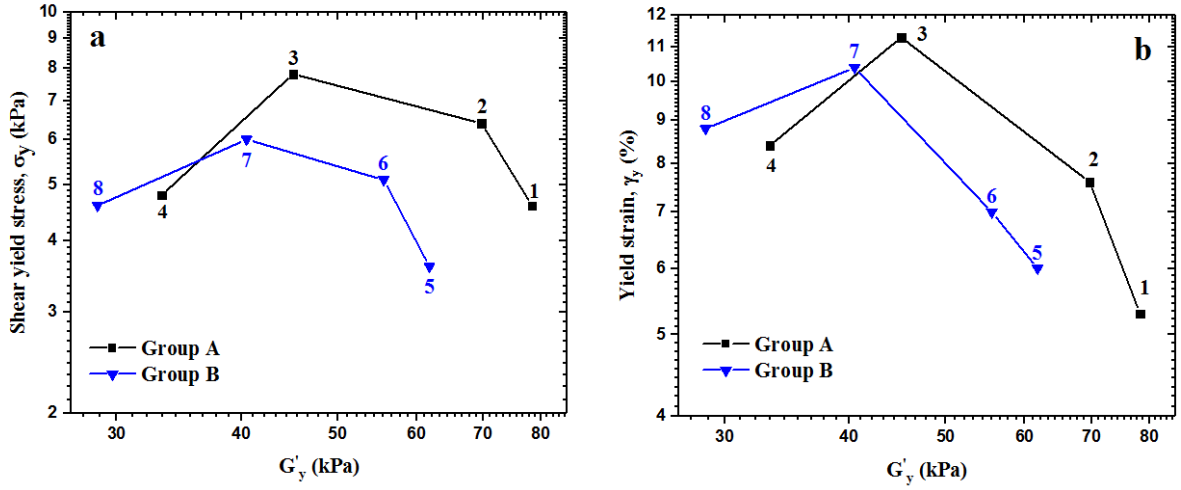

Figure 5-9. The yield stress,σ_y, and yield strain, γ_y, as functions of the equilibrium modulus G_y'

5.2.3.1 Effect of thermoplastic type (L-PP vs B-PP)

Figure 5-10 compares the viscoelastic moduli of TPV2 (B-PP+L-EPDM) and TPV3 (L-PP+L-EPDM) and those of TPV5 (B-PP+L-EPDM) and TPV6 (L-PP+L-EPDM) at low and high rubber concentrations. Although L-PP (linear) has viscoelastic moduli much higher than those of B-PP (branched), their effect is minimal on G′ in both cases since relaxation is dominantly controlled by the EPDM phase and the cured interface. There is a relatively higher influence on G″ (viscous component) over the whole frequency range. However, because G′>>G″, the overall effect of the loss modulus G″ can be ignored.

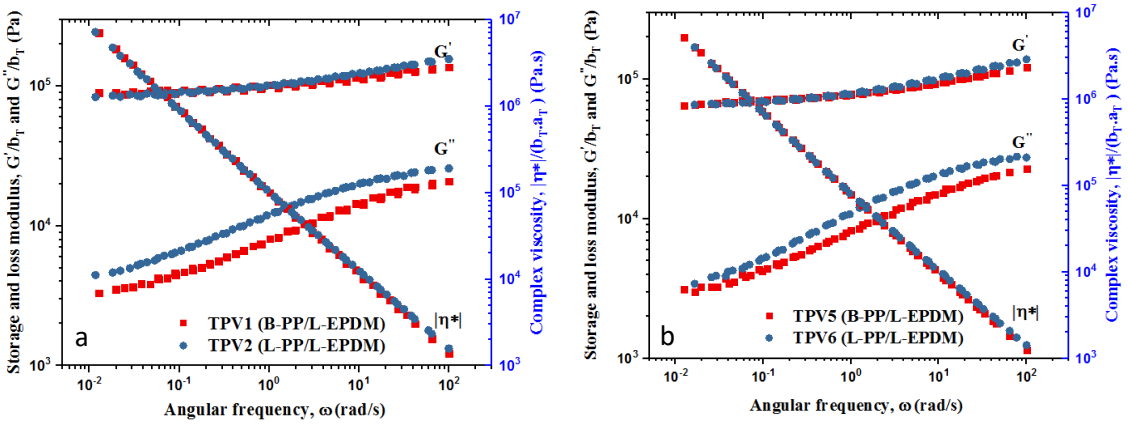

Figure 5-10. The linear viscoelastic moduli of a) TPV1 and 2, and b) TPV5 and 6 compared to show the effect of different thermoplastic used in the TPV formulation at T_{ref}=190 °C. Solid symbols represent storage modulus and open symbols represent loss modulus.

5.2.3.2 Effect of rubber type (L-EPDM vs B-EPDM)

Figure 5-11 compares the viscoelastic moduli of TPV3 (L-PP+L-EPDM) and TPV4 (L-PP+B-EPDM) and those of TPV7 (L-PP+L-EPDM) and TPV8 (L-PP+B-EPDM) at high (Group A) and low (Group B) rubber concentrations, respectively. The functions G′ and G″ are slightly higher at lower frequencies when the L-EPDM (linear) is used over B-EPDM (branched) although the individual viscoelastic moduli of B-EPDM are higher than those of L-EPDM. This can be attributed to the higher amount of oil in the L-EPDM (lower amount of rubber) compared to that in the B-EPDM, which causes a higher crosslink density at the same curing level during dynamic vulcanization. In addition, L-EPDM has a higher Mw, which makes it more elastomeric. Therefore, crosslinked L-EPDM can form a stronger rubber network due to a higher crosslink density and Mw. This was also discussed in view of the results plotted in **Figure 5-9**, where the B-EPDM appeared to produce the weakest network (smallest G_y' values).

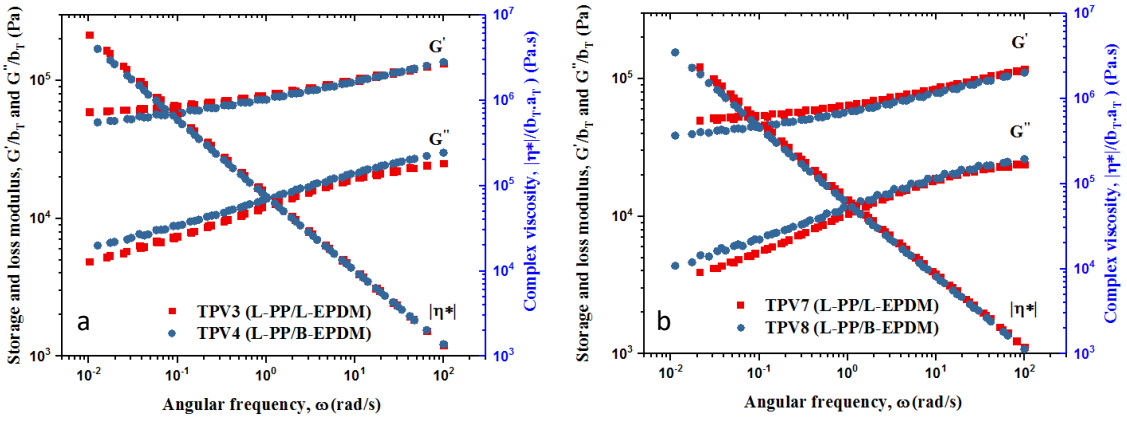

Figure 5-11. The linear viscoelastic moduli of a) TPV3 and TPV4, and b) TPV7 and TPV8 compared to show the effect of different thermoplastic used in the TPV formulation at T_{ref}=190°C. Solid symbols represent storage modulus and open symbols represent loss modulus.

5.2.3.3 Effect of curing level

Figure 5-12 compares the linear viscoelastic properties of TPV2 (high curing) and TPV3 (normal curing) that are made up of the same of L-PP and L-EPDM with the same filler concentration (left side) and the linear viscoelastic properties of TPV6 (high curing) and TPV7 (normal curing) that are made up of the same L-PP and L-EPDM with the same filler concentration (right side). Higher curing increases the G′ (elastic) significantly due to the stronger cured interface formed between

the two constituent polymers. In fact, as the values of G_y' listed in **Table 5-3** for these systems also show, a stronger rubber network is formed at a higher curing level.

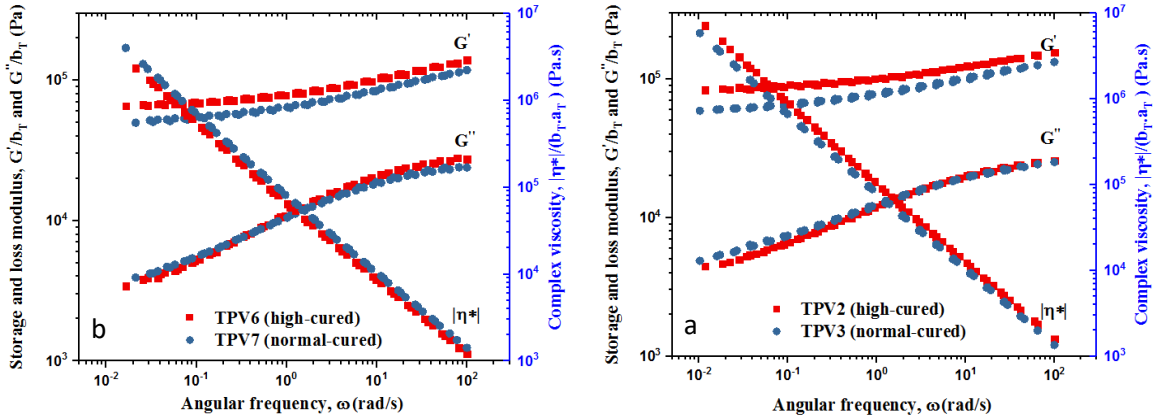

Figure 5-12. The effect of curing level on the linear viscoelastic moduli of TPV2 (high curing) and TPV3 (normal curing) with other parameters the same (left) and TPV6 (high curing) and TPV7 (normal curing) with other parameters the same (right) at T_{ref}=190°C. Solid symbols represent storage modulus and open symbols represent loss modulus.

5.2.3.4 Effect of crosslinked rubber concentration

Figure 5-13-a to **d** compares the linear viscoelastic properties of several TPVs in four different cases in each group. Group A has higher amount of EPDM. In all cases, when the amount of EPDM increases, the linear viscoelastic moduli (both G′ and G″) increase accordingly because either EPDM phase has higher elasticity or higher amount of rubber (proportionally lower amount of PP matrix) increases the linear voscoelastic moduli (both G′ and G″) accordingly.

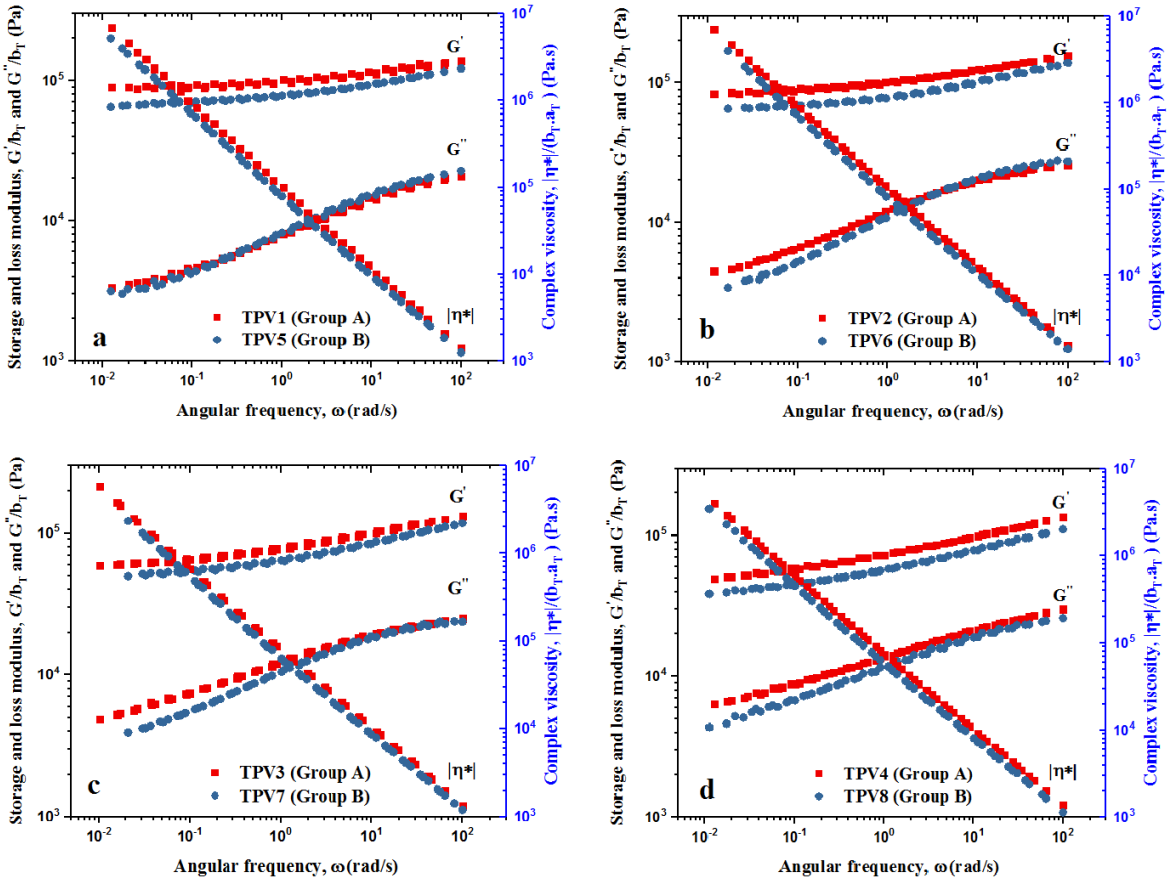

Figure 5-13. The effect of rubber concentration (high, normal) on the linear viscoelastic moduli of TPVs with other parameters the same (constituent polymers and level of curing) at T_{ref}=190°C. Solid symbols represent storage modulus and open symbols represent loss modulus.

5.2.4 Uniaxial extension of TPVs

As discussed above, uniaxial extension has been performed for TPVs at several Hencky strain rates at 190°C. **Figure 5-14** depicts the uniaxial stress growth coefficient, η_E^+, of TPV4 and TPV5 at 190°C together with those of their constituent polymers. Note that the uniaxial stress growth coefficients for TPVs have been multiplied by 6x for the sake of clarity, essentially to separate and show the data more clearly. It is clear from the plotted data that TPVs exhibit an "instability" at the early times of their extension due to the yielding of the material. In fact, at these early times the coefficient, η_E^+ go below the LVE envelop (continuous lines representing $3\eta^+$) change concavity and at longer times grow and follow practically the LVE curve again. This is definitely not due to sagging effects that are impossible to happen due to the strong network these materials form. This can also be seen from the corresponding coefficients, η_E^+, of their constituent polymers

(PP and EPDM) which, although much softer at the same temperature, show no signs of sagging or other instabilities. The observed effect is inherent to the yield stress in extension of these materials, which manifests itself as a change in the concavity where at some time the slope of the coefficient, η_E^+, approaches zero. This effect is shown for the first time in the case of polymer melt-like materials. Similar effects have been observed and reported previously for a thixotropic suspension [93]. These experimental results were modelled by Varchanis et al. [94] who developed a constitutive equation for an elastoviscoplastic material and has shown computationally the yielding obtained in uniaxial extension deformations. The computed elastic behavior during startup of uniaxial extension is initially observed, while at times beyond the elastic limit the slope of the stress curve decreases to zero showing its yielding behavior.

Another important observation to be noted is that the strong strain hardening of B-PP (**Figure 5-14**) is not manifesting itself when it is part of TPV5. Similarly, the strong strain hardening of B-EPDM is suppressed when it is part of TPV4 (**Figure 5-14b**).

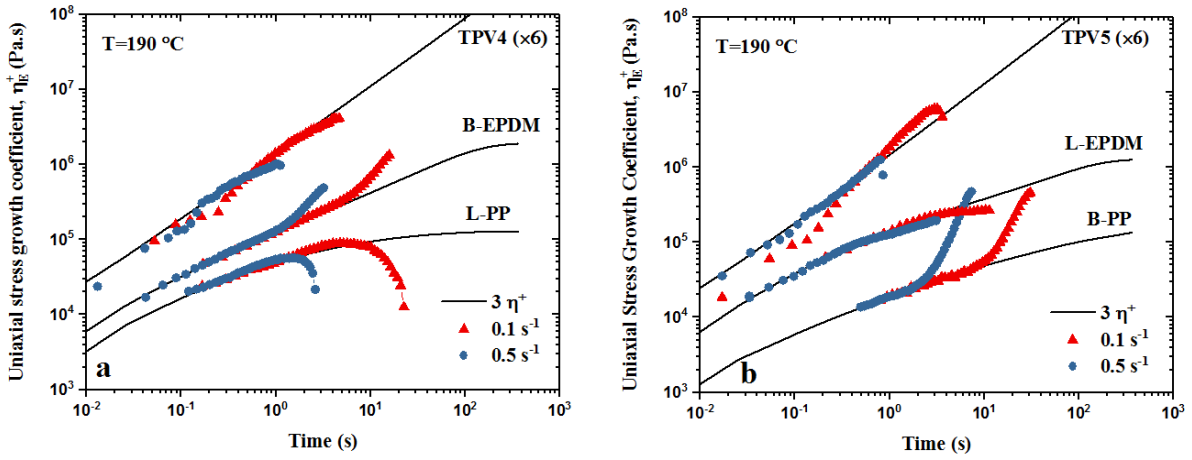

Figure 5-14. Comparison of the extensional behavior of TPV4 and TPV5 with those of their constituent components.

Figure 5-15-a depict typical uniaxial extension data for TPV4. **Figure 5-15-b** shows the same data in terms of uniaxial stress at various Hencky strain rates, multiplied by various factors to show the yield tensile strength at various Hencky strain rates more clearly. It can be concluded that the tensile yield stress is independent of the Hencky strain rate up to strains of $0.1s^{-1}$ (also see **Table 5-4**), which we define as the tensile yield stress, $\sigma_{y,E}$. **Table 5-4** lists the tensile yield stress, $\sigma_{y,E}$ of TPVs as an average at different Hencky strain rates (0.001-0.1 s^{-1}). Similar to our discussion of

yield in shear, yield in extension should also occur over a range of tensile stress values. The process starts at the point where the slope of the tensile stress curve decreases to zero or having the tendency to decreasing to zero [94] and it continues till flow initiation where the tensile curve reaches back again the LVE (shown with an arrow in **Figure 5-15** for different Hencky strain rates). Therefore, the tensile stress of fully flow initiation point is considered as the tensile yield stress$\sigma_{y,E}$. It has also been observed that the extensional yield stress slightly increases with the temperature (perhaps within experimental error). The temperature effect in extension is similar to that observed from the strain sweep results (**Figure 5-6**), where it was concluded that the temperature has no significant influence on the shear and thus on the extensional yield stress.

In solid mechanics, for sufficiently slow flows [44], the von Mises criterion relating these two yield stresses, defines this ratio, $\sigma_{y,E}/\sigma_y$, as $\sqrt{3} \approx 1.73$. However, this criterion assumes homogeneous extensional flow. For many complex materials this ratio has been reported to be much higher [44]. It should also be mentioned that normal forces in the solid phase prior to yielding also affect the von Mises criterion [95]. In particular this ratio has been calculated for different materials to be in the range between $\sqrt{3}$ and $3\sqrt{3}$ for various suspensions and pastes [44,96–98]. **Table 5-4** compares the ratio of tensile and shear yield stresses for TPVs studied in this work. As seen from the corresponding values listed in **Table 5-4**, in the case of TPVs this ratio of $\sigma_{y,E}/\sigma_y$takes values in the range of 1.4-3.25. The ratio of $\sigma_{y,E}/(G_y' \times \gamma_y)$ was also calculated using the critical yield strain determined from linear viscoelastic measurements, γ_y (listed in **Table 5-2**) and the equilibrium storage modulus, G_y', obtained from fitting Eq 5-3 to linear viscoelastic moduli (listed in **Table 5-3**). This procedure results in slightly higher yield stress ratio values (2-4.5) but still in the range of $\sqrt{3}$ and $3\sqrt{3}$. The deviation of this ratio from $\sqrt{3}$ could also be related to (i) inhomogeneity in the elongational flow and (ii) the normal stresses that develop in the solid state prior to yielding [95]. **Table 5-4** also lists the yield stress ratio by using as yield stress in shear obtained from the crossover of G′ and G″ (**Table 5-2**) which falls below $\sqrt{3}$ for all samples (practically less than 1). Since σ_y and $G_y' \times \gamma_y$ in **Table 5-4** represent the lower limit of shear yield stress and $\sigma_{y,C}$ the upper limit, a single value for this ratio could be somewhere in between those limits, still consistent with the von Mises criterion. Finally, considering the values listed in **Table 5-4**, one can conclude that the extensional yield stress increases with rubber particle concentration (Group A TPVs have higher values compared to those in Group B). Finally, the extensional yield

stress follows the same pattern as G_y' (apart from TPV8), therefore it can be concluded that it correlates with rubber strength. As a concluding remark, to the best of our knowledge this is the first time that yield evidence in extension is reported for polymer melts and definitely further investigation is needed.

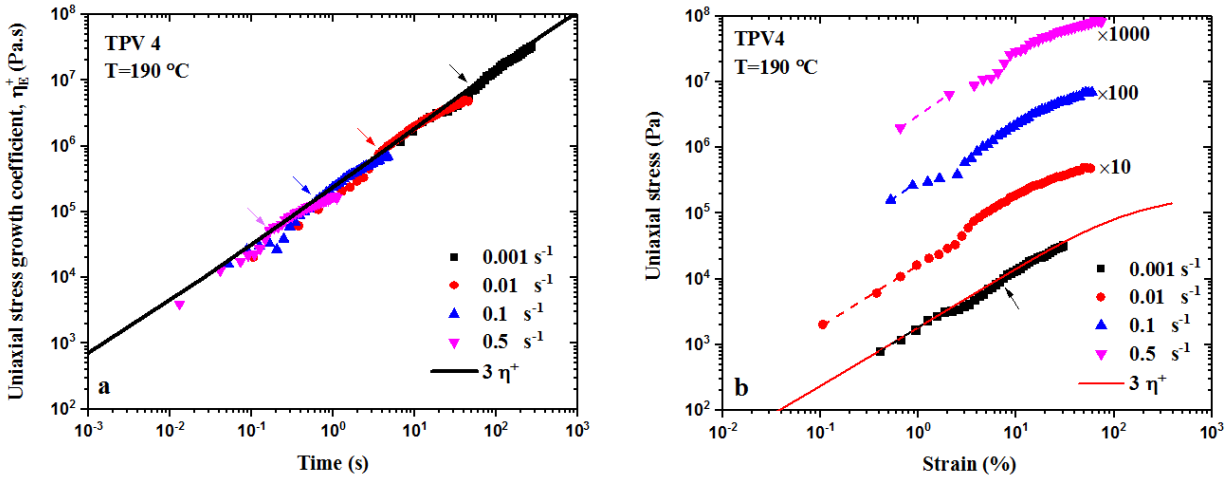

Figure 5-15. Uniaxial stress growth coefficient of TPV4 at 190°C. a) Uniaxial stress growth vs. time, and b) Uniaxial stress vs. strain. Arrows show the yielding point at different Hencky strain rates.

Table 5-4. Yield stresses in shear and extension of TPVs at 190°C and their ratio

Sample	$\sigma_{y,E}$ (kPa) at different Hencky strain rates				Average $\sigma_{y,E}$ (kPa)	Various measure of yield in shear (kPa)			Yield stress ratio in extension over shear		
	0.001 (s^{-1})	0.01 (s^{-1})	0.1 (s^{-1})	0.5 (s^{-1})	Mean (0.001-0.1)	σ_y	$G_y' \times \gamma_y$	$\sigma_{y,C}$	$\frac{\sigma_{y,E}}{G_y' \times \gamma_y}$	$\frac{\sigma_{y,E}}{\sigma_y}$	$\frac{\sigma_{y,E}}{\sigma_{y,C}}$
TPV1	14.1	15.8	14.5	23.1	14.8±0.9	4.6	4.15	18.5	3.56	3.21	0.8
TPV2	15.5	15	13.6	26	14.7±1	6.4	5.29	15.4	2.77	2.29	0.95
TPV3	13.3	13.5	13.7	20	13.5±0.2	7.8	5.09	22.5	2.65	1.90	0.6
TPV4	10.9	11.9	15	22.4	12.6±2.1	4.8	2.8	18.9	4.5	2.60	0.67
TPV5	11.6	11.4	12	15.6	11.7±0.1	3.6	3.71	12.3	3.15	3.25	0.95
TPV6	9.45	10.5	10.1	17.5	10±0.5	5.1	3.89	22.7	2.57	1.96	0.44
TPV7	7.52	8.3	9.5	18.9	8.4±1	6	4.2	22.7	2	1.40	0.37
TPV8	7.9	8.69	13.6	17	10.1±3	4.6	2.53	25.7	4	2.19	0.39

5.3 Conclusions

In this chapter, the effects of several parameters including the thermoplastic matrix and rubber types, amount, and curing levels on the rheological behavior of TPVs were investigated. Linear viscoelastic results showed that the storage modulus of TPVs follows the behavior of the thermoplastic matrix at high frequencies, while at the lower frequencies the strong interfacial associations between the two components dominate their relaxation. The storage modulus of TPVs is nearly independent of the frequency and always higher than the loss modulus by one order of magnitude at least.

The effects of long chain branching of the TPV constituents, the level of curing, and amount of crosslinked rubber particles on their rheology were found to affect the TPV rheology to various degrees. For example, increase of curing or increase of level of crosslinked rubber increases the rheological properties of TPVs (G′ and G′′), rendering the material stiffer and thus they yield and flow at larger levels of imposed stresses.

The relaxation modulus of TPVs follows a power law relation, $G(t) = G_c t^{-p} + G_y'$, where $G_y'$is the equilibrium modulus indicating the elastomeric nature of TPVs which was suggested to be related to their microstructure. Only three parameters are needed to describe the relaxation modulus. It remains to be seen if this modulus coupled with the damping function can predict the nonlinear rheological behavior of TPVs. These observations indicate that TPVs behave as nearly elastic solids at small deformations (linear viscoelasticity).

When large deformations are imposed on TPVs, yield phenomena occur in both shear and uniaxial extension. For these transient tests it was possible to obtain the yield stresses which were found to be similar in these two different types of deformation with their ratio (yield stress in extension to that in shear) to be in the range of $\sqrt{3}$ and $3\sqrt{3}$, which agrees with the von Mises criterion in solid mechanics for yield stress fluids.

6 Rheological Modelling of Thermoplastic Vulcanizates (TPVs) using the K-BKZ Constitutive Law

In this chapter, several model TPVs of known composition are studied rheologically in both shear and elongation to understand and model their response using the K-BKZ rheological law. The power-law relaxation model obtained in the previous chapter is applied on the model TPVs, as well, to prove its applicability to them. Afterwards, yield stress and wall slip are applied on K-BKZ model. Overall, it is shown that the use of the K-BKZ with yield stress and slip can capture well their rheological response.

6.1 Theoretical Background

6.1.1 Constitutive modelling for TPVs

In the previous chapter a simple expression for the relaxation modulus for TPVs was developed, which can be written as follows.

$$G(t) = G_c t^{-p} + G_y \qquad 6\text{-}1)$$

where G_c is a proportionality constant, p is the power-law exponent (universal for all TPVs) and $G_y$is the equilibrium modulus indicating the elastomeric nature of TPVs and absence of terminal relaxation. The memory function is defined by $m(t-t') \equiv -\frac{dG(t-t')}{dt'}$ and therefore can be written as:

$$m(t-t') = -pG_c(t-t')^{-p-1} \qquad 6\text{-}2)$$

The K-BKZ constitutive model proposed by Wagner [75] and modified by Luo and Tanner [76] was used to model the rheology of TPVs.

$$\tau(t) = \frac{1}{1-\theta}\int_{-\infty}^{t} m(t-t')\, h(I_C, I_{C^{-1}})\, [C^{-1}(t') + \theta C(t')]dt' \qquad 6\text{-}3)$$

Where h is damping function and $\boldsymbol{I_C}$, $\boldsymbol{I_{C^{-1}}}$ are the first invariants of the Cauchy-Green tensor C_t and its inverseC_t^{-1}, the Finger strain tensor. The material constant θ is given by:

$$\frac{N_2}{N_1} = \frac{\boldsymbol{\theta}}{1-\boldsymbol{\theta}} \tag{6-4}$$

where N_1 and N_2 are the first and second normal stress differences, respectively. It is noted that θ is not zero for polymer melts, which possess a non-zero second normal stress difference [38]. Its usual range is between -0.1 and -0.2 in accordance with experimental findings and numerical simulations [38,39]. Its effect on the predictions is minor [77,79,80].

The damping function used in the present work and shown below that it can capture the non-linear stress relaxation of TPVs can be written as [99].

$$h(I_C, I_{C^{-1}}) = \frac{\alpha}{\alpha+(\beta I_C+(1-\beta)I_{C^{-1}}-3)^{b/2}} \tag{6-5}$$

Where α and β are material constants. The parameter α can be determined from step-strain experiments in simple shear and the parameter β can be calculated from fitting uniaxial extension experiments. In simple shear, Equation 6-5 can be written (simplified) as:

$$h(I_C, I_{C^{-1}}) = \frac{\alpha}{\alpha+\gamma^b} \tag{6-6}$$

Yield stress materials, before yielding, behave nearly elastically and typically exhibit none or very little dissipation. This can be considered by the following formulation:

$$\tau(t) = \begin{cases} \int_{-\infty}^{t} (G_c(t-t')^{-p} + G_y)\dot{\gamma}\, dt \quad or \quad G_y\gamma & \tau \le \tau_y \\ \tau_y + \dfrac{1}{1-\theta}\displaystyle\int_{t_y}^{t} -pG_c(t-t')^{-p-1}\, h(I_C, I_{C^{-1}})\, [C^{-1}(t') + \theta C(t')]dt' & \tau > \tau_y \end{cases} \tag{6-7}$$

Where τ_y is yield stress, which is essentially $\tau_y = G_y\gamma_c$, where γ_c is the critical strain beyond which the material yields – marking the transition from elastic to visco-elasto-plastic behavior. The expression for the elastic part of the deformation has been written in two different forms. For the TPVs of high curing level, the response is purely elastic (no dissipation) and the stress can be calculated simply by $G_y\gamma$. However, for TPVs of low curing level the response deviates slightly from purely elastic and exhibits viscoelastic response and the form of Boltzmann's linear viscoelastic response is more appropriate resulting excellent predictions (presented below). For example, for G_y high enough $G_y \gg G_c(t-t')^{-p}$ and the two expressions become identical.

6.1.2 Implementation of slip in simple shear

Due to the presence of oil and rubber particles, TPVs slip significantly. Steady-shear experiments are analyzed in this work by means of K-BKZ Equation 6-7 to determine slip. Since Equation 6-7 is expressed in terms of the finite deformation tensor (strain), the steady shear simulations are performed by imposing only a portion of the nominal strain that best matches the experimental results. It is assumed that there is no slip in the linear response region (before yielding), therefore; slip only happens after yielding and flow initiation. Using the no-slip boundary condition, the K-BKZ over predicts the shear stress response of the material. However, using only a certain fraction *f* (to be determined) the calculations match the experimental data well. Therefore, we impose that the true strain, γ is:

$$\gamma = f\gamma_n \qquad 6\text{-}8)$$

Where is the nominal strain defined by the linear velocity of the plate divided by the distance between the plates, and f defines the fraction of the strain that the material follows. f is applied on strain tensor in non-linear shear flow. Based on these calculations to match the experimental data, the slip velocity can be calculated by:

$$V_s = (1 - f)\dot{\gamma}_n h/2 \qquad 6\text{-}9)$$

and plotted as a function of the wall shear stress. The results are presented below.

6.2 Results and Discussion

6.2.1 Linear viscoelastic behavior (LVE)

6.2.1.1 Effect of curing level on LVE

Figure 6-1 shows the frequency sweep of all the TPVs in this study. As can be seen TPVs with high curing level have higher storage modulus than the medium and low curing level ones. This is related to the stronger rubber network that is created at high curing level. The medium and low curing levels almost have similar linear viscoelastic behavior.

6.2.1.2 Effect of polymer type on LVE

Figure 6-2 shows effect of components of TPV on their LVE behavior at different curing levels. At low and medium curing level, storage modulus has a higher value when L-EPDM is the rubbery

component. That is due to higher molecular weight of L-EPDM compared to B-EPDM. The thermoplastic phase (PP) seems not to have a significant influence on the LVE behavior. On the other hand, for TPVs with high curing level, all storage moduli almost overlap over the whole frequency range. Thus, at high curing level, due to the strong elastic network through curing of the interface, the effect of components is negligible. These effects have been discussed in detail previously (previous chapter).

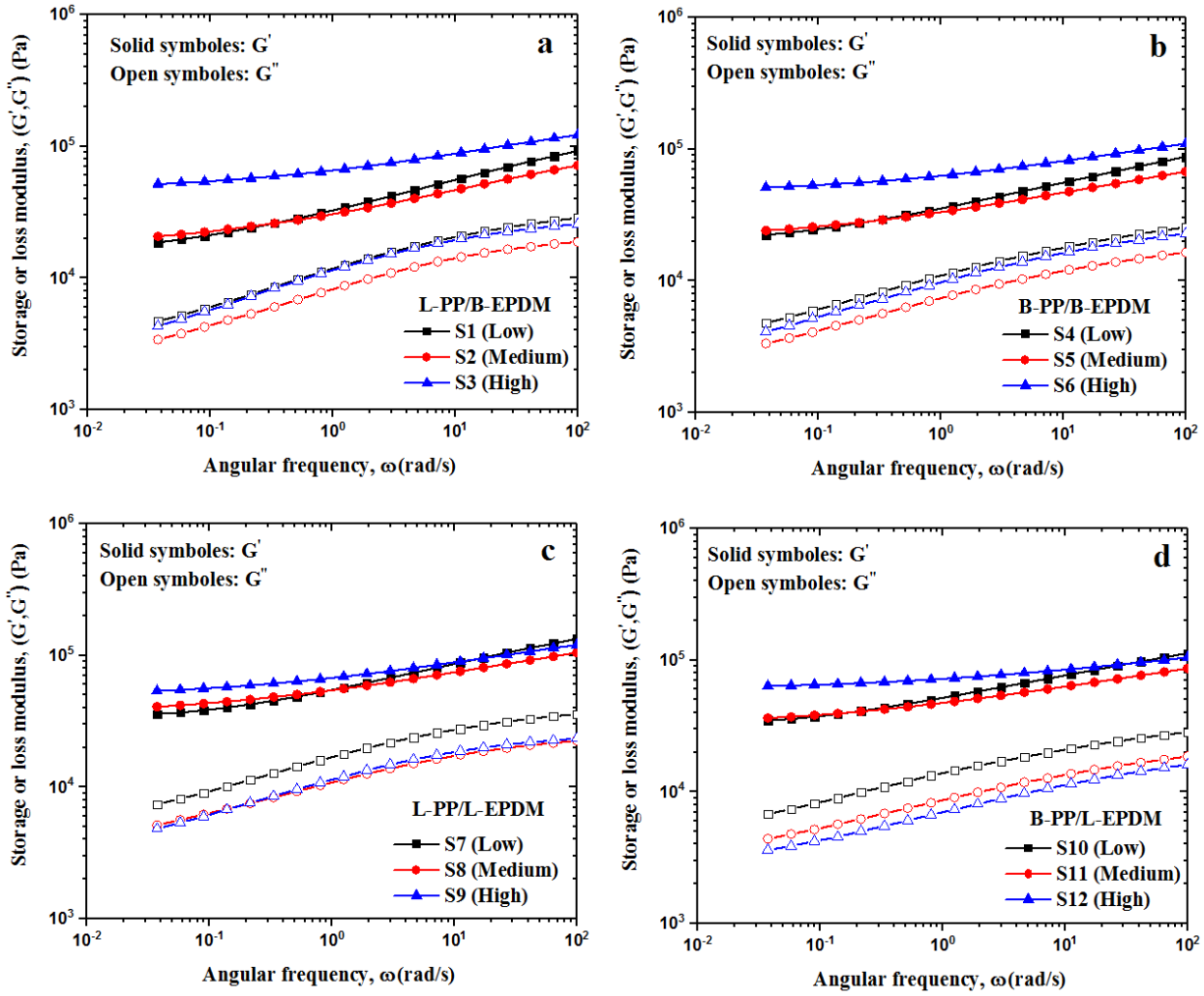

Figure 6-1. Storage and loss moduli vs. angular frequency of all the TPVs at T=190 ℃

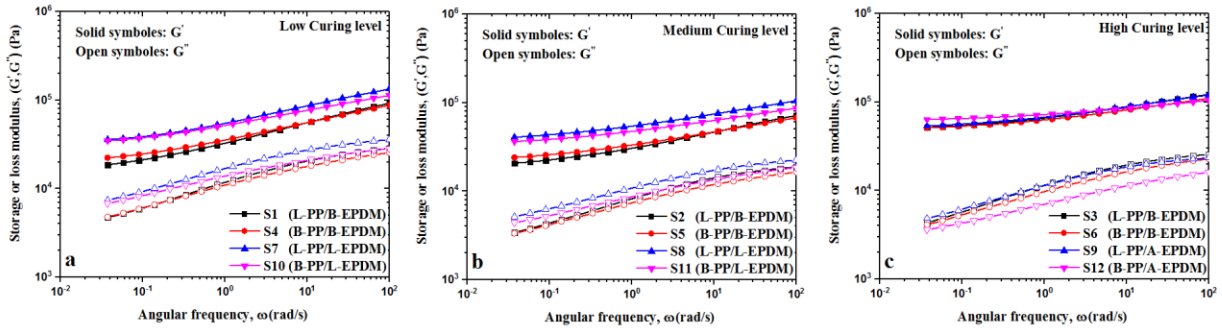

Figure 6-2. LVE of TPVs at different curing levels at T=190 ℃. a) low cured, b) medium cured, and c) high cured samples.

6.2.2 Linear relaxation modulus

In the previous chapter it was shown that the viscoelastic moduli of TPVs, G' and G'' can be modeled by (in agreement with Equation 6-1):

$$\frac{G'}{G'_y} = 1+(\omega\tau_R)^p \qquad 6\text{-}10)$$

$$\frac{G''}{G'_y} = \frac{G''_c}{G'_y}(\omega\tau_R)^p \qquad 6\text{-}11)$$

Where G''_c is the loss modulus coefficient (constant), τ_R is a characteristic time in the transition from the unyielding to the yielding zone and p is the power-law coefficient indicating the dependence of G' and G'' on frequency, ω. Since the damping factor, $tan\delta(\omega)=G''(\omega)/G'(\omega)$ is small in case of TPVs, Eq. 6-12 can be used as an approximation to calculate the relaxation modulus from the viscoelastic moduli [92]. This has been shown to indeed approximate the relaxation modulus of TPVs extremely well based on G' and G'' data,

$$G(t) \cong G'(\omega) - 0.560G''(\omega/2) + 0.200G''(\omega) \qquad 6\text{-}12)$$

Table 6-1 presents the relaxation fitting parameters of all the TPVs in this study. Based on **Table 6-1**, by increasing curing level G'_y increases, while τ_R decreases. This means that at high curing level, the transition from liquid like to solid like behavior happens at shorter frequencies (higher relaxation times) and the relaxation modulus gets close to its finite low-frequency limit quickly. Therefore, the TPV mostly behaves similar to a solid like material. It can also be observed that the exponent p is similar for all TPVs pointing to a universal relaxation behavior.

Table 6-1. Relaxation parameters at T=190 ℃.

sample	Curing level	G_C	G_y' (kPa)	P	τ_R (s)
S1	Low	2.47×10^4	5.8	0.252	466
S2	Medium	2.00×10^4	10.8	0.242	13
S3	High	2.69×10^4	36.7	0.232	0.408
S4	Low	2.44×10^4	8.7	0.233	135
S5	Medium	1.73×10^4	14.3	0.224	3.694
S6	High	2.17×10^4	39.2	0.236	0.129
S7	Low	3.94×10^4	11.8	0.228	303
S8	Medium	2.63×10^4	25.8	0.219	1.75
S9	High	2.69×10^4	38.3	0.222	0.322
S10	Low	3.53×10^4	13.4	0.206	174
S11	Medium	2.16×10^4	23.8	0.212	1.006
S12	High	1.60×10^4	55	0.230	0.007

The universal behavior of normalized storage and loss moduli vs. $\omega\tau_R$ for all the TPVs are displayed in **Figure 6-3**. As can be seen all the TPVs follow a master curve with parameters $p = 0.232$ and $\frac{G_c''}{G_y'} = 0.36$. $\lim_{\substack{\omega\to0\\ t\to\infty}}(G') = G_y' = G_y$

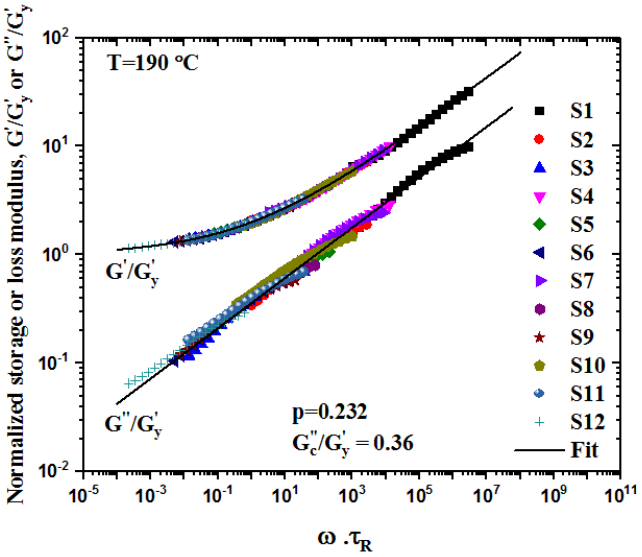

Figure 6-3. Master curve for LVE behavior of the TPVs at T=190 ℃.

6.2.3 Non-Linear viscoelastic behavior

To use K-BKZ model, damping function of the material should be determined. Therefore, the stress relaxation behavior of TPV S1 at 190°C is obtained using various step strains ranging from 0.05 to 2, (**Figure 6-4-a**). The line labelled as LVE in this figure represents the linear viscoelastic relaxation of the material and it has been calculated based on Equation 6-12. **Figure 6-4-b** shows the shifted curves to superpose on LVE which is used to calculate the damping function. Apart from the data at the early time scales<<1s, the data superposes well.

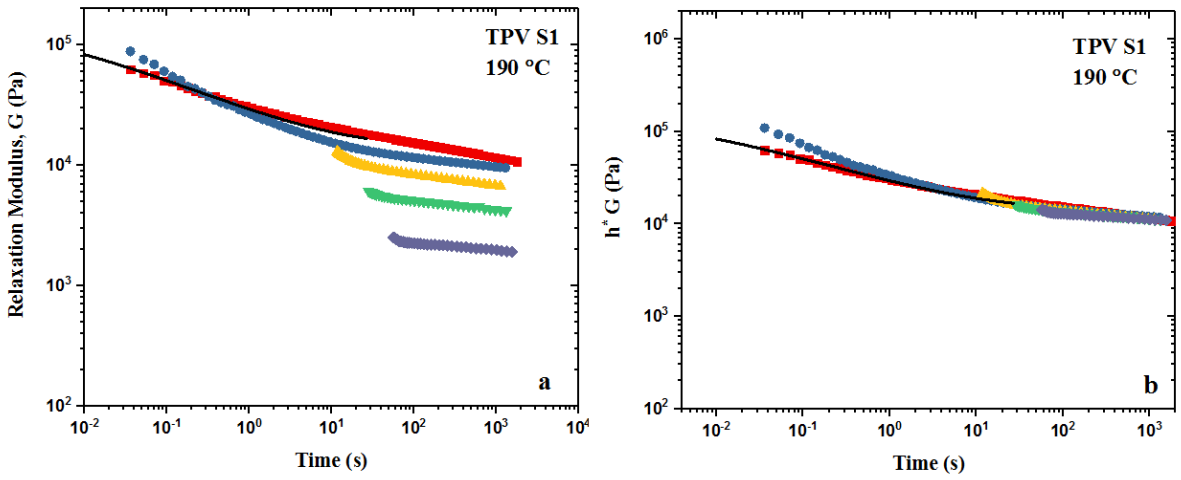

Figure 6-4. a) Stress relaxation of TPV S1, b) Shifted curves to find damping function. All experiments were done T = 190 ℃.

Using shifting values acquired from stress relaxation test, damping functions of S1-S3 are plotted in **Figure 6-5**. The damping functions are fitted with Equation 6-6 which seems to represent the results well.

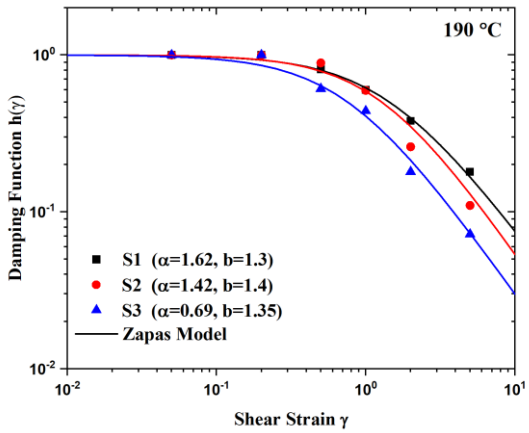

Figure 6-5. Damping function for S1-S3 at T=190 ℃.

6.2.4 Startup of steady shear and K-BKZ predictions

Figure 6-6 shows experimental data obtained from start-up of steady shear experiments in terms of the shear stress growth coefficient as a function of time for several values of the shear rate ranging from 0.01 to 20 s^{-1}. To find the yield stress that is used in Equation 6-7, it is assumed that the rubber particles form a viscoelastic network which governs the response of the materials at strains bellow critical yield strain. The yield strain is obtained from strain sweep test which was done at a frequency equal to 0.1 Hz. The yield stress corresponding to the yield strain in the strain sweep test was referred to as experimental yield stress. The experimental yield stresses obtained from strain sweep test, the yield stress from pure elastic assumption ($\tau_y = G_y\gamma_C$), and the critical strain for the onset of yielding and the corresponding value of the linear modulus are listed in **Table 6-2**. Critical yield strains obtained from strain sweep test assuming yielding happens at the region where the storage modulus is between 90% storage modulus of the plateau.

The predictions of the K-BKZ model as formulated by Equation 6-7 without slip (left) and with slip (right) are also shown in **Figure 6-6**. Predictions under no slip, overpredict the experimental data. On the other hand, predictions under slip match the experimental data well in all cases. As discussed above the level of slip in each case was calculated as a portion of the nominal shear strain to match the experimental data. Both the experimental data and predictions remarkably show the onset of yielding by a sudden deviation from the viscoelastic response (unyielded). The resemblance of the transients curves (experimental and calculated) is remarkable.

As discussed above the slip was imposed in terms of strain as a fraction of the nominal shear strain. Based on these values the slip velocity can be calculate by Equation 6-9. The slip velocity is plotted as a function of wall shear stress in **Figure 6-7**-b. The slip velocity is expressed as a power law ($V_S = A\sigma_w^m$) with a slope of 3.58 and A=1.92× $10^5 MPa^{-m}mm/s$), which is represented in **Figure 6-7** by the continuous line. The fitting was done using bi-square robust regression.

Table 6-2. Equilibrium Modulus, Yield stress and strain for TPVs S1-S3.

Sample	Eqm storage Modulus G_y' (kPa)	Critical yield strain γ_C (%)	Experimental yield stress (kPa) ($\omega = 0.1\ Hz$)	Elastic yield Stress, $\tau_y = G_y\gamma_C$ (kPa)
S1	5.8	17.8	4.5	1.03
S2	10.8	16.6	3.5	1.79
S3	36.7	7.5	3.9	2.75

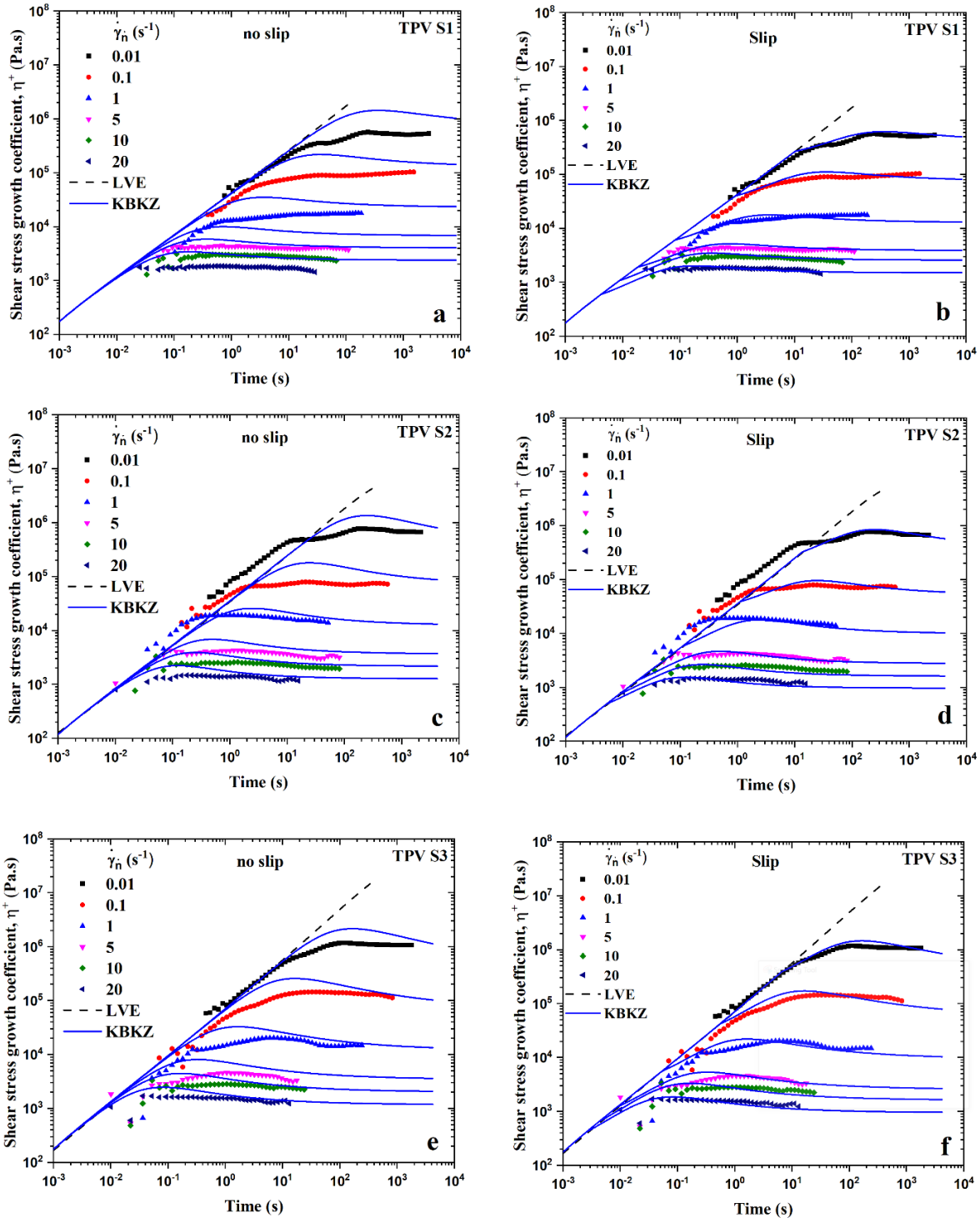

Figure 6-6. Start-up experimental results compared to model predictions, Left: no slip condition. Right: applying slip condition to the model

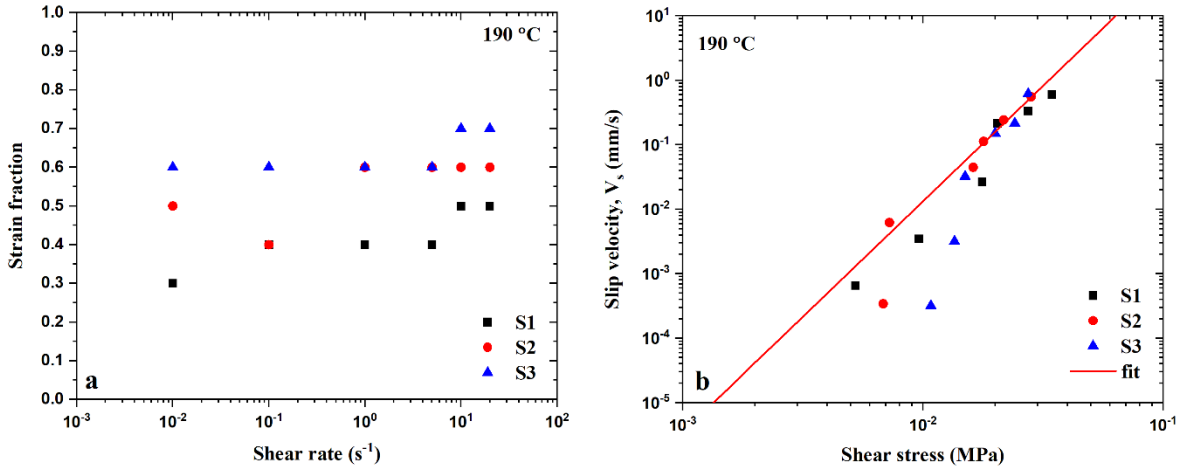

Figure 6-7. a) Strain fractions at different shear rates, b) The slip velocity of TPVs as a function of wall shear stress

6.2.5 Uniaxial extension and K-BKZ predictions

Figure 6-8 shows a comparison of uniaxial extensional results with the K-BKZ model (Equation 7). Similar to shear, the extensional yield stress was implemented into the model for uniaxial extension. To produce these results the yield stress in extension, $\tau_{y,E}$, is set by using according to von Misses criterion [44]. Model captures the correct curvature of experimental data (**Figure 6-8**). Initially the response is elastic (before yield), consequently the material yields exhibiting a strain hardening with concavity downwards (decreasing slow with time). However, at stress lvels well above the yield point, the concanity points upwards with a strong strain hardening behaviour due to the presence of the cured interface. The experimental data exhibit a similar curvature.

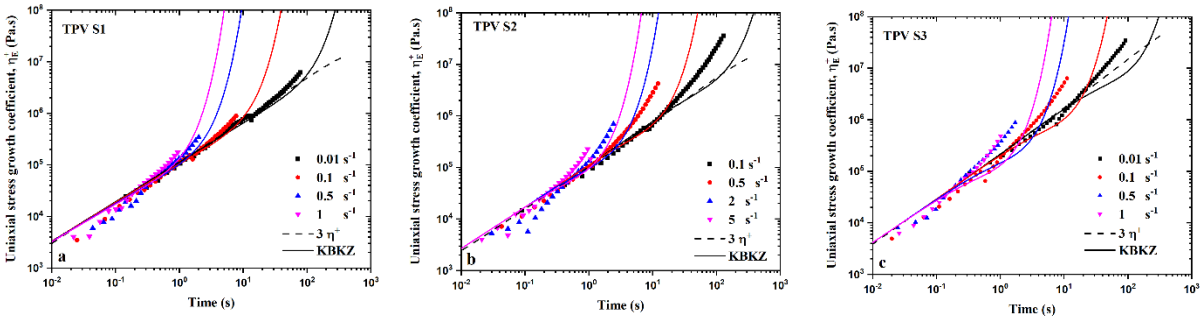

Figure 6-8. KBKZ extensional predictions using power-law relaxation function.

6.3 Conclusions

In this chapter, the K-BKZ constitutive model was used to predict the rheology of TPVs by using the power-law relaxation function. The effect of yield stress and slip velocity were also added into the model. The von Misses criterion was used to include the yield stress in extension. A convenient method was developed to include the effect of slip into the K-BKZ modelling in startup of steady shear. Essentially a fraction of the imposed nominal shear strain was used in the deformation tensor and this was calculated to match the experimental data. Based on these calculated portions, the slip velocity of TPVs was determined as a function of the wall shear stress and it was found to be similar for all TPVs.

In general, it was concluded that the nonlinear behavior of TPVs can be successfully predicted by the K-BKZ model considering all the aforementioned phenomena. The model successfully predicts shear behavior of TPVs. It deviates from extensional data at high curing levels. However, it predicts the curvature well.

7 Melt Fracture and Wall Slip of Thermoplastic Vulcanizates (TPVs)

In this chapter, a number of different TPVs with various characteristics, including the degree of curing and amount of cross-linked rubber are examined in capillary extrusion at two different temperatures (190°C and 205°C) relevant to real processing. First, the effect of the temperature on the yield stress is investigated using rheological measurements. Consequently, the flow behavior of the TPVs in capillary flow is studied concluding that TPVs slip massively (nearly plug flow) due to the presence of lubricant and the vulcanized rubber phase. Although there is little slip observed in PP samples, EPDMs themselves exhibit severe slip and melt fracture. Therefore, the TPV samples essentially follow the slip behavior of EPDMs. Finally, the melt fracture analysis of several TPVs is shown that with increase of temperature and amount of cross-linked rubber, the severity of TPVs' surface defects increases accordingly.

7.1 Linear Viscoelasticity (LVE) of TPVs

The linear rheological properties of the basic polymeric constituents of TPVs listed in **Table 4-1** were studied in Chapter 5 in detail as well as those of most TPVs listed in **Table 4-2**. Here we simply present the complex modulus, $\left|G^*(\omega)\right|$ of all TPVs studied in **Figure 7-1** at 190°C, 205°C, and 220 °C. The effect of T is not significant, and, in some cases, the experimental data is within experimental error. All data plotted in **Figure 7-1**, exhibit the tendency to approach a limiting value (equilibrium modulus, G_y^*) at smaller frequencies due to their elastomeric nature. This implies the absence of terminal relaxation as expected for elastomeric materials.

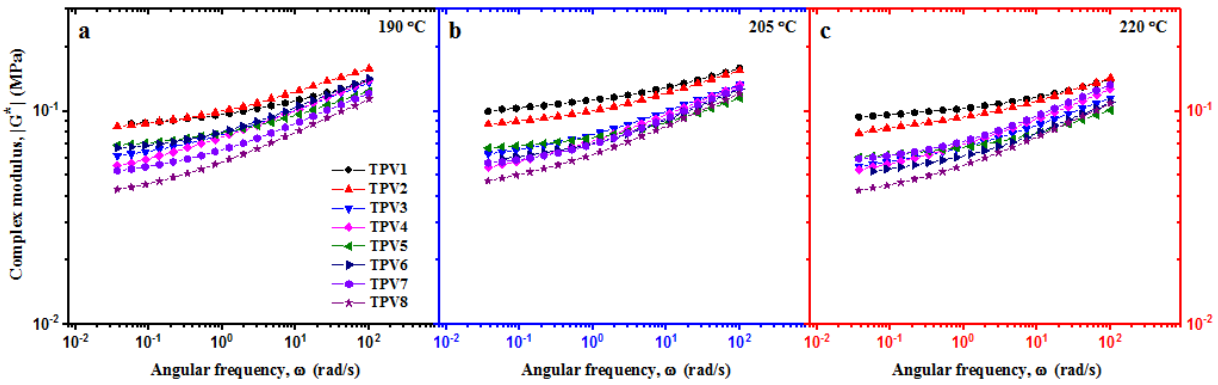

Figure 7-1. The linear viscoelastic moduli of all TPVs listed in **Table 4-2** at (a) T=190°C, (b) 205°C, and (c) 220 °C.

As concluded in Chapter 5, at higher frequencies the TPV response is controlled by the segmental dynamics of its constituent polymer (Rouse time response), however, at lower frequencies the effect of the interface of cured EPDM (dispersed) with PP (matrix) plays a significant role as there is no sign of terminal relaxation (see also **Figure 7-1**). Both G′ and G″ show solid-like behavior with a small dependence on frequency (G′ much less than G″) presented in Chapter 5. This was typically observed for all TPVs independent of the type of constituent polymeric components, level of curing (high or normal) and level of rubber concentration (high or low). This "simple" relaxation known as power-law relaxation has been observed also in the linear viscoelastic response of foods such as dough and yogurt [90,91,103] and it can be modelled by:

$$G'/G_y^{'} = 1+(\omega\tau_R)^p \text{ and } G''/G_y^{'} = \left(G_c^{''}/G_y^{'}\right)(\omega\tau_R)^p \qquad 7\text{-}1)$$

Where $G_c^{''}$ is the loss moduli coefficient (constant), τ_R is a characteristic time in the transition from the unyielding to the yielding zone and p is the power-law coefficient indicating the dependence of G′ and G″ on frequency, ω and $G_y^{'}$ indicates the existence of yield stress. The relaxation modulus of TPVs can be written as:

$$G(t) = G_c t^{-p} + G_y \qquad 7\text{-}2)$$

Where G(t) is the relaxation modulus and $G_y = G_y^{'}$.

Finally, Equations 7-1 and 7-2 can be combined to derive an equation for the complex modulus:

$$|G^*(\omega)|/G_y^*=1+(\omega\tau_R)^p \qquad 7\text{-}3)$$

It is noted that G_y^* should be very close to $G_y^{'}$. The universal viscoelastic moduli, G' and G", of all TPVs and their fitting using Equation 7-1, are plotted in **Figure 7-2** at the three temperatures of 190°C, 205°C, and 220°C.

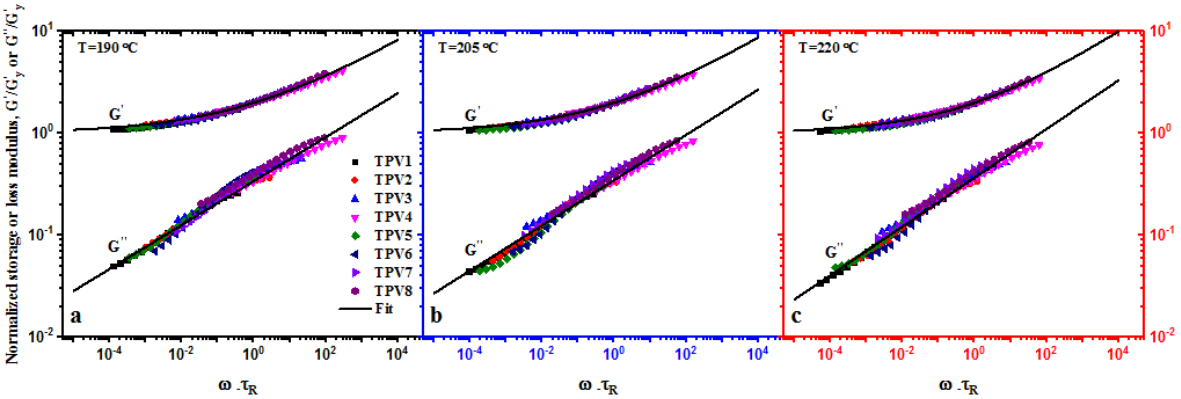

Figure 7-2. Fitting the universal viscoelastic moduli of TPVs with the model of Eq 7-1 to determine the parameters listed in **Table 7-1** and **Table 7-2**.

Table 7-1 lists the parameter values of $G_y^{'}$, τ_R, p, for all TPVs at 190°C, 205°C, and 220°C. The parameter $G_y^{'}$ and G_y^* can be viewed as fingerprints of the morphological structure of these complex multiphase systems. **Table 7-2** lists the coefficients of Equation 7-1 at different temperatures. From **Table 7-1** it can be concluded that the equilibrium (storage) modulus $G_y^{'}$ increases with temperature from 190°C to 205°C, which implies that the rubber particle network strengthens with temperature. From 205°C to 220°C in some cases, $G_y^{'}$ slightly decreases (within experimental error) or remains constant. The increase of $G_y^{'}$ with temperature might be either due to further crosslinking or increase of entropy in rubber upon deformation which consequently increases the modulus. In addition, $G_y^{'}$ increases with increase in the level of curing (TPV1 and TPV2 have higher cure level compared to TPV3 and TPV4, also TPV5 and TPV6 have higher cure level compared to TPV7 and TPV8), and with increase in the amount of rubber (TPVs of Group

A have more EPDM than their counterparts in Group B). These parameters will be used below to relate them with the onset of flow instabilities. Finally, the exponent, *p*, in the relaxation modulus also increases with temperature from 0.215 to 0.239 reflecting the influence of *T* on the relaxation modulus, essentially implying that the relaxation of the network occurs faster at a higher temperature.

Table 7-1. Parameters of the relaxation modulus (Equations 7-1 and 7-3) of all TPVs.

Sample	G_y' (kPa)			p			τ_R (s)		
Temperature (℃)	190	205	220	190	205	220	190	205	220
(Group A)									
TPV1	78.3	91.4	88.4	0.258	0.245	0.273	0.003	0.002	0.001
TPV2	69.7	75.7	69.1	0.231	0.251	0.236	0.027	0.011	0.012
TPV3	45.1	48.8	43.7	0.222	0.232	0.232	0.213	0.100	0.074
TPV4	33.3	34.3	36.2	0.200	0.202	0.214	2.864	1.535	0.631
(Group B)									
TPV5	61.8	62.9	57.7	0.274	0.311	0.316	0.009	0.005	0.008
TPV6	55.6	50.7	45.0	0.270	0.274	0.277	0.049	0.041	0.035
TPV7	40.5	46.0	50.0	0.242	0.266	0.282	0.191	0.084	0.055
TPV8	28.7	33.2	31.5	0.234	0.236	0.250	0.928	0.547	0.315

Table 7-2. Variation of model coefficients with the temperature.

190 ℃	**205** ℃	**220** ℃
$\boldsymbol{G'/G'_y = 1 + (\omega\tau_R)^{0.215}}$ $\boldsymbol{G''/G'_y = 0.34(\omega\tau_R)^{0.215}}$ $\boldsymbol{\lvert G^*\rvert/G^*_y = 1 + (\omega\tau_R)^{0.209}}$	$\boldsymbol{G'/G'_y = 1 + (\omega\tau_R)^{0.222}}$ $\boldsymbol{G''/G'_y = 0.35(\omega\tau_R)^{0.222}}$ $\boldsymbol{\lvert G^*\rvert/G^*_y = 1 + (\omega\tau_R)^{0.217}}$	$\boldsymbol{G'/G'_y = 1 + (\omega\tau_R)^{0.239}}$ $\boldsymbol{G''/G'_y = 0.37(\omega\tau_R)^{0.239}}$ $\boldsymbol{\lvert G^*\rvert/G^*_y = 1 + (\omega\tau_R)^{0.235}}$

7.2 Capillary Flow

7.2.1 Capillary flow of PPs and EPDMs

The basic polymeric constituents of TPVs were first tested in capillary flow at 190°C and 205°C to determine possible pressure effects on their viscosity (flow curve) and the existence of wall slip. **Figure 7-3** presents an example for the L-PP. First **Figure 7-3-a** depicts the apparent flow curves of L-PP using three capillary dies having the same diameter and different lengths. These are plotted

in terms of the apparent shear stress ($\sigma_A \equiv \Delta P / 4(L/D)$ as a function of the apparent shear rate $\left(\dot{\gamma}_A \equiv 32Q/\pi D^3\right)$, where ΔP is the pressure drop along the capillary die including the entrance and exit, *Q* is the volumetric flow rate and *D* is the capillary diameter. These apparent flow curves lie above the Linear Viscoelastic data (LVE) obtained from parallel-plate rheometry (reported previously in Chapter 5) due to the effect of ends pressure, ΔP_{end}. The latter should be determined in order to calculate the true wall shear stress. **Figure 7-3-b** shows the Bagley plot (pressure as a function of apparent shear rate) typically used to determine the ends pressure, ΔP_{end}. This is plotted in **Figure 7-3-c** as a function of the apparent shear rate. Using the ends pressure, the true shear stress can be calculated from $\sigma_w = (\Delta P - P_{end}) / 4\left(L/D\right)$ and the true shear rate from $\dot{\gamma}_w \equiv [(3n+1)/4n]\dot{\gamma}_A$ where *n* is defined by $n \equiv d(\log \sigma_w) / d(\log \dot{\gamma}_A)$, that is the local slope of the apparent flow curve [104]. The flow curve is compared with the LVE data in **Figure 7-3-d** and the agreement implies the consistency of the experimental data from the two different flow geometries. For this high molecular weight PP of relatively narrow molecular weight distribution, slip effects are minimal and due to minor effects of slip there is a slight decrease of capillary data compared to LVE [105,106].

The procedure was repeated for the B-PP and the two EPDMs at 190°C and 205°C. The ends pressure corrected flow curves are plotted in **Figure 7-4** and **Figure 7-5** at 190^{o}C and 205^{o}C, respectively. First, slip effects are minimal for the case of PPs as discussed above [45,46]. This is due to the high molecular weight and relatively narrow molecular weight distribution of L-PP and the branched structure of B-PP [105,106]. However, both EPDMs do slip significantly particularly at higher shear rates. There appear significant differences between LVE and capillary flow curves consistent with the assumption of slip. In particular, the flow curve for both EPDMs deviate significantly from the LVE (no slip) at high shear rates, which imply strong slip effects and possible appearance of volume defects/melt fracture. Based on these data, the slip velocity for both EPDMs has been calculated and the results are presented below together with those of TPVs. Similar results with those plotted in **Figure 7-4-c** and **Figure 7-4-d** have also been reported for polyisobutylene elastomers [68].

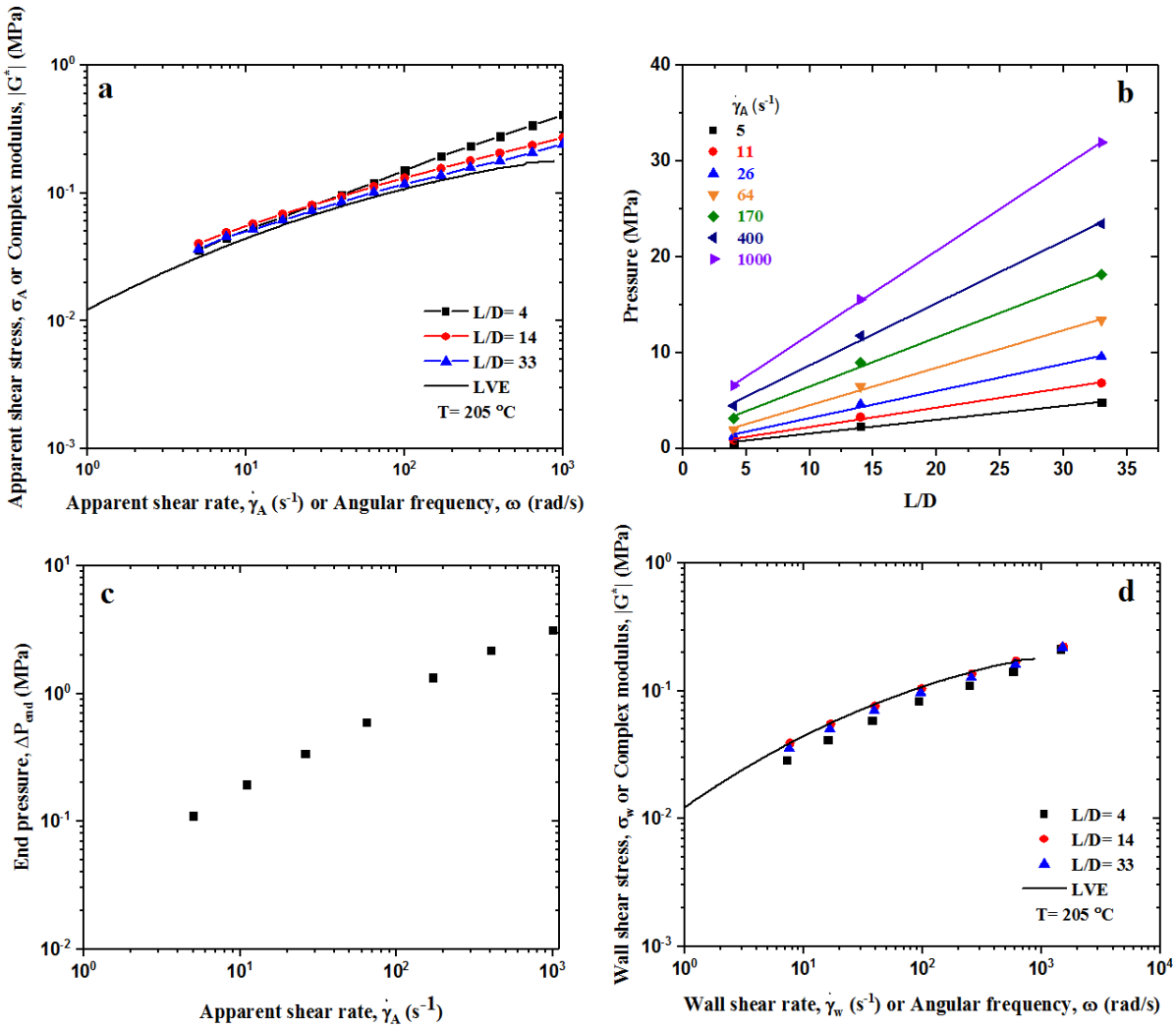

Figure 7-3. (a) The apparent flow curves of L-PP using three capillary dies having the same D and different L/D at 205°C, (b) the Bagley plot to determine the ends pressure, (c) the ends pressure versus the apparent shear rate (d) the flow curves corrected for the ends pressure effects.

7.2.2 Capillary flow of TPVs

Capillary experiments were also performed for all TPVs quite similar to those presented for PPs and EPDMs. **Figure 7-6** presents typical results for TPV1 at 190°C. First, **Figure 7-6-a** shows the comparison between LVE and the apparent flow curves of TPV1 at T=190°C without the application of the ends pressure. **Figure 7-6-b** is the Bagley plot to determine the ends pressure, ΔP_{end}. This is plotted in **Figure 7-6-c**. Finally, **Figure 7-6-d** shows the comparison between LVE and the capillary flow curves corrected for the ends pressure effects. The capillary data at different L/D ratios now collapse into a single curve (compare **Figure 7-6-a** with that of **Figure 7-6-d**).

Moreover, the capillary data are significantly lower than that of LVE. This is mainly due to two reasons (i) existence of the yield stress which causes failure of the Cox-Merz rule (in yield stress materials the Cox-Merz rule does not apply) [102] and (ii) due to significant slip effects. The slip effects in TPVs are studied next.

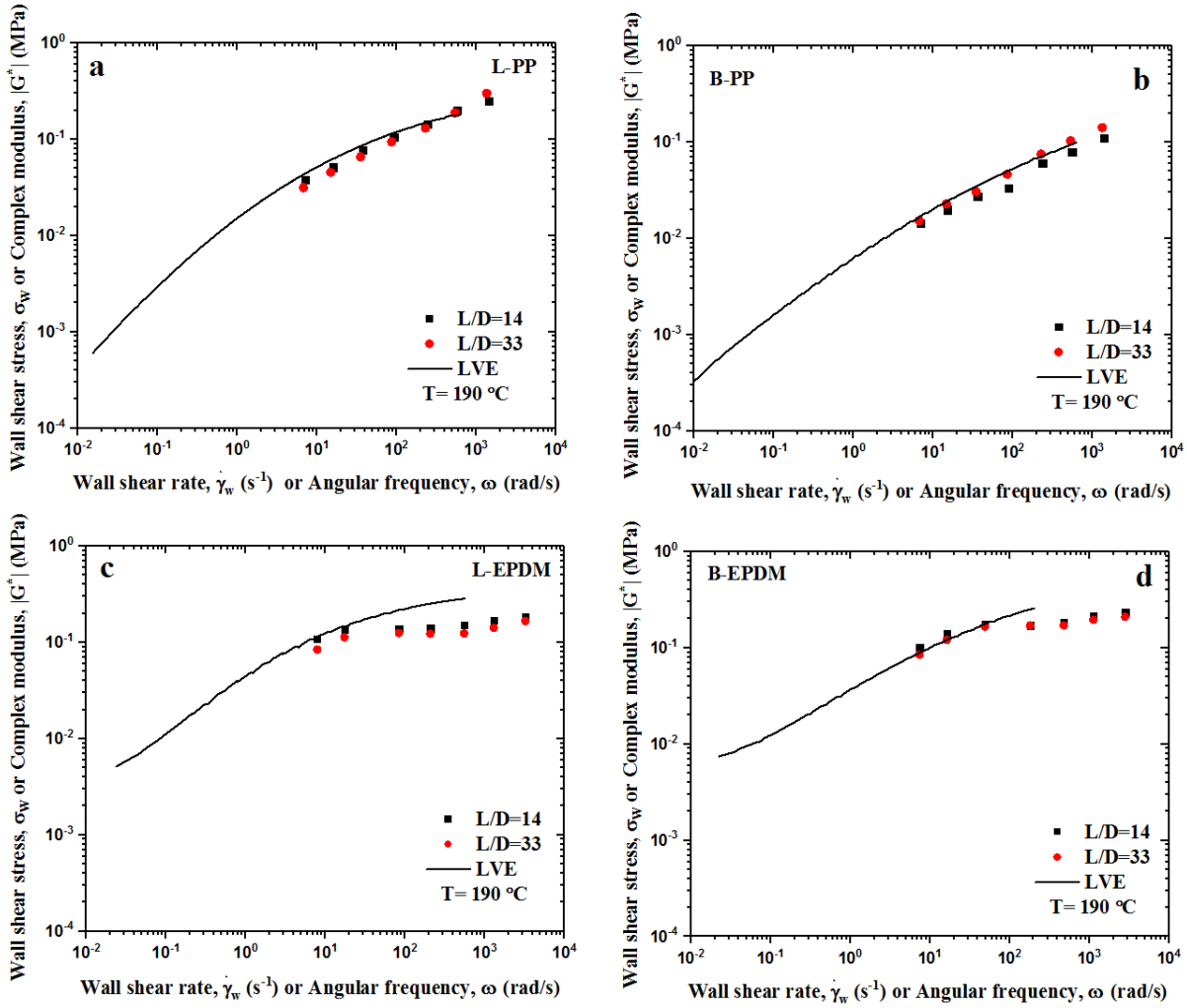

Figure 7-4. The flow curves of PPs and EPDMs at 190 ℃. While slip effects in PP are minimal, EPDMs do slip significantly at high shear rates (significant differences between LVE and capillary flow curves)

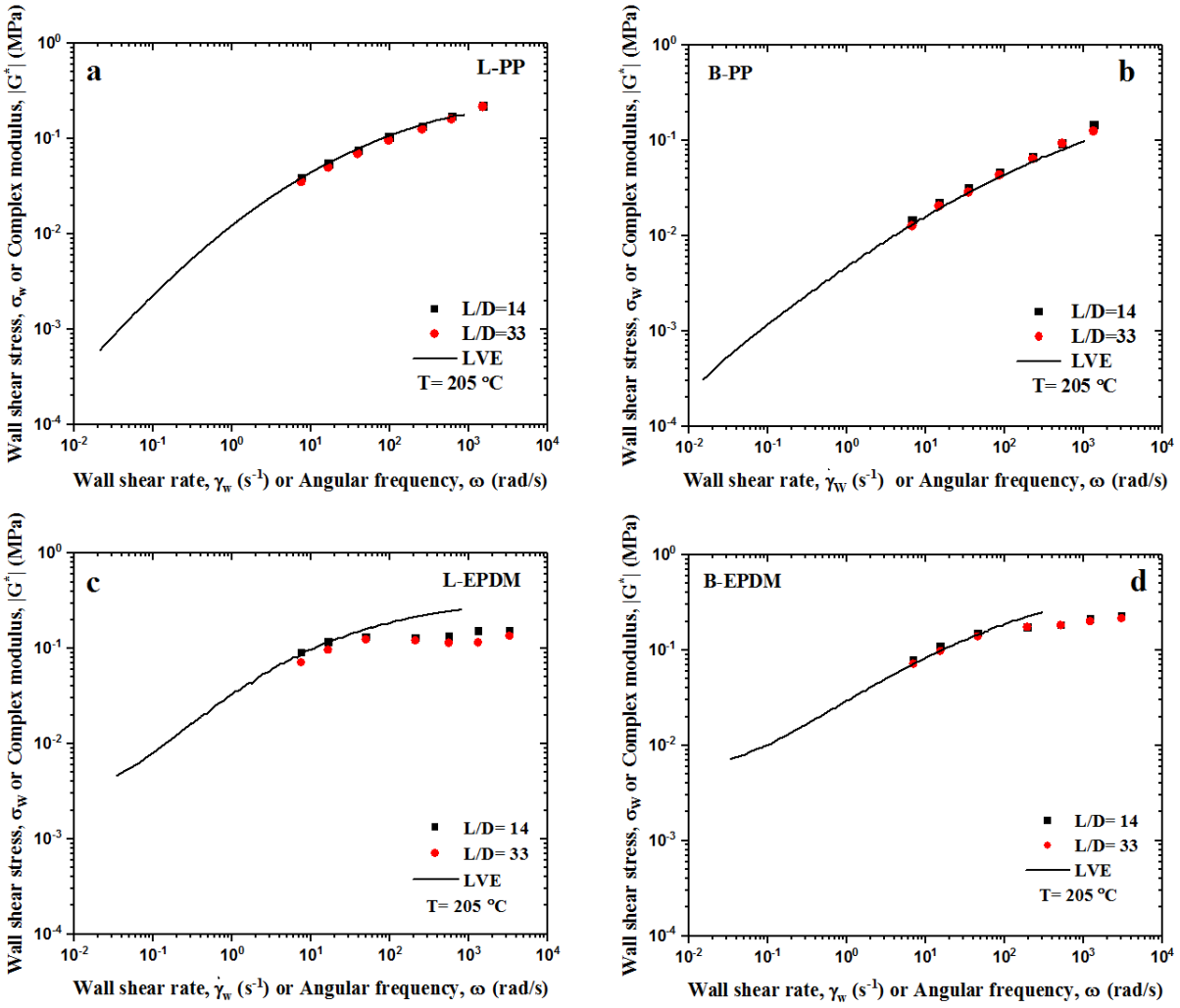

Figure 7-5. The flow curves of PPs and EPDMs at 205 ℃. While slip effects in PP are minimal, EPDMs do slip significantly at high shear rates (significant differences between LVE and capillary flow curves)

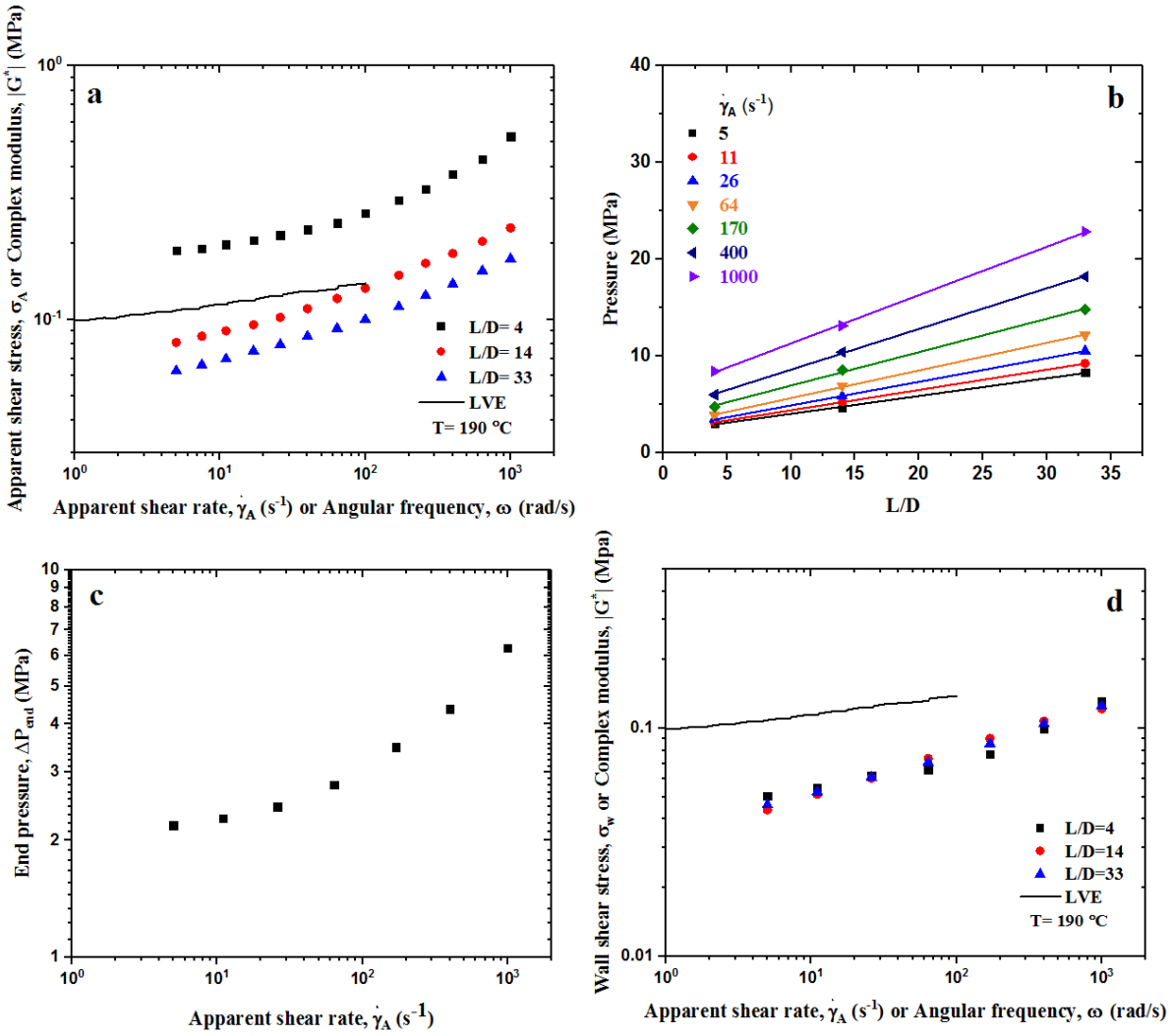

Figure 7-6. (a) The apparent flow curves of TPV1 using three capillary dies having the same D and different L/D at 190°C, (b) the Bagley plot to determine the ends pressure, (c) the ends pressure versus the apparent shear rate and (d) the flow curves corrected for the ends pressure effects.

7.3 Slip of TPVs and Their Basic Constituent Polymers (PP and EPDM)

To demonstrate slip, capillary experiments were performed for one TPV using two dies having a different diameter, *D* and same *L/D* ratio (similar pressure gradients). The results in terms of the end pressure-corrected flow curves are plotted in **Figure 7-7**. Clearly the flow curve depends on the die diameter and the experimental data are consistent with the assumption of slip. Using the Mooney technique, slip was calculated and it was found essentially to correspond to a nearly plug flow [48]. Mooney analysis has resulted shear rates corrected for the effects of slip around zero and in some cases slightly negative. This implies that for all practical purposes, TPVs can be

assumed to exhibit a nearly plug flow velocity profile. Thus at a given apparent shear rate, the slip velocity, *Vs* can be calculated by $V_S = \dot{\gamma}_A D/8$ which results from the definition of the apparent shear rate, $\dot{\gamma}_A \equiv 32Q/\pi D^3$ by setting $Q = \pi D^2 V_S/4$. The results are presented below after examining the slip of TPVs in parallel plate geometry.

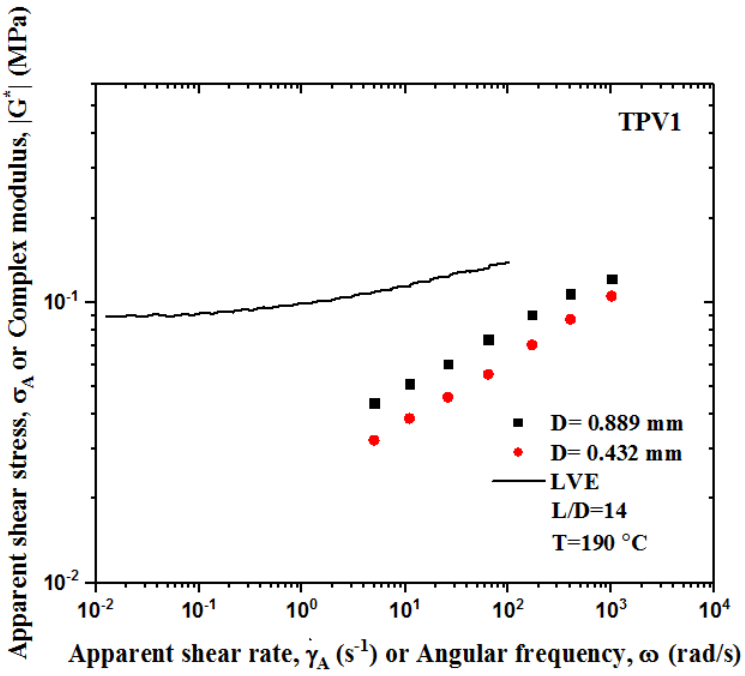

Figure 7-7. (a) The flow curves of TPV1 using two capillary dies having the same L/D and different *D* at 190°C to demonstrate slip effects in TPVs.

Figure 7-8 plots the shear stress growth coefficient of TPV1 in simple shear at various shear rates at 190°C. The LVE curve is also plotted as reference. Since these materials possess a yield stress and slip, the agreement of steady-shear experiments and LVE is lost at low strain levels below the yield stress value. As seen from **Figure 7-8**, LVE lies well above the shear stress response, similar to what is depicted and discussed in **Figure 7-7** for yield stress materials (failure of the Cox-Merz rule). We have used these experimental data and the assumption of plug flow to calculate slip in simple shear. Essentially slip can be calculated by, $V_S = \dot{\gamma}_n h/2$, where $\dot{\gamma}_n$ is the nominal shear rate (values are specified in **Figure 7-8**).

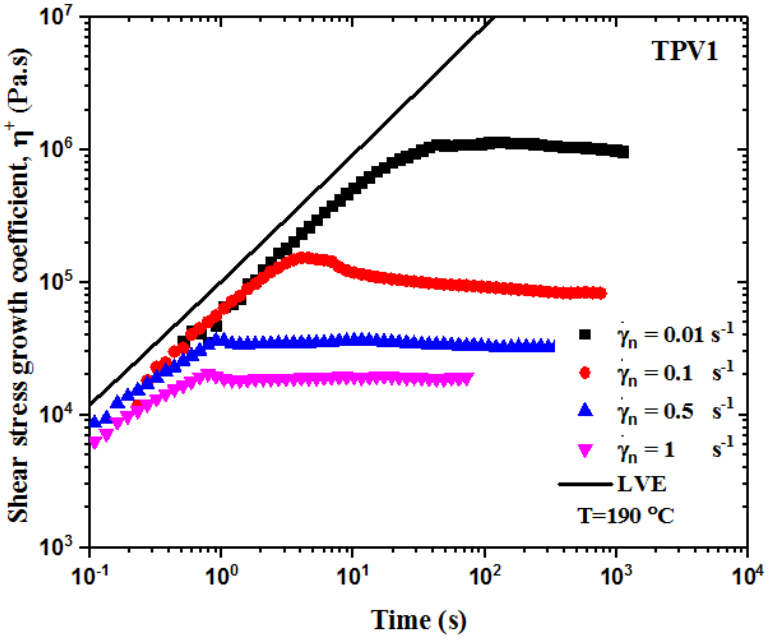

Figure 7-8. Start-up of steady shear tests of TPV1 at various shear rates at 190°C.

Figure 7-9 shows the slip velocity of TPV1 as a function of wall shear stress obtained from capillary and parallel-plate at 190°C. The two sets of data from parallel-plate and capillary are consistent (one set is extension of the other) and thus the assumption of nearly plug flow is validated, although the two sets of capillary data do not agree (although they exhibit the same trend). The slip velocity expressed as a power law ($V_S = A\sigma_w^m$) results a slope of 3.29 and A=8.5× $10^4 MPa^{-m}mm/s$), which is represented by the continuous line in **Figure 7-9**. The significant slip of TPVs is due to the presence of EPDM, which do slip easily due to their elastomeric nature (high elasticity which at high shear rates renders the materials behaving solid-like).

Figure 7-10 plots the slip velocity of the two EPDMs at different temperatures and compares this with that of TPV1 at 190°C. First, the slip velocity of EPDM increases with increase of temperature consistent the time-Temperature superposition (tTS) principle. Second, the linear EPDM slips more than the branched EPDM again consistent with previous findings for polyethylene (linear PEs slip significantly more than their branched counterparts) [29,30]. Finally, TPV1 shows a similar slip trend with that of EPDMs indicating the consistency of the experimental results that

the EPDM phase controls the slip of TPVs (similar behavior). Similar results have been reported for polyisobutylenes which are also elastomeric in nature similar to EPDMs [49,50].

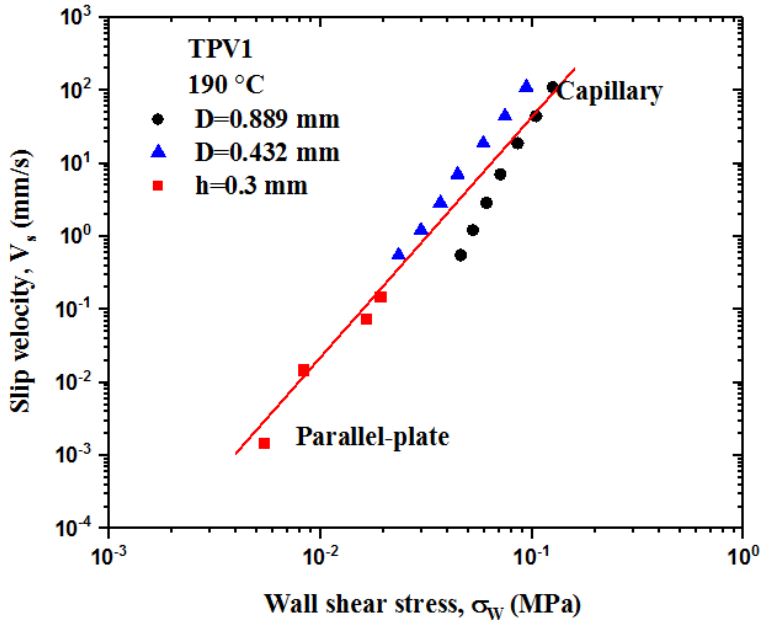

Figure 7-9. The slip velocity of TPV1 from capillary and parallel-plate rheometers as a function of wall shear stress at 190°C.

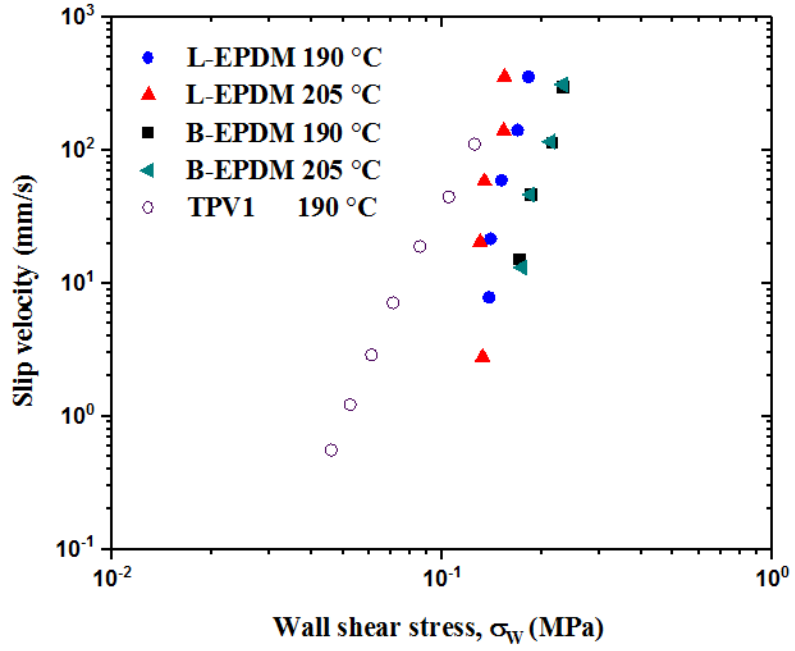

Figure 7-10. The slip velocity of EPDMs at 190 and 205°C, compared to that of TPV1 at 190°C.

Using the assumption of plug flow (validated above for TPV1), the flow curves of all TPVs determined from capillary rheometry (**Figure 7-11-a**) were used to calculate their slip velocity at 190°C. These are plotted in **Figure 7-11-b**. The general trend is that the lower the flow curve in terms of shear stress, the higher the slip velocity calculated (expected). The slip velocities of TPVs in Group B are higher than those in Group A, although no firm conclusion can be drawn as these slip calculations are based on the assumption of plug flow.

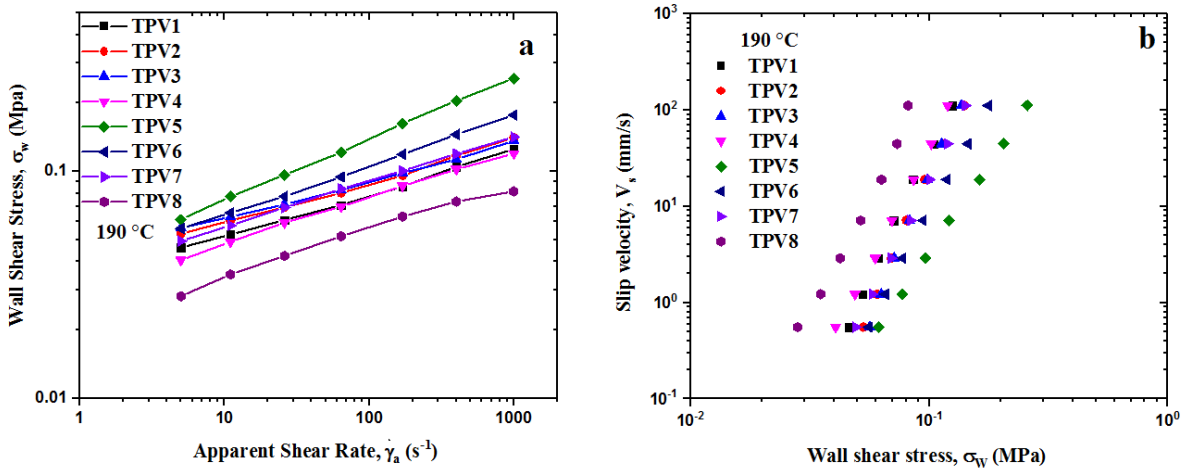

Figure 7-11. The flow curves of all TPVs listed in Table II at 190°C and the corresponding slip velocities at 190°C.

7.4 Melt Fracture

7.4.1 Melt fracture of PPs and EPDMs

Melt fracture phenomena, such as sharkskin (small amplitude periodic distortions on the extrudate surface), stick-slip or oscillating (alternating smooth and distorted surfaces) and gross melt fracture (GMF) (large amplitude/ chaotic distortions affecting the whole volume of the melt) either as helical or chaotic distortions, have been known to occur during the extrusion of most polymers (more dominant in linear polymers) when the wall shear stress exceeds a critical value [49,50]. These phenomena cause problems in the processing of polymers by setting an upper limit to the throughput applied during extrusion. PPs and EPDMs also exhibit these phenomena and many reports exist in the literature for PPs [35,36] and EPDMs [51,52] and other elastomeric materials such as PDMS [63], PIB [68,107], and SBR [26]. The stick-slip instability with large pressure oscillation is normally observed for linear polymers after the sharkskin defect, which is a result of

a cyclic transition between weak and strong slip. The size of pressure oscillations depends on the material compressibility and the geometrical characteristics of the die used for the extrusion. On the other hand, for PS [108], or SBR[26] a volume defect (helical or chaotic) develops above a critical stress, corresponding to a change in the slope of the flow curve [26]. A similar behavior has been reported for EPDMs where there is a change in the slope that occurs simultaneous with volume defect development [51,52].

Figure 7-12 and **Figure 7-13** present extrudate images obtained in the capillary extrusion of the two PPs and EPDMs at various shear rates at 190^{o}C. The geometrical characteristics of the die used were L/D=33 and D=0.89 mm. As seen from **Figure 7-12**, PPs at certain shear rates possess the shape of regular helices (type of GMF) with no sharkskin (surface) melt fracture. At higher rates the helical distortions take the form of chaotic ones (severe form of melt fracture). The critical shear rates and shear stresses for the onset of these phenomena are listed in **Table 7-3**. While PP exhibit relatively mild melt fracture phenomena at relatively high shear rates, EPDMs exhibit well-developed sharkskin and chaotic GMF even at very low shear rate (as low as 5 s^{-1}) due to their elastomeric nature. In fact, a more or less helical volume instability is superimposed on sharkskin and it develops severely with increasing shear rate leading to a chaotic GMF. Similar phenomena have been reported for other elastomeric polymers such as PDMS [63], PIB [107] and SBR [26].

L-PP, *T*=190 ℃, *D*=0.889mm, *L/D*=33			
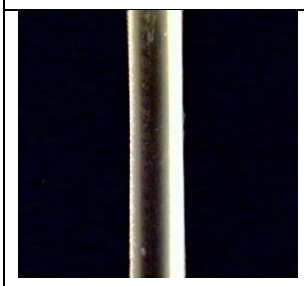	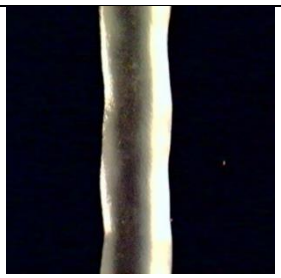		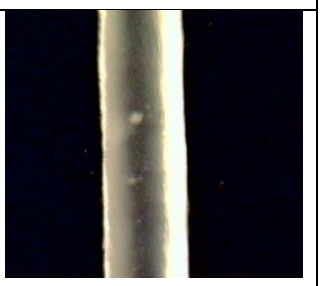
$\dot{\gamma} = 5\ s^{-1}$, Smooth	$\dot{\gamma} = 170\ s^{-1}$, Gross (helical)	$\dot{\gamma} = 260\ s^{-1}$, Gross (helical)	$\dot{\gamma} = 1000\ s^{-1}$, Gross
B-PP, T=190 ℃, L/D=33			
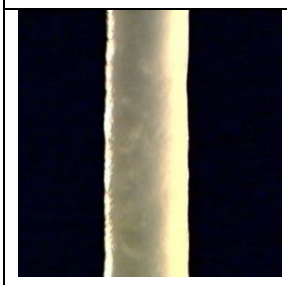	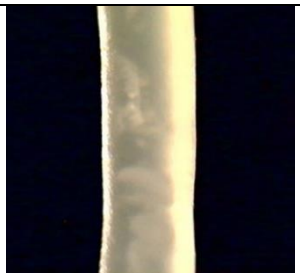	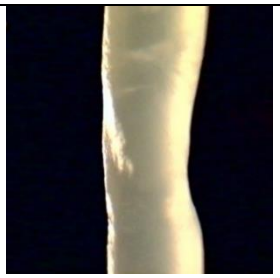	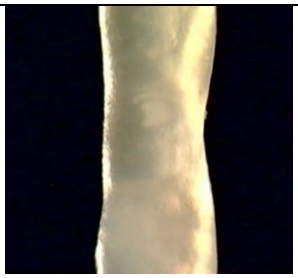
$\dot{\gamma} = 5\ s^{-1}$, Smooth	$\dot{\gamma} = 260\ s^{-1}$, Gross	$\dot{\gamma} = 640\ s^{-1}$, Gross	$\dot{\gamma} = 1000\ s^{-1}$, Gross

Figure 7-12. Extrudate images of L-PP (first row) and B-PP produced (second row) by capillary extrusion at 190°C.

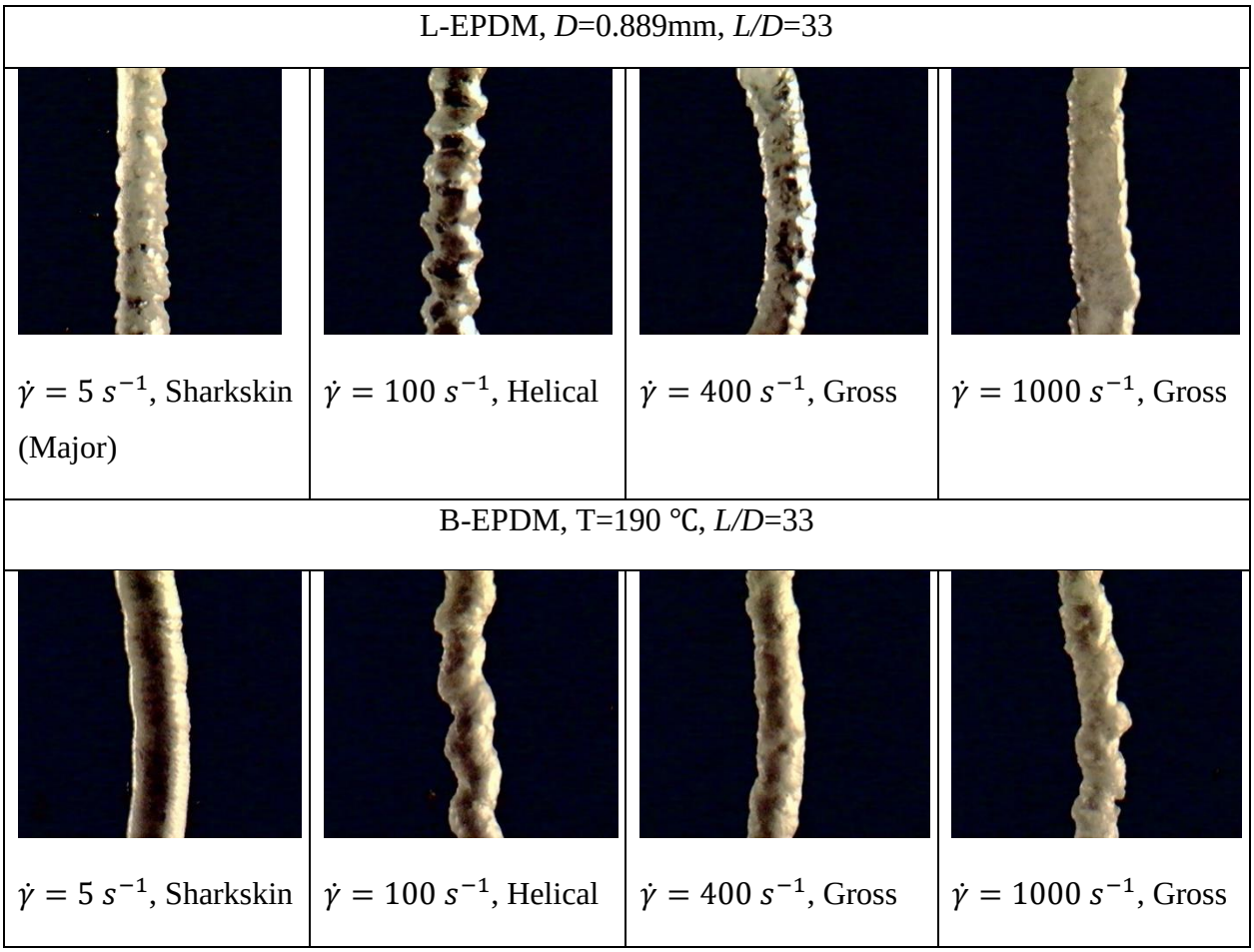

Figure 7-13. Extrudate images of L-EPDM (first row) and B-EPDM (second row) produced by capillary extrusion at 190°C.

Table 7-3. Critical shear rates and stresses for the onset of Melt Fracture (MF) phenomena of PPs and EPDMs at 190°C and 205°C.

Resin		**Critical shear rate (s^{-1})/shear stress (MPa)**		
		Sharkskin	Helical instability	Gross melt fracture
L-PP	T= 190 ℃	-	170/0.15	820/0.311
	T= 205℃	-	170/0.1437	820/0.225
B-PP	T= 190 ℃	-	-	450/0.133
	T= 205℃	-	170/0.074	-
L-EPDM	T= 190℃	5/0.102	17/0.148	285/0.178
	T= 205℃	5/0.087	17/0.137	70/0.145
B-EPDM	T= 190 ℃	5/0.100	70/0.201	330/0.240
	T= 205℃	5/0.860	70/0.141	260/0.232

7.4.2 Melt fracture of TPVs

As discussed above the melt fracture behavior of TPVs was studied in capillary rheometry at 190^{o}C and 205^{o}C. As a general remark the distortions observed in the capillary extrusion of TPVs are much milder compared to those seen in PPs and EPDMs at similar shear rates and temperatures. Two types of instabilities have been observed, which are classified in the context of this work as minor and severe surface distortions. Essentially no gross melt fracture appears in the case of TPV extrusion. **Figure 7-14** illustrates these two types of extrudate distortion (minor and severe surface melt fracture) using the real extrudate image and the processed image with photoshop to observe more clearly the edge profile. It has to be mentioned that although these instabilities/distortions are limited to the surface, they are not periodic such as those seen in EPDM and therefore they cannot be referred to as sharkskin (term reserved for periodic surface distortions). Below the effects of temperature, shear rate, curing degree and EPDM concentration on melt fracture is examined.

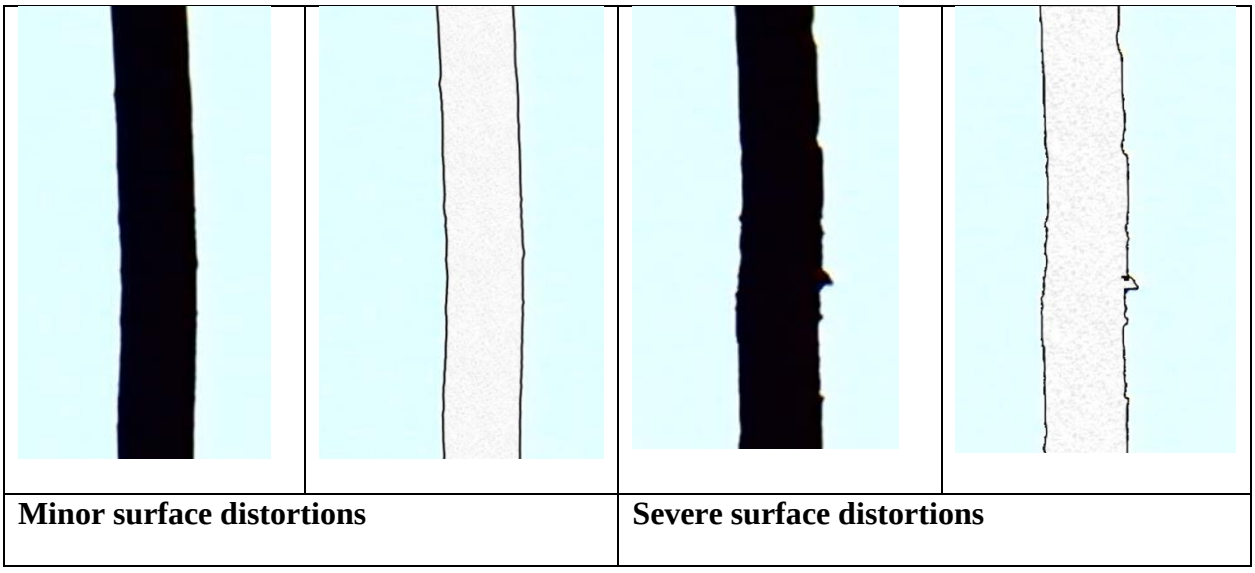

Figure 7-14. Typical extrudate images and their corresponding surface profiles that exhibit minor and severe surface distortions.

Effect of curing level and temperature: The effect of curing level on the melt fracture of the TPVs is shown in the **Figure 7-15** (TPV2 and TPV3 at 190℃). As it can be observed from all images, the defects are limited to the surface and they become less severe or disappear with increase of the shear rate. It appears that the first surface distortions appear at wall shear stresses

in the range of 45-78 kPa (listed in **Table 7-4**) of the same order of magnitude with the yield stress values reported by Ghahramani et al [2] (shear yield stresses in the range of 20-25 kPa and yield stresses in extension in the range of 9-15 kPa, all listed in **Table 7-5**). The polymer extruded at such shear rates include yielded and un-yielded regions that relax differently upon extrusion resulting these minor instabilities, which are definitely non-periodic. At higher shear rates/stresses, well above the yield stress, most of polymer volume is in a yielded state (except the core region or dead flow regions) resulting more uniform and smoother extrudates.

The surface defects in TPV3 are more severe than those in TPV2 at the same shear rate. This is due to higher yield stress of TPV3 [2]. Therefore, a higher flow rate is needed in the case of TPV3 to eliminate these surface instabilities. Temperature also has an unexpected effect in the processing of TPVs. **Figure 7-15** presents images of TPV3 at 190 and 205℃. It can be observed that the severity of surface defects increases with temperature. As discussed above the equilibrium storage and shear moduli, $G_y^{'}$ and G_y^{*} (fingerprints of the morphological structure of these complex multiphase systems related to the yield stress) increase with temperature. In other words, increase of temperature increases the strength of the rubber network strengthening, causing this surprising result.

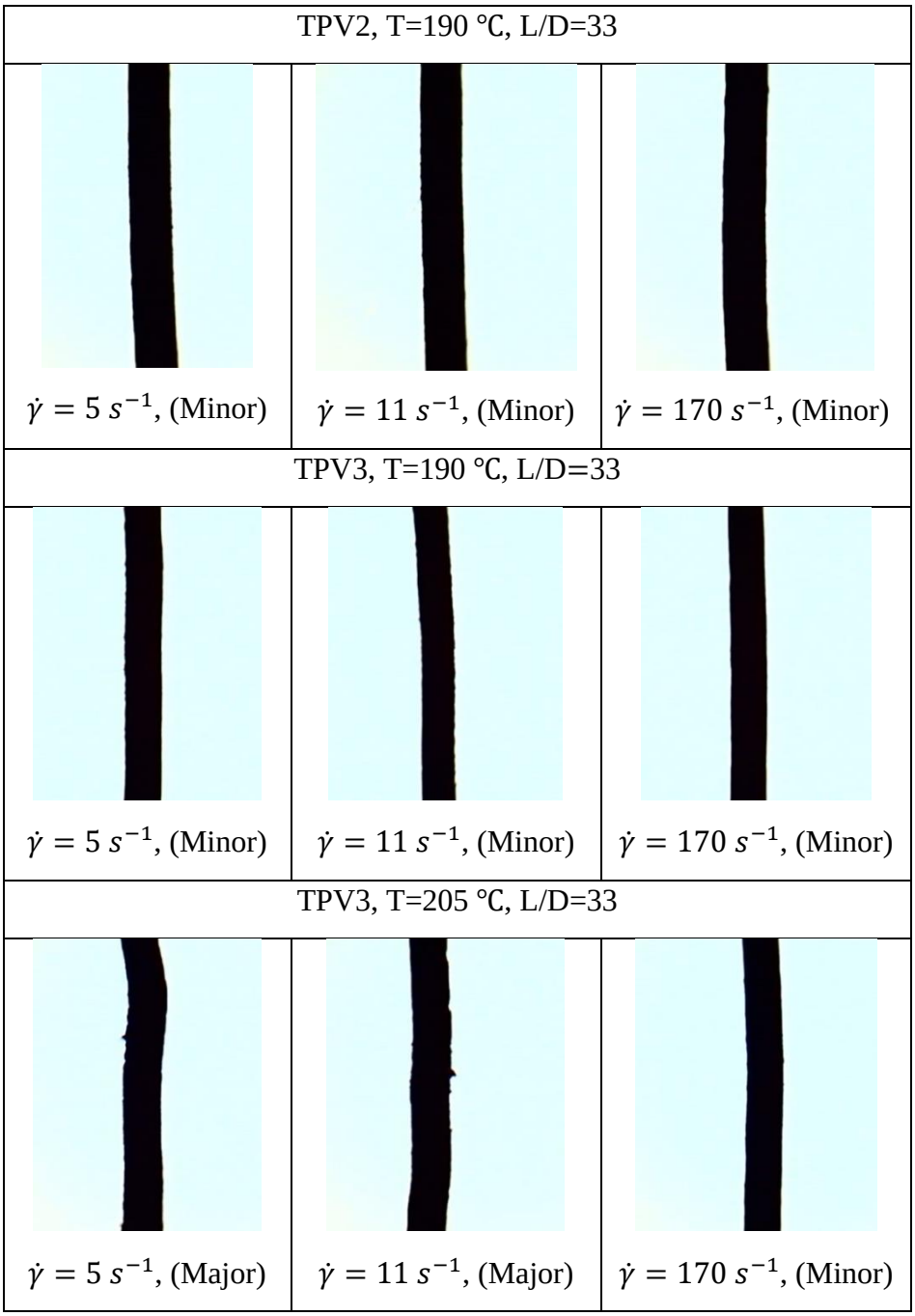

Figure 7-15. The effect of curing level (TPV2 and TPV3 at 190℃) and that of temperature (TPV3 at 190 and 205℃) on the surface extrudate distortion of TPVs.

The effect of crosslinked rubber concentration: Figure 7-16 shows surface fractures of TPV1 (Group A) and TPV5 (Group B) at 190 ℃. While TPV1 shows some minor sharkskin, TPV5 is almost completely smooth at all shear rates. Therefore, increase of the amount of crosslinked rubber particles, increases the severity of surface defects. This again can be explained on the basis

of a higher yield stress (**Table 7-4**), and higher equilibrium storage and shear moduli, G'_y and G^*_y (fingerprints of the morphological structure) of TPV1 compared to those of TPV5. Finally, it was also concluded that the thermoplastic type (L-PP vs B-PP) or rubber type (L-EPDM vs B-EPDM) does not have a clear influence on the TPV's surface fracture.

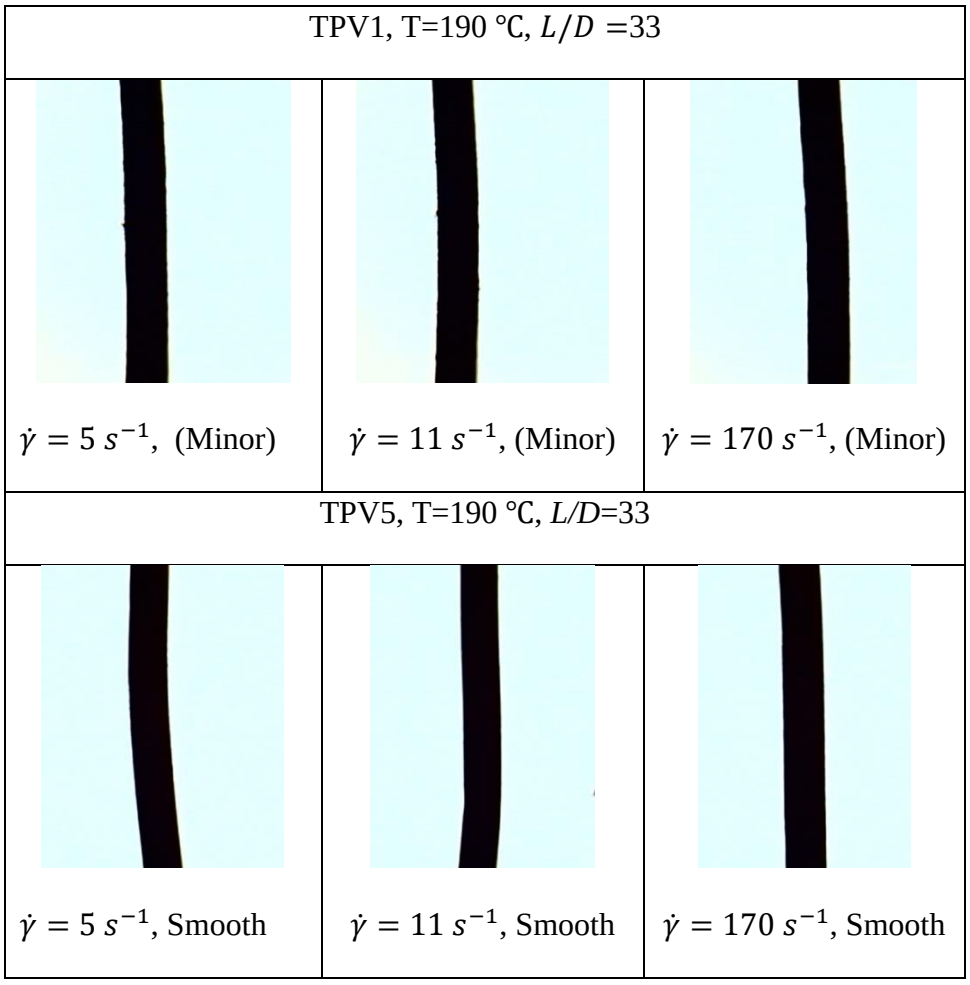

Figure 7-16. Comparison of extrudate surfaces with different amount of crosslinked rubber (TPV1 and TPV5 at 190 ℃)

Table 7-4. The critical shear rates and stresses at 190ºC and 205ºC for the end of surface instabilities of TPVs listed in **Table 4-2**.

Sample	Critical shear rate s^{-1}/ shear stress (MPa) for end of instability			
	Major Sharkskin		**Minor Sharkskin**	
	190 ℃	**205** ℃	**190** ℃	**205** ℃
TPV1	<5/0.063	<5/0.065	>1000/0.173	>1000/0.171
TPV2	<5/0.077	<5/0.066	>1000/0.190	>1000/0.162
TPV3	<5/0.073	18/0.083	640/0.164	820/0.156
TPV4	<5/0.057	18/0.068	>1000/0.168	>1000/0.163
TPV5	<5/0.078	<5/0.074	<5/0.078	640/0.218
TPV6	8/0.078	<5/0.069	64/0.116	820/0.175
TPV7	<5/0.066	<5/0.068	>1000/0.190	820/0.168
TPV8	<5/0.045	<5/0.037	170/0.090	820/0.106

Table 7-5. Yield stresses in shear and extension of TPVs at 190ºC

Sample	Yield stress in Shear σ_y (kPa)	Yield stress in Extension $\sigma_{y,E}$ (kPa)
TPV1	18.5	14.8
TPV2	15.4	14.7
TPV3	22.5	13.5
TPV4	18.9	12.6
TPV5	12.3	11.7
TPV6	22.7	10
TPV7	22.7	8.4
TPV8	25.7	10.1

7.5 Extensional Viscosity

Figure 7-17 shows the comparison of extensional behavior of TPV 4 and TPV 5 with their components. The change in concavity of TPVs' curves represents yield stress [102]. As can be seen, the strong strain hardening of components is not observed in the TPVs. However, **Figure 7-18** shows that the strain hardening becomes more obvious at elevated temperatures. The yield stress is also remains the same or slightly increases with the temperature. This is probably due to network strengthening with the temperature similar to G_y'.

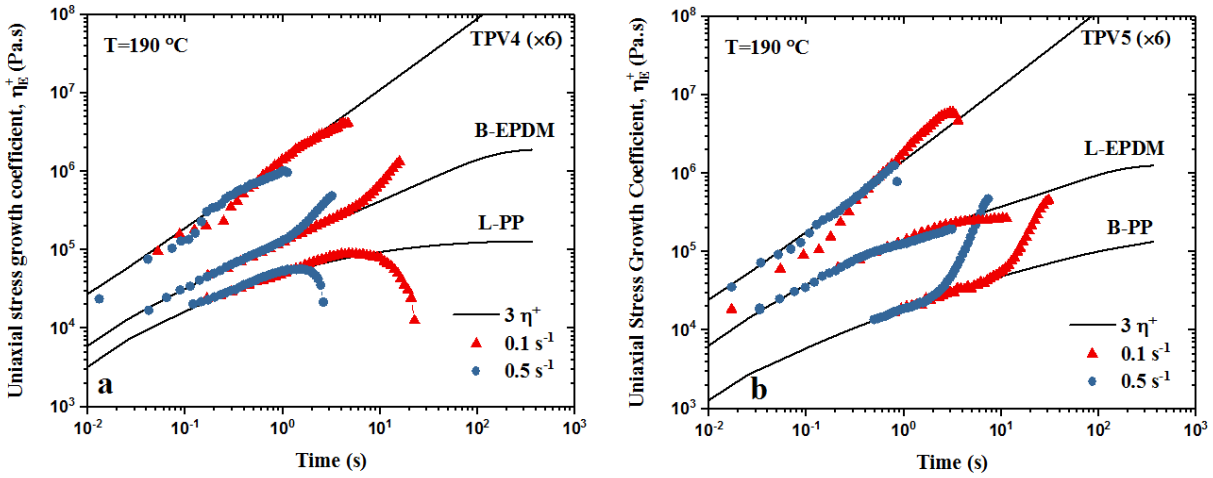

Figure 7-17. Comparison of extensional behavior of TPV4 and TPV5 with those of their constituent components. The data for TPV5 and TPV4 have been multiplied by 6 times for the sake of clarity.

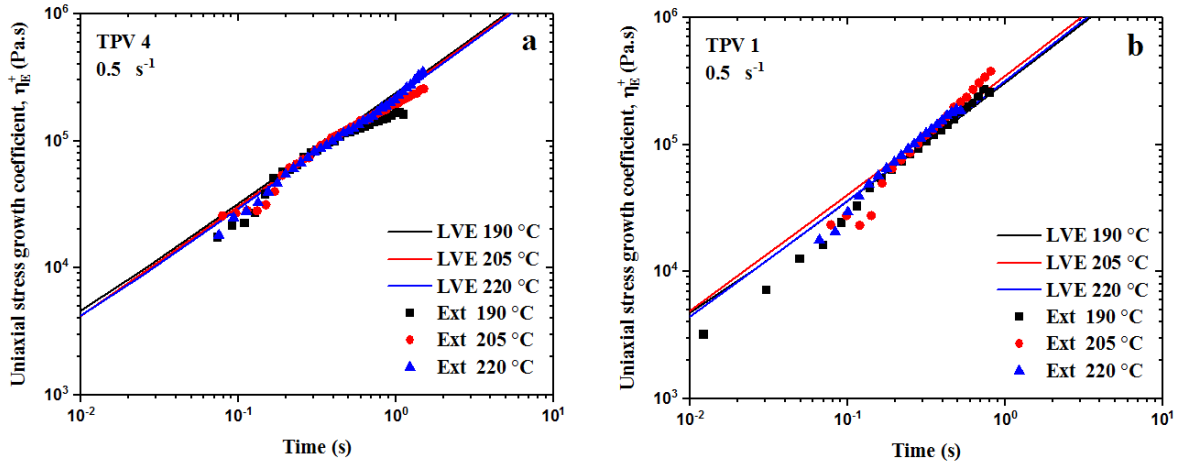

Figure 7-18. Extensional behavior of a) TPV4, and b) TPV 1 at different temperatures.

7.6 Conclusions

In this chapter, the effects of several parameters including the temperature, thermoplastic matrix and rubber particles types, filler and curing levels on the melt fracture of TPVs were investigated. Depending on the molecular characteristics of the constituent polymers, the level of curing, and amount of crosslinked rubber, their processing (extrusion) exhibits various difficulties such as melt fracture (extrudate distortions).

Based on the results of this work, raising the temperature or the amount of rubber particles increases the rubber network strength and consequently creates more surface defects. It also causes more strain hardening in the extensional flow field for all combinations of PP and EPDM independent of linear or branched structure.

Moreover, the slip velocity of EPDMs increases with the temperature and linearity of the polymer. It was also concluded that the slip effect for PPs is negligible due to the high molecular weight and relatively narrow molecular weight distribution of L-PP and the branched structure of B-PP. The results showed that TPV's slip behavior follows its constituent EPDM at high shear rates and based on Mooney analysis [48] it was concluded that the TPV flow in the capillary is almost a plug flow.

Melt fracture analysis showed that TPV surface fracture is increased with decreasing the curing level (especially at high shear rates) which is probably due to yield stress increment in the TPVs.

In summary, yield stresses (in shear and extension) and the equilibrium storage and shear moduli, $G_y^{'}$ and G_y^{*} (fingerprints of the morphological structure) play a critical role in the melt fracture behavior of TPVs. It appears that these parameters correlate inversely proportional with the critical shear stress for the onset of surface instabilities.

8 Conclusions and Recommendations

In this PhD thesis, the linear and non-linear viscoelastic and flow behavior of several groups of TPVs was fully investigated using rheology to understand how to reduce the flow instabilities such as slip and melt fracture. The critical parameters influencing flow instabilities of TPVs were determined and the relationship between these parameters in shear, extensional, and capillary (pressure driven flow field) was studied, as well. This chapter summarizes the important results obtained from the experiments and modeling reported in the thesis. Recommendations for further work are also provided.

8.1 Conclusions

- All TPVs showed a universal non-terminal relaxation behavior i.e., they do not relax the stress at long times or low frequencies. The behavior can be modeled by a simple power-law model $G(t) = G_c t^{-p} + G'_y$, where G'_y is the equilibrium modulus indicating the elastomeric nature of TPVs which was suggested to be related to their microstructure.
- The yield stress increases by increasing the rubber content. It decreases by the curing level as the network becomes stiffer and the yield strain decreases which consequently decrease the yield stress. The TPVs behave more similar to their thermoplastic phase at high frequencies (rose timescale) and follow their rubber behavior at low frequencies.
- For the first time the yield stress for polymer melts in the extensional flow field was observed. The yield stress manifests itself as a change of the curvature of the stress-strain curve. The ratio of extensional yield stress and shear yield stress was found to deviate from von Misses criterion and be in the range of $\sqrt{3}$ and $3\sqrt{3}$ consistent with reported finding for other similar materials.
- It was concluded that TPVs slip massively. The combination of the presence of slip and yield stress originated from the strong rubber network cause a significant reduction in the stress from capillary experiment compared to linear viscoelastic behavior. The slip velocity in capillary flow was obtained from Mooney technique.
- The non-linear behavior of the TPVs can be modeled using K-BKZ model. To incorporate slip in the model, a fraction of the imposed strain should be applied on the model. It is supposed that the TPVs do not slip in the linear viscoelastic region and they show a pure

elastic behavior before yielding (at high curing levels). The slip measurements from parallel-plate and capillary flow were found to be consistent

- TPVs mostly show surface fracture as opposed to melt fracture. The surface fracture is not sharkskin as it is not periodic, and it decreases by increasing shear rate. Therefore, the origin of surface fracture in TPVs differ from other polymers. It was concluded that a minimum stress is required to eliminate or reduce the surface fracture which is the yield stress. By increasing rubber content, the yield stress increases. Thus, more surface fracture is seen in TPVs with high rubber content. The fracture increases with the temperature, as well.
- It was concluded that the yield stress is a key parameter determining the processability of the TPVs. Any parameter that increases yield stress, leads to higher flow instabilities, for example by increasing rubber content, yield stress and consequently flow instability increase.
- As a general picture of the parameters affecting melt fracture, it can be concluded that higher curing level, higher rubber content, and higher molecular wight of the rubber phase contribute significantly to the melt fracture of the TPVs. The effect of the curing level is more profound than the effect of the molecular weight the rubber phase. Moreover, polymer components' molecular structure and molecular weight of the PP phase have a minor influence on the melt fracture of the TPVs. In addition, lower temperature, and higher shear rate assist with the reduction of the melt fracture.

8.2 Future Recommendations

- It is recommended to study the melt fracture of TPVs using different die geometries such as slit to address the edge and stress concentration effects on their melt fracture. In addition, other more complex geometries can be used that create dead zones for unyielded regions to study how unyielded regions affect melt fracture phenomena
- It would be helpful to study the slip behavior at higher temperatures to investigate if the TPVs show the same behavior at higher temperatures. On the same time the K-BKZ model can be used to check if it is still valid. The slip behavior in capillary flow can be studied also by using capillary dies of different diameter to study the effect of pressure on slip. It

is typically expected that increasing pressure (normal force), the slip should decrease (analog of friction of elastomers on solid substrates).

- The presence of oil has a significant influence on the slip behavior of TPVs. It would be also useful to study the effect of oil content on the rheological properties of TPVs and how much if affects the TPVs wall slip behavior.

References

[1] K. Naskar, Thermoplastic elastomers based on PP/EPDM blends by dynamic vulcanization, Rubber Chem. Technol. 80 (2007) 504–519.

[2] N. Ning, S. Li, H. Wu, H. Tian, P. Yao, H.U. Guo-Hua, M. Tian, L. Zhang, Preparation, microstructure, and microstructure-properties relationship of thermoplastic vulcanizates (TPVs): A review, Prog. Polym. Sci. 79 (2018) 61–97.

[3] M. van Duin, Recent Developments for EPDM-Based Thermoplastic Vulcanisates, in: Macromol. Symp., Wiley Online Library, 2006: pp. 11–16.

[4] K. Lu, M. van Duin, J. Loos, G. de With, On the volume organisation of thermoplastic vulcanisates (TPVs) as revealed by scanning transmission electron microscopy (STEM) tomography, Polymer (Guildf). 53 (2012) 4171–4177.

[5] S. Shahbikian, P.J. Carreau, M. Heuzey, M.D. Ellul, H.P. Nadella, J. Cheng, P. Shirodkar, Rheology/morphology relationship of plasticized and nonplasticized thermoplastic elastomers based on ethylene–propylene–diene–terpolymer and polypropylene, Polym. Eng. Sci. 51 (2011) 2314–2327.

[6] W.G.F. Sengers, P. Sengupta, J.W.M. Noordermeer, S.J. Picken, A.D. Gotsis, Linear viscoelastic properties of olefinic thermoplastic elastomer blends: melt state properties, Polymer (Guildf). 45 (2004) 8881–8891.

[7] K. Naskar, U. Gohs, G. Heinrich, Influence of molecular structure of blend components on the performance of thermoplastic vulcanisates prepared by electron induced reactive processing, Polymer (Guildf). 91 (2016) 203–210.

[8] V.M. Litvinov, EPDM/PP thermoplastic vulcanizates as studied by proton NMR relaxation: phase composition, molecular mobility, network structure in the rubbery phase, and network heterogeneity, Macromolecules. 39 (2006) 8727–8741.

[9] K. Jayaraman, V.G. Kolli, S. Kang, S. Kumar, M.D. Ellul, Shear flow behavior and oil distribution between phases in thermoplastic vulcanizates, J. Appl. Polym. Sci. 93 (2004) 113–121.

[10] S. Shahbikian, P.J. Carreau, M. Heuzey, M.D. Ellul, J. Cheng, P. Shirodkar, H.P. Nadella, Morphology development of EPDM/PP uncross-linked/dynamically cross-linked blends, Polym. Eng. Sci. 52 (2012) 309–322.

[11] S. Shahbikian, P.J. Carreau, M.C. Heuzey, M.D. Ellul, H.P. Nadella, J. Cheng, P. Shirodkar, Morphology and rheology of nonreactive and reactive EPDM/PP blends in transient shear flow: plasticized versus nonplasticized blends, Rubber Chem. Technol. 84 (2011) 325–353.

[12] R.R. Babu, N.K. Singha, K. Naskar, Effects of mixing sequence on peroxide cured polypropylene (PP)/ethylene octene copolymer (EOC) thermoplastic vulcanizates (TPVs). Part. II. Viscoelastic characteristics, J. Polym. Res. 18 (2011) 31–39.

[13] C. Nakason, P. Wannavilai, A. Kaesaman, Effect of vulcanization system on properties of thermoplastic vulcanizates based on epoxidized natural rubber/polypropylene blends, Polym. Test. 25 (2006) 34–41.

[14] S. Varghese, R. Alex, B. Kuriakose, Natural rubber–isotactic polypropylene thermoplastic blends, J. Appl. Polym. Sci. 92 (2004) 2063–2068.

[15] C. Nakason, M. Jarnthong, A. Kaesaman, S. Kiatkamjornwong, Thermoplastic elastomers based on epoxidized natural rubber and high-density polyethylene blends: Effect of blend compatibilizers on the mechanical and morphological properties, J. Appl. Polym. Sci. 109 (2008) 2694–2702.

[16] J. George, N.R. Neelakantan, K.T. Varughese, S. Thomas, Failure properties of thermoplastic elastomers from polyethylene/nitrile rubber blends: Effect of blend ratio, dynamic vulcanization, and filler incorporation, J. Appl. Polym. Sci. 100 (2006) 2912–2929.

[17] N. Ning, Y. Hua, H. Wu, L. Zhang, S. Wu, M. Tian, H. Tian, G.-H. Hu, Novel heat and oil-resistant thermoplastic vulcanizates based on ethylene-vinyl acetate rubber/poly (vinylidene fluoride), RSC Adv. 6 (2016) 91594–91602.

[18] C. Xu, Y. Wang, B. Lin, X. Liang, Y. Chen, Thermoplastic vulcanizate based on poly (vinylidene fluoride) and methyl vinyl silicone rubber by using fluorosilicone rubber as interfacial compatibilizer, Mater. Des. 88 (2015) 170–176.

[19] D. Yuan, Z. Chen, C. Xu, K. Chen, Y. Chen, Fully biobased shape memory material based on novel cocontinuous structure in poly (lactic acid)/natural rubber TPVs fabricated via peroxide-induced dynamic vulcanization and in situ interfacial compatibilization, ACS Sustain. Chem. Eng. 3 (2015) 2856–2865.

[20] G. Martin, C. Barrès, P. Sonntag, N. Garois, P. Cassagnau, Morphology development in thermoplastic vulcanizates (tpv): Dispersion mechanisms of a pre-crosslinked epdm phase, Eur. Polym. J. 45 (2009) 3257–3268.

[21] H. Wu, M. Tian, L. Zhang, H. Tian, Y. Wu, N. Ning, T.W. Chan, New understanding of morphology evolution of thermoplastic vulcanizate (TPV) during dynamic vulcanization, ACS Sustain. Chem. Eng. 3 (2014) 26–32.

[22] C.F. Antunes, A. V Machado, M. Van Duin, Morphology development and phase inversion during dynamic vulcanisation of EPDM/PP blends, Eur. Polym. J. 47 (2011) 1447–1459.

[23] F. Goharpey, A.A. Katbab, H. Nazockdast, Formation of rubber particle agglomerates during morphology development in dynamically crosslinked EPDM/PP thermoplastic elastomers. Part 1: effects of processing and polymer structural parameters, Rubber Chem. Technol. 76 (2003) 239–252.

[24] S. Li, H. Tian, B. Zhang, G.-H. Hu, C.-Y. Liu, L. Zhang, M. Tian, Nonlinear and linear viscoelastic behaviors of thermoplastic vulcanizates containing rubber nanoparticle agglomerates, Polymer (Guildf). 181 (2019) 121793.

[25] U. Yilmazer, D.M. Kalyon, Slip effects in capillary and parallel disk torsional flows of highly filled suspensions, J. Rheol. (N. Y. N. Y). 33 (1989) 1197–1212.

[26] M. Jugo Viloria, M. Valtier, B. Vergnes, Volume instabilities in capillary flow of pure SBR and SBR compounds, J. Rheol. (N. Y. N. Y). 61 (2017) 1085–1097.

[27] P. Yao, H. Wu, N. Ning, L. Zhang, H. Tian, Y. Wu, G. Hu, T.W. Chan, M. Tian, Properties and unique morphological evolution of dynamically vulcanized bromo-isobutylene-isoprene rubber/polypropylene thermoplastic elastomer, RSC Adv. 6 (2016) 11151–11160.

[28] S.S. Banerjee, A.K. Bhowmick, Viscoelastic properties and melt rheology of novel polyamide 6/fluoroelastomer nanostructured thermoplastic vulcanizates, J. Mater. Sci. 51

(2016) 252–261.

[29] E. Prut, T. Medintseva, V. Dreval, Mechanical and Rheological Behavior of Unvulcanized and Dynamically Vulcanized i-PP/EPDM Blends, in: Macromol. Symp., Wiley Online Library, 2006: pp. 78–85.

[30] P. Ma, P. Xu, W. Liu, Y. Zhai, W. Dong, Y. Zhang, M. Chen, Bio-based poly (lactide)/ethylene-co-vinyl acetate thermoplastic vulcanizates by dynamic crosslinking: structure vs. property, RSC Adv. 5 (2015) 15962–15968.

[31] K.A. Iyer, J.M. Torkelson, Importance of superior dispersion versus filler surface modification in producing robust polymer nanocomposites: The example of polypropylene/nanosilica hybrids, Polymer (Guildf). 68 (2015) 147–157.

[32] M. Tian, J. Han, H. Wu, H. Tian, Q. She, W. Chen, L. Zhang, Effect of the compatibility on the morphology and properties of acrylonitrile–butadiene rubber/polypropylene thermoplastic vulcanizates, J. Appl. Polym. Sci. 124 (2012) 1999–2006.

[33] P. Ma, P. Xu, Y. Zhai, W. Dong, Y. Zhang, M. Chen, Biobased poly (lactide)/ethylene-co-vinyl acetate thermoplastic vulcanizates: morphology evolution, superior properties, and partial degradability, ACS Sustain. Chem. Eng. 3 (2015) 2211–2219.

[34] W. Pechurai, K. Sahakaro, C. Nakason, Influence of phenolic curative on crosslink density and other related properties of dynamically cured NR/HDPE blends, J. Appl. Polym. Sci. 113 (2009) 1232–1240.

[35] P. Yao, H. Wu, N. Ning, L. Zhang, H. Tian, Y. Wu, G.-H. Hu, T.W. Chan, M. Tian, Microstructure and properties of bromo-isobutylene–isoprene rubber/polyamide 12 thermoplastic vulcanizate toward recyclable inner liners for green tires, RSC Adv. 6 (2016) 30004–30013.

[36] A.F. Jolfaei, J.N. Gavgani, A. Jalali, F. Goharpey, Effect of organoclay and compatibilizers on microstructure, rheological and mechanical properties of dynamically vulcanized EPDM/PP elastomers, Polym. Bull. 72 (2015) 1127–1144.

[37] S.S. Banerjee, K.D. Kumar, A.K. Sikder, A.K. Bhowmick, Nanomechanics and origin of rubber elasticity of novel nanostructured thermoplastic elastomeric blends using atomic

force microscopy, Macromol. Chem. Phys. 216 (2015) 1666–1674.

[38] E. V Prut, N.A. Erina, J. Karger-Kocsis, T.I. Medintseva, Effects of blend composition and dynamic vulcanization on the morphology and dynamic viscoelastic properties of PP/EPDM blends, J. Appl. Polym. Sci. 109 (2008) 1212–1220.

[39] Y. Tang, K. Lu, X. Cao, Y. Li, Nanostructured thermoplastic vulcanizates by selectively cross-linking a thermoplastic blend with similar chemical structures, Ind. Eng. Chem. Res. 52 (2013) 12613–12621.

[40] R.R. Fernandes, D.E. V Andrade, A.T. Franco, C.O.R. Negrão, The yielding and the linear-to-nonlinear viscoelastic transition of an elastoviscoplastic material, J. Rheol. (N. Y. N. Y). 61 (2017) 893–903.

[41] H. Kim, C.W. Macosko, Processing-property relationships of polycarbonate/graphene composites, Polymer (Guildf). 50 (2009) 3797–3809.

[42] E. N'Gouamba, J. Goyon, P. Coussot, Elastoplastic behavior of yield stress fluids, Phys. Rev. Fluids. 4 (2019) 123301.

[43] C.J. Dimitriou, R.H. Ewoldt, G.H. McKinley, Describing and prescribing the constitutive response of yield stress fluids using large amplitude oscillatory shear stress (LAOStress), J. Rheol. (N. Y. N. Y). 57 (2013) 27–70.

[44] X. Zhang, O. Fadoul, E. Lorenceau, P. Coussot, Yielding and flow of soft-jammed systems in elongation, Phys. Rev. Lett. 120 (2018) 48001.

[45] S.G. Hatzikiriakos, Wall slip of molten polymers, Prog. Polym. Sci. 37 (2012) 624–643.

[46] S.G. Hatzikiriakos, Slip mechanisms in complex fluid flows, Soft Matter. 11 (2015) 7851–7856.

[47] M. Ebrahimi, Wall slip of polydisperse linear polymers: effects of molecular weight characteristics, and surface conditions, (2017).

[48] M. Mooney, Explicit formulas for slip and fluidity, J. Rheol. 2 (1931) 210–222.

[49] S.G. Hatzikiriakos, K.B. Migler, Polymer processing instabilities: control and

understanding, CRC Press, 2004.

[50] B. Vergnes, Extrusion defects and flow instabilities of molten polymers, Int. Polym. Process. 30 (2015) 3–28.

[51] W. Qiye, L. Peng, M. Jingxia, Z. Na, A. Peng, W. Jingan, The rheological behavior of EPDM Nordel IP and POE engage produced by CGC and INSITE^{TM} technology, J. Appl. Polym. Sci. 101 (2006) 2847–2853.

[52] B. Vergnes, S. d'Halewyn, M.F. Boube, Wall slip and instabilities in the flow of EPDM compounds, in: Theor. Appl. Rheol., Elsevier, 1992: pp. 399–401.

[53] J. Wu, Q. Pan, G. Huang, Study on the morphology, rheology and surface of dynamically vulcanized chlorinated butyl rubber/polyethylacrylate extrudates: effect of extrusion temperature and times, J. Mater. Sci. 42 (2007) 4494–4501.

[54] M. Ponsard-Fillette, C. Barres, P. Cassagnau, Viscoelastic study of oil diffusion in molten PP and EPDM copolymer, Polymer (Guildf). 46 (2005) 10256–10268.

[55] A.A. Katbab, H. Nazockdast, S. Bazgir, Carbon black-reinforced dynamically cured EPDM/PP thermoplastic elastomers. I. Morphology, rheology, and dynamic mechanical properties, J. Appl. Polym. Sci. 75 (2000) 1127–1137.

[56] T. Himmel, M.H. Wagner, Experimental determination of interfacial slip between polyethylene and thermoplastic elastomers, J. Rheol. (N. Y. N. Y). 57 (2013) 1773–1785.

[57] M. Ansari, Y.W. Inn, A.M. Sukhadia, P.J. DesLauriers, S.G. Hatzikiriakos, Melt fracture of HDPEs: Metallocene versus Ziegler–Natta and broad MWD effects, Polymer (Guildf). 53 (2012) 4195–4201.

[58] M. Ansari, T. Zisis, S.G. Hatzikiriakos, E. Mitsoulis, Capillary flow of low-density polyethylene, Polym. Eng. Sci. 52 (2012) 649–662.

[59] M. Ebrahimi, T. Tomkovic, G. Liu, A.A. Doufas, S.G. Hatzikiriakos, Melt fracture of linear low-density polyethylenes: Die geometry and molecular weight characteristics, Phys. Fluids. 30 (2018) 53103.

[60] J.J. Baik, C. Tzoganakis, A study of extrudate distortion in controlled-rheology

polypropylenes, Polym. Eng. Sci. 38 (1998) 274–281.

[61] I.B. Kazatchkov, S.G. Hatzikiriakos, C.W. Stewart, Extrudate distortion in the capillary/slit extrusion of a molten polypropylene, J. Plast. Film Sheeting. 11 (1995) 38–57.

[62] J. Vlachopoulos, S. Lidorikis, Melt fracture of polystyrene, Polym. Eng. Sci. 11 (1971) 1–5.

[63] N. El Kissi, J.-M. Piau, F. Toussaint, Sharkskin and cracking of polymer melt extrudates, J. Nonnewton. Fluid Mech. 68 (1997) 271–290.

[64] N. Noroozi, J.A. Thomson, N. Noroozi, L.L. Schafer, S.G. Hatzikiriakos, Viscoelastic behaviour and flow instabilities of biodegradable poly (ε-caprolactone) polyesters, Rheol. Acta. 51 (2012) 179–192.

[65] N. Othman, B. Jazrawi, P. Mehrkhodavandi, S.G. Hatzikiriakos, Wall slip and melt fracture of poly (lactides), Rheol. Acta. 51 (2012) 357–369.

[66] B. Jazrawi, N. Noroozi, M. Ansari, S.G. Hatzikiriakos, Processing aids for biodegradable polymers, J. Appl. Polym. Sci. 128 (2013) 3592–3600.

[67] E.E. Rosenbaum, S.G. Hatzikiriakos, C.W. Stewart, Flow implications in the processing of tetrafluoroethylene/hexafluoropropylene copolymers, Int. Polym. Process. 10 (1995) 204–212.

[68] E. Chatzigiannakis, M. Ebrahimi, M.H. Wagner, S.G. Hatzikiriakos, Wall slip of polyisobutylenes: Effect of molecular characteristics, Rheol. Acta. 56 (2017) 85–94.

[69] M. Zuliki, S. Zhang, T. Tomkovic, S.G. Hatzikiriakos, Capillary flow of sodium and zinc ionomers, Phys. Fluids. 32 (2020) 23106.

[70] R. Dangtungee, P. Supaphol, Melt rheology and extrudate swell of sodium chloride-filled low-density polyethylene: Effects of content and size of salt particles, Polym. Test. 29 (2010) 188–195.

[71] F. Baldi, J. Ragnoli, F. Briatico-Vangosa, Measurement of the high rate flow properties of filled HDPE melts by capillary rheometer: Effects of the test geometry, Polym. Test. 37 (2014) 201–209.

[72] J.Z. Liang, J.N. Ness, Studies on melt flow properties of low density and linear low density polyethylene blends in capillary extrusion, Polym. Test. 16 (1997) 173–184.

[73] K. Lewandowski, K. Piszczek, S. Zajchowski, J. Mirowski, Rheological properties of wood polymer composites at high shear rates, Polym. Test. 51 (2016) 58–62.

[74] F. Snijkers, D. Vlassopoulos, Cone-partitioned-plate geometry for the ARES rheometer with temperature control, J. Rheol. (N. Y. N. Y). 55 (2011) 1167–1186.

[75] M.H. Wagner, Analysis of stress-growth data for simple extension of a low-density branched polyethylene melt, Rhological Acta. 15 (1976) 133–135. https://doi.org/10.1007/BF01517504.

[76] X.-L. Luo, R.I. Tanner, Finite Element Simulation of Long and Short Circular Die Extrusion Experiments Using Integral Models, Int. J. Numer. Methods Eng. 25 (1988) 9–22. https://doi.org/10.1002/nme.1620250104.

[77] E. Mitsoulis, S.G. Hatzikiriakos, Bagley correction: the effect of contraction angle and its prediction, Rheol. Acta. 42 (2003) 309–320.

[78] E. Mitsoulis, S.G. Hatzikiriakos, K. Christodoulou, D. Vlassopoulos, Sensitivity analysis of the Bagley correction to shear and extensional rheology, Rheol. Acta. 37 (1998) 438–448.

[79] S. Costanzo, G. Ianniruberto, G. Marrucci, D. Vlassopoulos, Measuring and assessing first and second normal stress differences of polymeric fluids with a modular cone-partitioned plate geometry, Rheol. Acta. 57 (2018) 363–376.

[80] T. Tomkovic, E. Mitsoulis, S.G. Hatzikiriakos, Contraction flow of ionomers and their corresponding copolymers: Ionic and hydrogen bonding effects, Phys. Fluids. 31 (2019) 33102.

[81] H. Niu, Y. Wang, X. Liu, Y. Wang, Y. Li, Determination of plateau moduli and entanglement molecular weights of ultra-high molecular weight isotactic polypropylene synthesized by Ziegler-Natta catalyst, Polym. Test. 60 (2017) 260–265.

[82] S. Paavola, T. Saarinen, B. Löfgren, P. Pitkänen, Propylene copolymerization with non-conjugated dienes and α-olefins using supported metallocene catalyst, Polymer (Guildf). 45

(2004) 2099–2110.

[83] J.A. Langston, R.H. Colby, T.C.M. Chung, F. Shimizu, T. Suzuki, M. Aoki, Synthesis and characterization of long chain branched isotactic polypropylene via metallocene catalyst and T-reagent, Macromolecules. 40 (2007) 2712–2720.

[84] S.G. Hatzikiriakos, Long chain branching and polydispersity effects on the rheological properties of polyethylenes, Polym. Eng. Sci. 40 (2000) 2279–2287.

[85] X. Wang, X. Luo, A polymer network based on thermoplastic polyurethane and ethylene–propylene–diene elastomer via melt blending: morphology, mechanical properties, and rheology, Eur. Polym. J. 40 (2004) 2391–2399.

[86] A.R.R. Menon, Melt rheology of ethylene propylene diene rubber modified with phosphorylated cashew nut shell liquid prepolymer, Iran. Polym. J. (2003).

[87] S.A. Rogers, B.M. Erwin, D. Vlassopoulos, M. Cloitre, A sequence of physical processes determined and quantified in LAOS: Application to a yield stress fluid, J. Rheol. (N. Y. N. Y). 55 (2011) 435–458.

[88] D. Bonn, M.M. Denn, L. Berthier, T. Divoux, S. Manneville, Yield stress materials in soft condensed matter, Rev. Mod. Phys. 89 (2017) 35005.

[89] Q. Wu, J. Fang, M. Zheng, Y. Luo, X. Wang, L. Xu, C. Zhang, Morphology evolution and rheological behaviors of PP/SR thermoplastic vulcanizate, Polymers (Basel). 11 (2019) 175.

[90] R.I. Tanner, S.-C. Dai, F. Qi, Bread dough rheology and recoil: 2. Recoil and relaxation, J. Nonnewton. Fluid Mech. 143 (2007) 107–119.

[91] C.I. Hicks, H. See, C. Ekwebelam, The shear rheology of bread dough: modeling, Rheol. Acta. 50 (2011) 701–710.

[92] F.R. Schwarzl, Numerical calculation of stress relaxation modulus from dynamic data for linear viscoelastic materials, Rheol. Acta. 14 (1975) 581–590.

[93] M.J. Armstrong, A.N. Beris, S.A. Rogers, N.J. Wagner, Dynamic shear rheology of a thixotropic suspension: Comparison of an improved structure-based model with large amplitude oscillatory shear experiments, J. Rheol. (N. Y. N. Y). 60 (2016) 433–450.

[94] S. Varchanis, G. Makrigiorgos, P. Moschopoulos, Y. Dimakopoulos, J. Tsamopoulos, Modeling the rheology of thixotropic elasto-visco-plastic materials, J. Rheol. (N. Y. N. Y). 63 (2019) 609–639.

[95] S. Varchanis, S.J. Haward, C.C. Hopkins, A. Syrakos, A.Q. Shen, Y. Dimakopoulos, J. Tsamopoulos, Transition between solid and liquid state of yield-stress fluids under purely extensional deformations, Proc. Natl. Acad. Sci. 117 (2020) 12611–12617.

[96] K. Niedzwiedz, H. Buggisch, N. Willenbacher, Extensional rheology of concentrated emulsions as probed by capillary breakup elongational rheometry (CaBER), Rheol. Acta. 49 (2010) 1103–1116.

[97] N. Louvet, D. Bonn, H. Kellay, Nonuniversality in the pinch-off of yield stress fluids: role of nonlocal rheology, Phys. Rev. Lett. 113 (2014) 218302.

[98] J. Boujlel, P. Coussot, Measuring the surface tension of yield stress fluids, Soft Matter. 9 (2013) 5898–5908.

[99] E. Mitsoulis, 50 years of the K-BKZ constitutive relation for polymers, Int. Sch. Res. Not. 2013 (2013).

[100] N. Ghahramani, S. Zhang, K. A Iyer, A.K. Doufas, S.G. Hatzikiriakos, Melt fracture and wall slip of thermoplastic vulcanizates, Polym. Eng. Sci. (2020).

[101] N. Ghahramani, K.A. Iyer, A.K. Doufas, S.G. Hatzikiriakos, Rheology of thermoplastic vulcanizates (TPVs), J. Rheol. (N. Y. N. Y). 64 (2020) 1325–1341.

[102] S. Ghahramani, Nikoo, Hatzikiriakos, Rheology of TPVs, (2020).

[103] G. Ghoshal, U.S. Shivhare, U.C. Banerjee, Rheological properties and microstructure of xylanase containing whole wheat bread dough, J. Food Sci. Technol. 54 (2017) 1928–1937.

[104] J.M. Dealy, K.F. Wissbrun, Melt rheology and its role in plastics processing: theory and applications, Springer Science & Business Media, 2012.

[105] M. Ansari, Y.W. Inn, A.M. Sukhadia, P.J. DesLauriers, S.G. Hatzikiriakos, Wall slip of HDPEs: Molecular weight and molecular weight distribution effects, J. Rheol. (N. Y. N. Y). 57 (2013) 927–948.

[106] M. Ebrahimi, M. Ansari, S.G. Hatzikiriakos, Wall slip of polydisperse linear polymers using double reptation, J. Rheol. (N. Y. N. Y). 59 (2015) 885–901.

[107] E. Chatzigiannakis, M. Ebrahimi, M.H. Wagner, S.G. Hatzikiriakos, Melt fracture of polyisobutylenes, Polym. Test. 60 (2017) 30–38.

[108] C. Combeaud, Y. Demay, B. Vergnes, Experimental study of the volume defects in polystyrene extrusion, J. Nonnewton. Fluid Mech. 121 (2004) 175–185.